INTERFEROMETRY OF SOLID THIN FILMS

Charles Ray Brown
(M. S. thesis)

December 1973

Prepared for the U. S. Atomic Energy Commission
under Contract W-7405-ENG-48

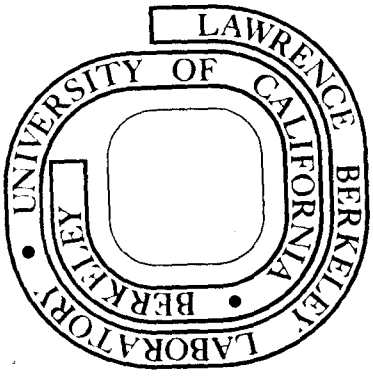

LBL-2264
c.1

DISCLAIMER

INTERFEROMETRY OF SOLID THIN FILMS

Contents

INTERFEROMETRY OF SOLID THIN FILMS

Charles Ray Brown

Inorganic Materials Research Division, Lawrence Berkeley Laboratory
and Department of Chemical Engineering; University of California
Berkeley, California

ABSTRACT

Experiments were conducted to determine the validity of previously-derived interference color series and the accuracy obtainable by using white light interference for measuring the thickness of thin, transparent films on metal substrates. Film thickness profiles were derived from observed interference colors and compared to profiles derived from two different step-height measurements that were independent of the optical properties of film and substrate. In addition, film thickness was determined by two other optical techniques, spectroscopy and ellipsometry.

Satisfactory agreement was obtained with film profiles obtained by visual interpretation of interference colors and use of previously determined color series. The practical distinction between neighboring hues is not as sharp as theoretically predicted. But colors of lower saturation than previously assumed can still be observed in practice.

---

*M. S. Thesis, research conducted under the direction of R. H. Muller.

I. INTRODUCTION

White light optical interference is a sensitive, non-destructive technique for observing extended thin films. Since light does not measurably disturb the film, white light interference has been used in previous work[1,2,4] for the quantitative determination of local thickness of draining electrolytes on partially submerged, polished metal substrates. In addition to their visual and photographic observation, interference colors have been characterized spectroscopically.[2] Ellipsometry of liquid layers was used by Gu[3] to study draining electrolytes on platinum substrates.

In order to derive a film profile from observed interference colors resulting from white light interference in a tapered, transparant, thin film, a model of thin film interference is used. The surfaces of the film and substrate are geometrically planar and multiple reflection occurs at material interfaces. The fact that there are phase changes at absorbing substrates was included by Muller.[5] From the intensity distribution calculated for the wedge film, a color series can be calculated for visual analysis. Turney[2] compiled color charts for different metal-liquid reflectivities and arbitrary phase changes. Thus, film profiles could be derived either from spectroscopic intensity distributions or from color series derived for a specific phase change and reflectivity.

The purpose of this work was to experimentally test computed color series derived from the model of multiple beam interference in thin films. In order to do this, experimental thin films must cover a wide range of phase change and metal-film reflectance in order to examine

different areas of several of the computed color charts. The film-thicknesses derived from the interference colors are, then, compared with thicknesses derived using methods not dependent upon phase change and reflectance (optical properties of the film and substrate). Ellipsometry and spectroscopy are optical methods that have been used, also. Solid dielectric films have been used because they are stable for the consecutive examination by several techniques.

Vacuum deposited layers have been used for both substrates and transparent films.[8] Vapor deposition of the material in a vacuum results in clean, microscopically smooth surfaces.[6,7] The optical properties of deposited thin films are constant above a critical film thickness. These properties are well-defined and are reproducible.

The dielectric was deposited in the shape of a wedge in order to obtain a series of interference colors on each specimen. The film thickness profile of the dielectric film was derived from three optical measurements. These were: (1) photography of interference colors, (2) ellipsometry, and (3) spectroscopy of white light interference. These film profiles were then compared with two independently derived profiles. These were: (1) mechanical step-height measurement using a profilometer, and (2) optical step-height measurement of a coated step on the film using an interference microscope.

The optically-derived thickness profiles were compared with independently derived step-height profiles in order to determine the utility of the computed interference color series for the visual derivation of film thickness.

II. TECHNIQUES OF MEASUREMENT

A. Interferometry of Thin Films

Light interference is a non-destructive technique for the measurement of transparent thin film thicknesses. It offers high resolution combined with the capability of simultaneously observing extended areas of film.

Optical interference in thin films depends on the optical properties of the substrate and film as well as the film thickness. For solid films prepared in high vacuum the refractive index of materials used for optical coatings is, generally, independent of thickness for films thicker than 475 Angstrom[9] and shows negligible variation in literature values.[10] The optical properties of deposited metals are, however, sensitive to both the structure and thickness of the deposited film and, generally, are different from the refractive indices of the bulk material.[11] The optical properties of the metal films are spectrally dependent also with literature values showing a wide variation in index values. Therefore, separate studies of refractive index of the substrates are required.

The explanation of optical interference is given elsewhere.[12,13] White light interference is preferred for the study of thin films because the interference results in non-repetitive color variations for films up to about 1.5 microns thickness.

1. Sign Convention

The conventions and definitions describing the interaction of light with a material interface are those used in ellipsometry.[14]

The complex index of refraction of an absorbing medium is defined as $n_c = n - ik$, where n is the refractive index and k is the index of

extinction. For a dielectric medium, k is equal to zero and the medium is characterized by a real index of refraction n. The medium containing the incident beam is assumed to be a dielectric medium with refractive index n_o.

The coordinate system is shown in Fig. 1. The direction of a positive vector is shown by an arrowhead. Subscripts p and s designate the component "in the plane of incidence" and "normal to the plane of incidence," respectively. Superscript (") denotes the reflected wave, and superscript (') the transmitted wave. Phi, ϕ, is the angle of incidence and reflection with respect to the normal at the dielectric-incident medium interface while ϕ' is the angle of refraction.

Superscript "1" denotes the dielectric-metal interface, subscript "2" denotes the dielectric-incident medium interface, and "3" denotes the incident-medium-dielectric interface. Figure 2 is a description of the use of this notation in identifying the Fresnel coefficients and the local relative phase changes.

As a ray of light falls upon a film-covered surface, multiple reflection occurs at the film surface and at the film-substrate interface as shown in Fig. 3(a). The system of reflected and refracted waves in Fig. 3(a) is equivalent to the system shown in Fig. 3(b),[16] where E" is a wave equivalent to all waves reflected at the film, E' and E'" are the equivalents of all waves in the film, and E_m is the equivalent of all waves in the substrate. The substrate is to be of infinite extent in the -y direction.

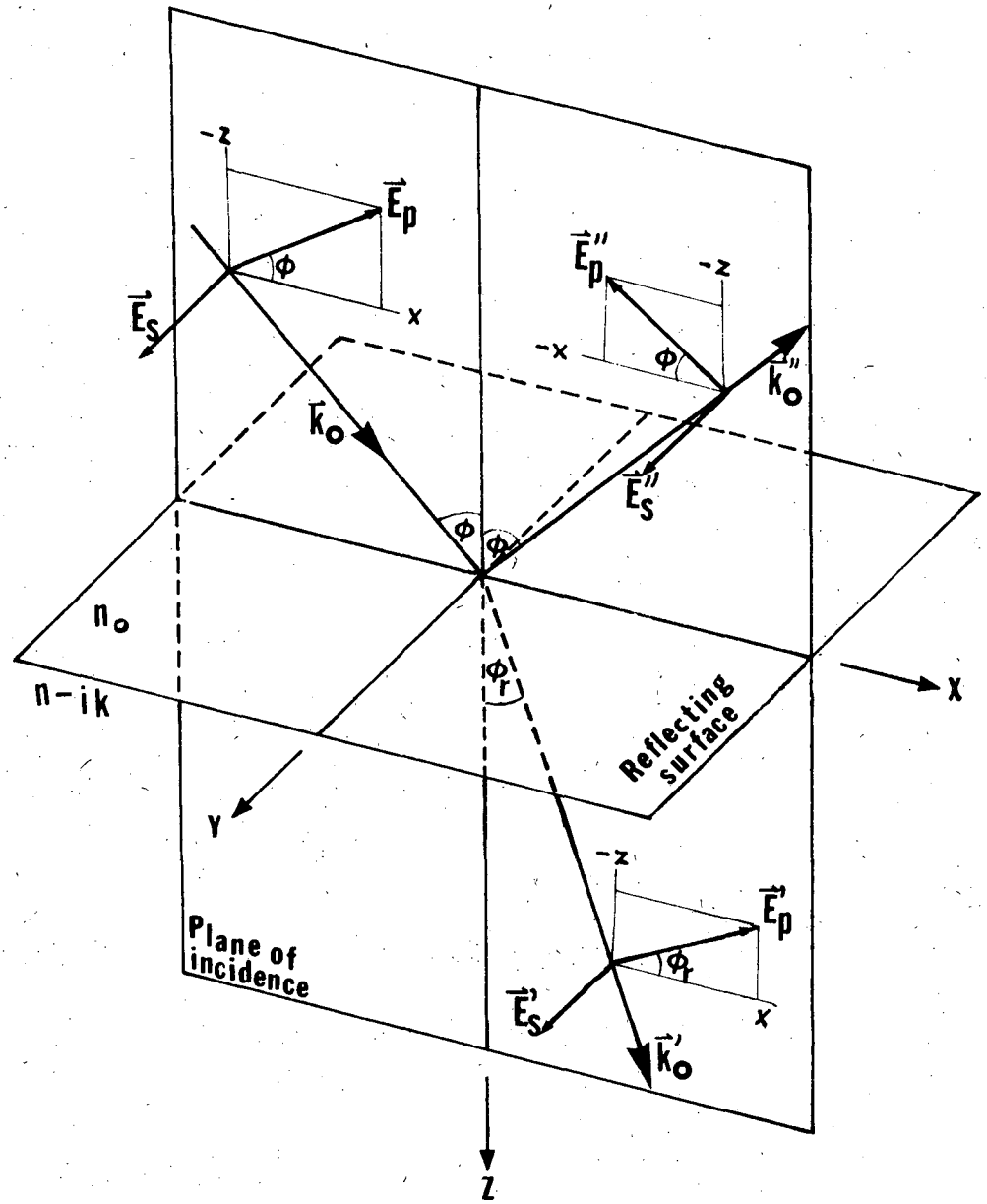

XBL 7110-7420

Fig. 1. Coordinate system and sign conventions for the electric field (positive direction of E_p and E_s in incident, reflected in refracted waves is indicated by arrows). The propagation vectors are represented by k_o, k_o' and k_o''. Subscript p stands for polarization parallel to the plane of incidence and subscript s stands for polarization normal to the plane of incidence. The complex index of refraction of the adsorbing medium is designated n-ik.

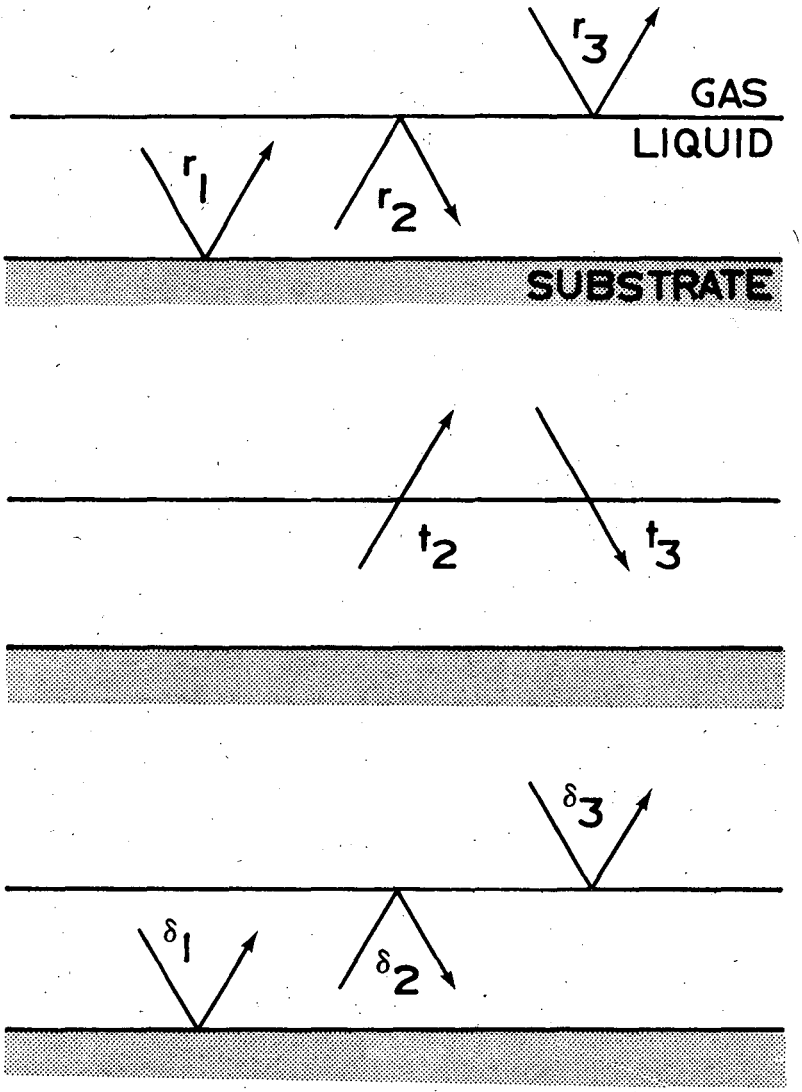

XBL 7012-7485

Fig. 2. Identification of reflection and transmission coefficients, with associated phase changes due to reflection from different interfaces.

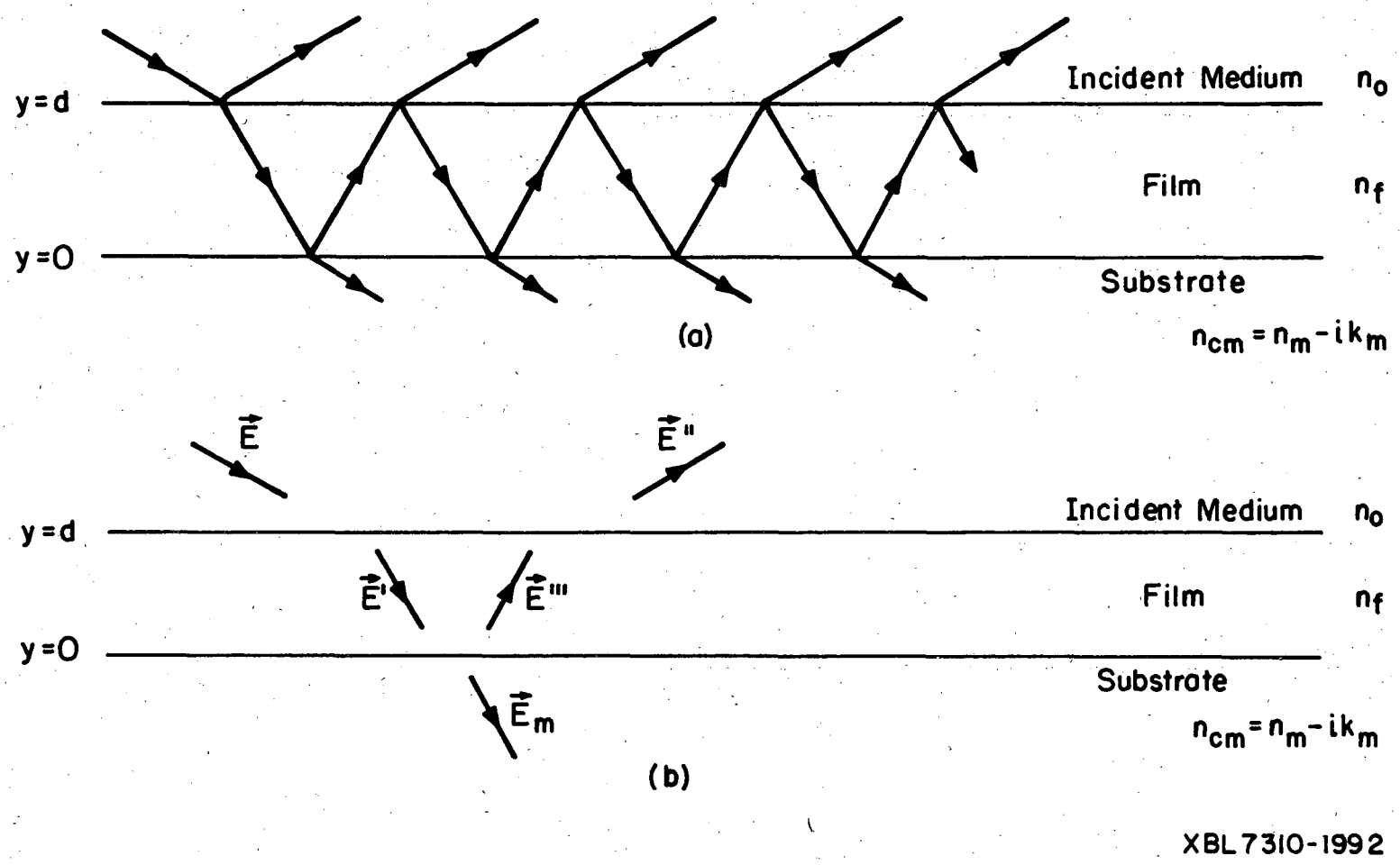

Fig. 3. Reflection from idealized film covered surface. (a) Representation by multiple beam reflection. (b) Representation in terms of equivalent waves.

2. Fresnel Coefficients

The local Fresnel reflection coefficients for a dielectric-covered metal surface are given by:[15]

$$r_{1s} = \frac{E_{1s}}{E_s} = \frac{n_o \cos\phi - n_f \cos\phi'}{n_o \cos\phi + n_f \cos\phi'} \tag{1}$$

$$r_{1p} = \frac{E_{1p}}{E_p} = \frac{n_f \cos\phi - n_o \cos\phi'}{n_f \cos\phi + n_o \cos\phi'} \tag{2}$$

$$r_{2s} = \frac{E_s'''}{E_s'} = \frac{n_f \cos\phi' - n_{cm} \cos\phi_m'}{n_f \cos\phi' + n_{cm} \cos\phi_m'} \tag{3}$$

$$r_{2p} = \frac{E_p'''}{E_p'} = \frac{n_{cm} \cos\phi' - n_f \cos\phi_m'}{n_{cm} \cos\phi' + n_f \cos\phi_m'} \tag{4}$$

where by Snell's law:

$$\cos\phi' = \sqrt{1 - \frac{n_o^2 \sin^2\phi}{n_f^2}} \tag{5}$$

$$\cos\phi_m' = \sqrt{1 - \frac{n_o^2 \sin^2\phi}{n_{cm}^2}} \tag{6}$$

The transmission (amplitude) coefficients for a unit incident ray are[17]

$$t_{3s} = \frac{2n_o \cos\phi}{n_o \cos\phi + n_f \cos\phi'} \tag{7}$$

$$t_{3p} = \frac{2n_o \cos\phi}{n_f \cos\phi + n_o \cos\phi'} \tag{8}$$

$$t_{2s} = \frac{2n_f \cos\phi'}{n_f \cos\phi' + n_o \cos\phi} \tag{9}$$

$$t_{2p} = \frac{2n_f \cos\phi'}{n_o \cos\phi' + n_f \cos\phi} \tag{10}$$

The complex reflection coefficient may be expressed in exponential form:

$$r = |r| e^{i\delta} \tag{11}$$

Without the use of complex arithmetic, the reflection coefficients can be formulated as follows:[3]

$$|r_{1s}| = \sqrt{\frac{A^2 + B^2 - 2A\cos\phi + \cos^2\phi}{A^2 + B^2 + 2A\cos\phi + \cos^2\phi}} \tag{12}$$

$$|r_{1p}| = |r_{1s}| \sqrt{\frac{A^2 + B^2 - 2A\sin\phi\tan\phi + \sin^2\phi\tan^2\phi}{A^2 + B^2 + 2A\sin\phi\tan\phi + \sin^2\phi\tan^2\phi}} \tag{13}$$

where

$$A = \sqrt{\frac{1}{2n_o^2}\left[\sqrt{(n^2 - k^2 - n_o^2\sin^2\phi)^2 + 4n^2k^2} + (n^2 - k^2 - n_o^2\sin^2\phi)\right]} \tag{14}$$

$$B = \sqrt{\frac{1}{2n_o^2}\left[\sqrt{(n^2 - k^2 - n_o^2\sin^2\phi)^2 + 4n^2k^2} - (n^2 - k^2 - n_o^2\sin^2\phi)\right]} \tag{15}$$

The absolute phase change δ_m is defined as the difference between the absolute phase of the light wave before and after reflection. m is equal to 1, 2 or 3 at interfaces.

The overall reflection coefficients for a film-covered surface are given by the Drude Eqs. (16) and (17).

$$r_s = \frac{E''_s}{E_s} = \left\{ \frac{r_{1s} + r_{2s} e^{-i\delta_o}}{1 + r_{1s} r_{2s} e^{-i\delta_o}} \right\} e^{+i\delta'_o} \tag{16}$$

$$r_p = \frac{E''_p}{E_p} = \left\{ \frac{r_{1p} + r_{2p} e^{-i\delta_o}}{1 + r_{1p} r_{2p} e^{-i\delta_o}} \right\} e^{+i\delta'_o} \tag{17}$$

where δ_o is the phase change associated with the optical path difference due to passage of the beam through the film (as observed in the image):

$$\Delta S = 2n_f d \cos\phi' \tag{18}$$

$$\delta_o = \frac{2\pi}{\lambda} \Delta S = \frac{4\pi n_f d \cos\phi'}{\lambda} \tag{19}$$

where λ is the wavelength of light in vacuum, δ'_o is the phase change had no film been present, and d is the film thickness:

$$\delta'_o = \frac{4\pi d n_o \cos\phi}{\lambda} \tag{20}$$

The ratio of the overall reflection coefficients can be expressed in complex exponential form

$$\rho = \frac{r_p}{r_s} = \tan\psi e^{i\Delta} \tag{21}$$

where the modulus of ρ, $\tan\psi$, is the relative amplitude and Δ is the relative phase change:

$$\Delta = \delta_p - \delta_s \tag{22}$$

The absolute phase changes can then be expressed without the use of complex arithmetic by:

$$\delta_s = \tan^{-1}\left(-\frac{2B\cos\phi}{A^2 + B^2 - \cos\phi}\right) \tag{23a}$$

and

$$\delta_p = \tan^{-1}\left(\frac{2B\cos\phi(A^2 + B^2 - \sin^2\phi)}{A^2 + B^2 - \frac{1}{n_o^4}(n^2 + k^2)\cos^2\phi}\right)$$

The total phase change between the reflection from the dielectric-metal and dielectric-incident media is:[2]

$$\delta_{TOT} = \delta_3 - \delta_1 \tag{24}$$

Metallic reflection coefficients, r_{1s} and r_{1p}, and phase changes, δ_{1p} and δ_{1s}, are calculated by program MER.[5]

The relative phase for external reflection from a dielectric, δ_3, is 0 for s and p polarizations below Brewster's angle ($\phi + \phi' = \pi/2$). Above Brewster's angle δ_p becomes π.

The intensity from the multiple beam model is:[2,18]

$$I(d,\lambda) = r_3^2 + \frac{(t_2t_3r_1)^2 + 2t_2t_3r_1r_3\cos(\delta+\delta_1-\delta_3) - 2t_2t_3r_1^2r_2r_3\cos(\delta_2+\delta_3)}{1+(r_1r_2)^2 - 2r_1r_2\cos(\delta+\delta_1+\delta_2)} \tag{25a}$$

from which the Michelson fringe visibility V, which is a measure of fringe constrast

$$V(\lambda) \equiv \frac{I_{max} - I_{min}}{I_{max} + I_{min}} \tag{25b}$$

is determined by program MINIM[2] for different angles of incidence.

Intensity maxima and minima occur at film thicknesses associated with the relations derived from Eq. (25a), that is:[2]

$$I_{min}^{(d,\lambda)} = r_3^2 + \frac{(t_2t_3r_1)^2 - 2t_2t_3r_1r_3 + 2t_2t_3r_1^2r_2r_3}{1 + (r_1r_2)^2 - 2r_1r_2} \qquad (26)$$

and

$$I_{max}^{(d,\lambda)} = r_3^2 + \frac{(t_2t_3r_1)^2 + 2t_2t_3r_1r_3 + 2t_2t_3r_1^2r_2r_3}{1 + (r_1r_2)^2 + 2r_1r_2} \qquad (27)$$

Program MBINF calculates the intensity function, Eq. (25a), for variable film thickness at discrete wavelengths covering the visible spectrum.[2] In order to determine the film thickness at a discreet location on a wedge shaped film, several maxima and minima must be observed to decide which order of interference is associated with the film thickness.

3. Elements of Colorimetry

According to the tristimulus theory, the sensation of color can be described using three primary or tristimulus colors.[19] The colorimetry system allows any color to be given in quantitative terms.

The three tristimulus primaries are known as primary X, primary Y and primary Z. The amounts of these primaries in an equal energy spectrum for the range $380 \leq \lambda \leq 780$ nm are tabulated as $\bar{x}(\lambda)$, $\bar{y}(\lambda)$ and $\bar{z}(\lambda)$, respectively. For light of spectral intensity distribution $I(\lambda)$, the amounts of the primaries are

$$X = \int_{380}^{780} I(\lambda)\ \bar{x}(\lambda)\ d\lambda \qquad (28)$$

$$Y = \int_{380}^{780} I(\lambda)\ \bar{y}(\lambda)\ d\lambda \qquad (29)$$

$$Z = \int_{380}^{780} I(\lambda)\ \bar{z}(\lambda)\ d\lambda \qquad (30)$$

The intensity function $I(\lambda)$ is a product of the spectral emissivity of the light source $P(\lambda)$, the attenuation due to passage through filters or reflection from colored surfaces or interference, and the response factor of the receptor. No correction is required when the eye is the receptor. The normalized chromaticity values, which allow color to be specified without regard to intensity, are:

$$x = \frac{X}{X + Y + Z} \tag{31}$$

$$y = \frac{Y}{X + Y + Z} \tag{32}$$

$$z = \frac{Z}{X + Y + Z} \tag{33}$$

4. Chromaticity Charts

When white light is incident onto a thin film, the resulting colors can be predicted using Eq. (25a) and Eqs. (28) through (33). The intensity function, $I(\lambda)$ in Eqs. (28) through (30) is then a product of the spectral emissivity of the light source, the spectral distribution $I(d,\lambda)$ of Eq. (25a) and the response attenuation of the receptor. The weighted distribution coefficients $P(\lambda)\ \bar{x}(\lambda)$, $P(\lambda)\ \bar{y}(\lambda)$, $P(\lambda)\ \bar{z}(\lambda)$ for CIE standard illuminants are tabulated.[20] Chromaticity values and the primaries are calculated for variable optical path difference by program CHROM.[2]

A chromaticity diagram based on a standard source (source A in this case) as achromatic stimulus is shown in Fig. 4. The white area of the chart was chosen to be the minimum resolution of an observer as given by Wright.[21] Turney[2] assumed an achromatic region ten times this size. The color regions correspond to the spectral bands of

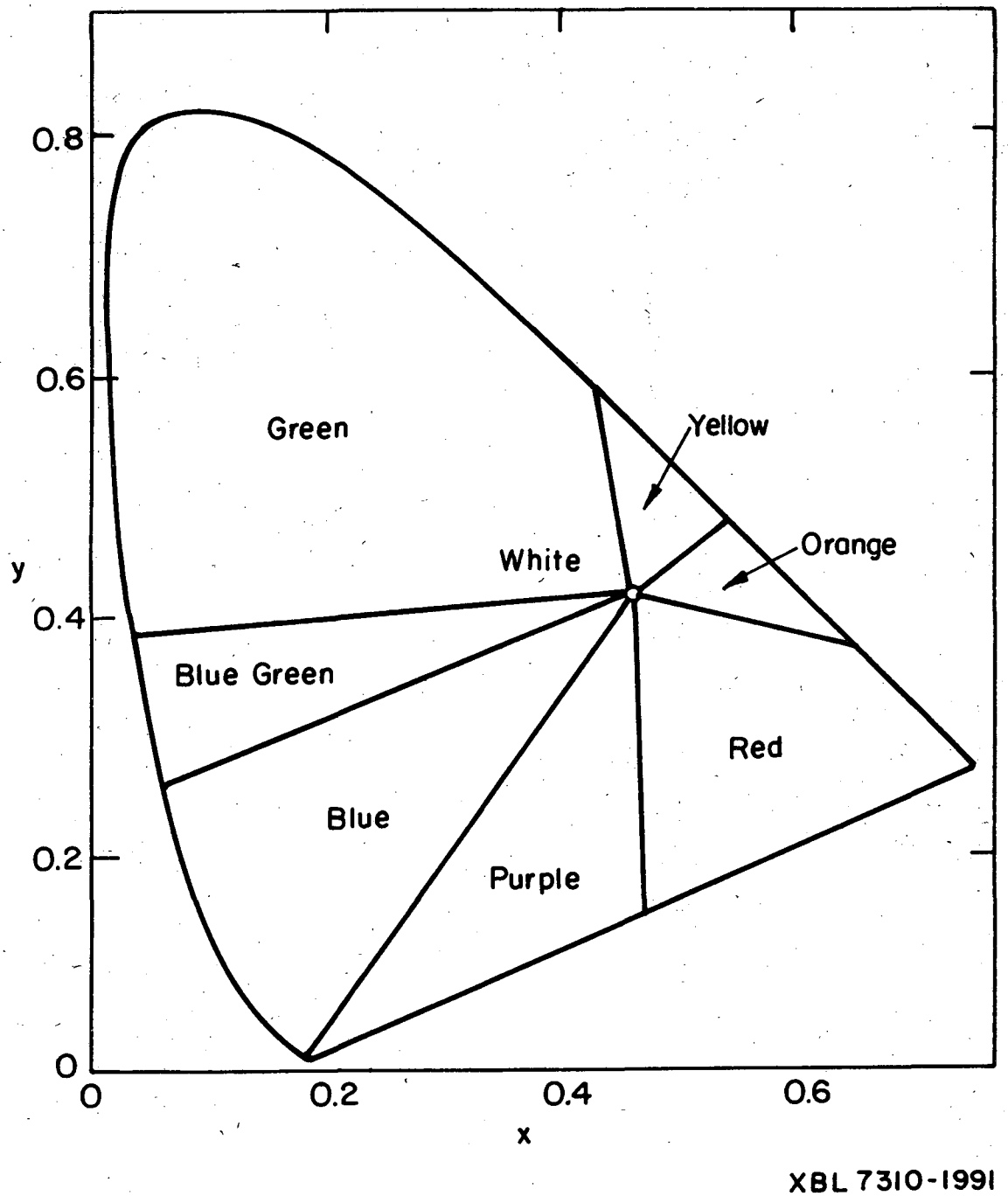

Fig. 4. Definition of color names employed in the colorimetric analysis of interference colors on the chromaticity diagram for white light standard source A.

Table I. Visible Spectrum

Color	Range of λ (nm)
Purple	410-424
Blue	424-491
Green	491-575
Yellow	575-585
Orange	585-647
Red	647-700

Table I in accord with CIE convention.[19] A color chart for medium and low reflectance substrate materials is available.[2] Figures 5(a) and 5(b) show the charts. It can be seen from the charts that differences in film thickness of a minimum of 200 angstroms are discernible by color changes provided the colors of the series are optically saturated. Purity of colors is represented by increasing displacement from the achromatic center of the chromaticity diagram.

B. Interference Microscopy

An alternative optical technique to white light interference measurement of film thickness is step-height measurement by double-beam interference microscopy. This technique requires coating the sample with a reflecting material prior to measurement. The incident beam is split and, before reuniting in the occular, both beams undergo reflections from mirror surfaces. One of the mirrors is an optically flat reference mirror while the other is the sample. This coating equilizes reflectivity and phase change in reflection from bare and film-covered substrate parts. Interference arises in the reunited beam due to an optical path difference resulting from differences in the surface topographies of the reference and sample surfaces. Hence, step measurement at the film edge gives the film thickness provided the film has a rectangular cross-section.

A fringe displacement equal to the spacing between interference fringes corresponds to a variation in topography of half the wavelength of the light used. Difficulty in locating the center of a fringe due to the gradual change of intensity of the fringe near the edges limits measurement of step height to films thicker than 250Å. A major

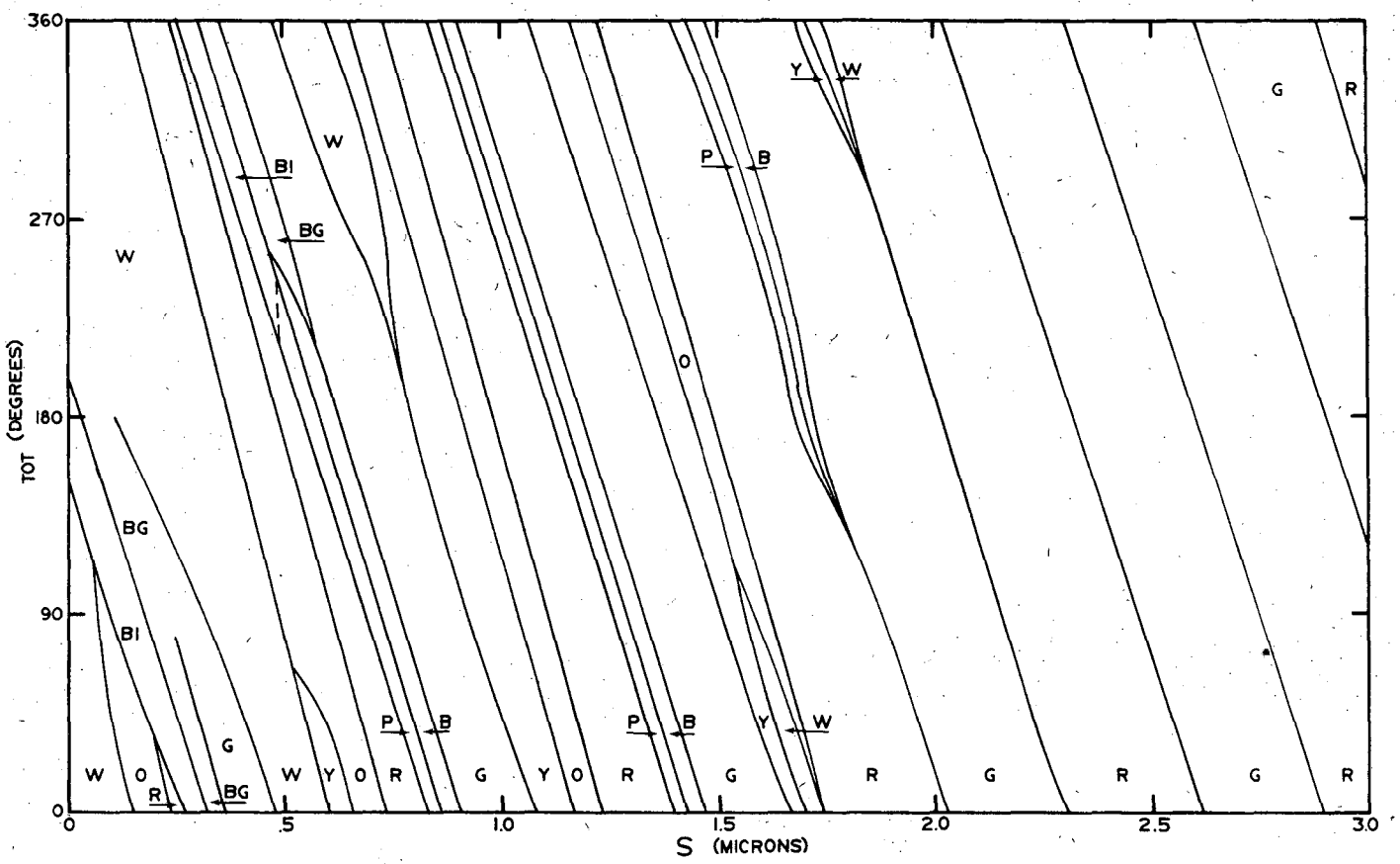

Fig. 5a. Generalized color chart according to Turney: r_1=0.60.
Color names: R=red, P=purple, B or Bl=blue, BG=glue-green,
G=green, Y=yellow, O=orange, W=white.

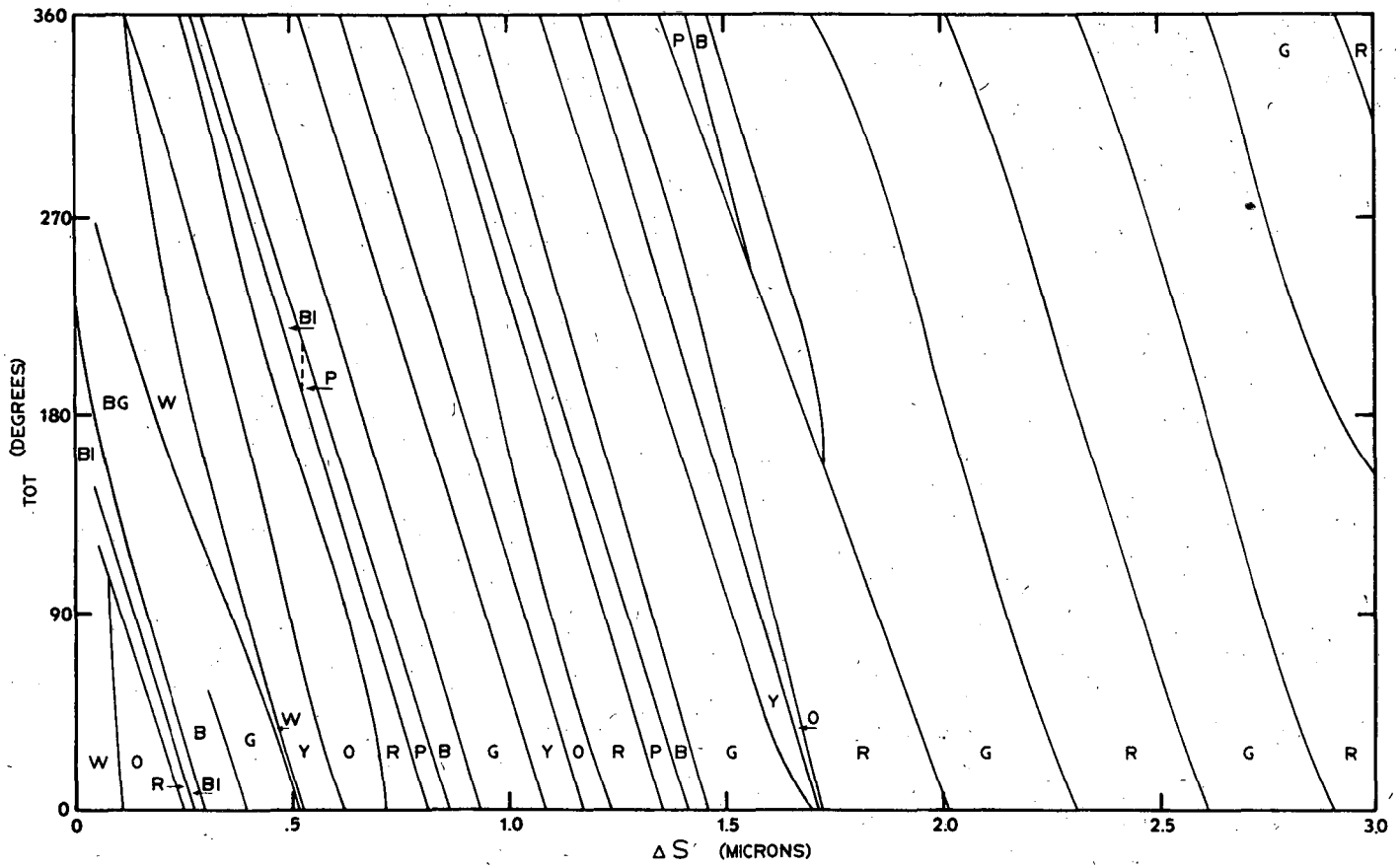

Fig. 5b. Generalized color chart according to Turney: r_1=0.20. Color names as in Fig. 5a.

disadvantage of the technique is that the film cannot be used again for optical investigation.

C. Ellipsometry

Ellipsometry is the measurement of elliptically polarized light which results from optical reflection. Two parameters are measured: the change in relative amplitude, $\tan\psi$, and the change in relative phase, Δ, of two orthogonal components of light. These parameters are included in Eqs. (21) and (22). The resolution of ellipsometry is quite high due to the following reasons: (1) relative rather than absolute measurements are performed, (2) azimuth angles (angles resulting from rotation around an optic axis) are measured with quite high resolution with available instruments. In many cases, an increase in film thickness by one wavelength results in an azimuth change of a full turn.[22] Under these conditions an angular resolution of 0.01° results in an average resolution in film thickness of 3×10^{-5} wavelengths or about 0.2 Å.

Rearranging Eq. (21) by applying complex algebra gives the definitions:

$$\Delta = \tan^{-1} \frac{\mathrm{Im}(\rho)}{\mathrm{Re}(\rho)} \tag{34}$$

and

$$\psi = \tan^{-1}\{|\rho|\} \tag{35}$$

It is clear from the dependency of ψ and Δ on ρ and Eqs. (16) through (21) that both ψ and Δ are dependent on the angle of incidence, the vacuum wavelength, the refractive index of the incident medium,

the optical constants of the substrate and the film, and the thickness of the film. A compilation of computer programs which calculate film thickness from ellipsometric measurements is given by Mathieu.[23] All computations are based on the assumptions that both film and substrate are flat with uniform optical properties.

D. Profilometry

Principles of operation of stylus instruments have been outlined by Bickel (1963).[24] A stylus is mounted in a measuring head which can be traversed across the specimen. Its path is the basis or datum for measuring the profile or cross-section of the specimen. The motions of the stylus perpendicular to the scanning direction may be recorded as a graph showing the geometric differences between the profile and the datum. These differences may also be statistically evaluated to obtain characteristic numerical values.

1. Skid and Skidless Modes

In the skidless mode, the datum line is generated by a smooth, straight slideway for the measuring head. Measurement in skidless mode is done by a "true-datum" device according to Reason (1944)[25] and measurement in skid-mode is thus done by a "surface-datum" device. In the skid mode, the datum line is generated by a member or skid-shoe sliding on the surface. The surface-datum method produces a distorted surface profile. The distortion depends on the surface profile, on the size and shape of the skid and on the distance between the stylus and the skid.[24] Stylus measurement in skid mode of very rough surfaces characteristic of specimens which have been mechanically polished,

milled or ground exhibits large errors. These errors diminish as the surface becomes smoother.

The true-datum method produces a faithful surface profile of a flat surface as the datum line is generated independent of the specimen. Steeply sloping hills, grooves in the film and steps are accurately reproduced using a skidless-mode stylus arrangement to within the limits of the instrument's resolution. The skidless mode, then, is the more satisfactory method to measure thin film profiles and step heights of films.

2. Stylus Resolution Due to the Finite Size of the Stylus Tip

The lateral resolution of the stylus instrument is limited by the radius of the stylus which contacts the specimen. The effective profile, which is the locus of the center of curvature of the tracer tip, is reported by Hasunuma (1966)[26] to be a set of gently sloping hills. The linear response of the stylus tip and the form of the curve traced by a stylus tip along a cosine curve model of the specimen surface was considered by Nakamura (1966).[27] In measuring it was shown that the wave is deformed due to the shape and size of the stylus tip. Nakamura computed the minimum amplitude and pitch (defined as twice the wavelength) of a cosine wave of inclination angle 15° below which a trace record using a standard ASA stylus tip of radius 2.54 microns deforms an input cosine wave of amplitude greater than 3 microns and a period of 63 microns by 10%. Assuming this 10% tolerance level, the minimum amplitude measurable was 0.6 microns and the minimum pitch was 10 microns. A faithful trace record for the same stylus tip for triangular wave

form input of inclination angle 15° is limited to wave amplitudes greater than 0.9 microns and to pitches greater than 95 microns.

The error accrued on input wave height (defined at twice the amplitude of the wave) increases with increasing inclination angle. Since the inclination of surface protuberances is usually 15° or smaller (Nakamura (1966)[27]), the error in measuring wave height for surface roughness on the order of a micron is generally less than 10%. It can be deduced from these findings that trace records of square wave forms such as rectangular grooves of depth in the range of a micron will have deformation errors greater than 10%. The deformation errors in wave height measurements are eliminated if the groove is wide enough to approximate a step. In general, steps prepared for the purpose of measuring thin film thickness by tracer methods should be at the edge of the thin film to avoid step-height errors due to the size of the stylus.

3. Stylus Resolution Due to Surface Damage

Surface damage produced by the stylus in traversing the specimen has been studied using a scanning electron microscope by Guerrero and black.[28] The result of their SEM study showed that the surface damage produced by the stylus is the result of an unconstrained loading situation and is equivalent to many other forms of plastic deformation; in particular, plowing.

A study of surface damage to a thin chromium film by a spherical, diamond stylus of load 50 mg and tip radius 2.54 microns was done here using a Gould Corporation Profilometer (Model 21-1120-00) in the skidless mode. A plow track was produced on the metal film by

traversing the stylus to and fro laterally. The track depth and width were then recorded by passing the stylus across the groove longitudinally. The trace record indicated the stylus had cut a path 0.027 microns deep per pass and roughly 0.254 microns maximum width. Since the stylus resolution is limited by the finite radius of the stylus tip in this range of surface irregularities, no satisfactory calculation of indentor (contact) pressure, which is quite sensitive to the measured track width, can be made using this estimation.

Track widths measured by Guerrero and Black using the SEM ranged from 0.5 to 1 micron at the widest point for a conically-shaped, diamond tipped stylus of radius 12.5 microns under a load of 200 mg on stainless steel. Assuming the maximum track width corresponds to the area where the full stylus load is applied and that the track width for a 2.54 micron radius tip is roughly 0.25 microns, the indentor pressure (load divided by half the contact area as the dynamic load is applied to roughly the front half of the stylus tip) is on the order of 56,000 psi for a 50 mg load. R. R. Austin et al. (1973)[29] report yield stresses of dielectrics used in optical coatings on the order of 40,000 psi, so that the stylus is expected to damage these films.

Guerrero and Black (1972)[28] report the theoretical limit on stylus resolution due to surface damage for a spherical tip of radius R, a ratio of yield stress to indentor pressure of three, where Y = yield stress and L is the stylus load by an equation for the plow-track depth:

$$d_{dam} = L/6Y\pi R \quad . \tag{36}$$

For a dielectric thin film of yield stress 42,000 psi (3000 kg/cm^2), typical of films used in anti-reflection coatings, the track depth estimated by Eq. (35) for a 2.54 micron radius stylus under a load of 50 mg is 0.035 microns. This value is larger than the plow-track measurement on the chromium film. Stylus resolution for profile measurement, then, is negligibly affected by surface damage effects when compared to the effect of stylus size on resolution of surface traces. However, surface damage is the prime limitation on stylus resolution for step height meausrements since the size of the stylus tip does not affect the measurement of the step. Hence, step measurement is restricted to steps larger than 350 angstroms.

4. Seismic Restrictions to Stylus Resolution

Seismic vibrations can be a limiting factor before a trace record of the specimen's surface is made. A 750 lb granite slab was used to reduce the amplitude of seismic noise reaching the stylus. The frequency and amplitude of all background vibrations at the surface of the granite insulation in this experiment were 11 cycles per second and 85 angstroms, respectively. The insulation reduced seismic noise from an undamped amplitude of 0.37 microns to 0.0085 microns. The depth of a plow track produced by a lightweight (50 mg) stylus is roughly 250Å which is about three times greater than the seismic uncertainty. Therefore, under the present circumstances, seismic noise is small compared to surface damage and has a negligible effect on stylus resolution.

5. Stylus Resolution Restrictions due to Skipping

Skipping is the phenomenon whereby the stylus encounters friction resistance due to local contamination (residual cutting lubricants in the case of machined films, oxide films, etc.) during plowing deformation. Guerrero and Black observed differences in the tracks of the stylus on a stainless steel surface with respect to the direction of motion of the stylus as a result of the stylus response to the local topography and friction conditions coupled with the plowing deformation. The effect may be quite pronounced with mechanically or ultrasonically cleaned metal surfaces because large quantities of impurities are usually imbedded in the surface during these processes. Vacuum deposited, homogeneous thin films, however, are usually free of imbedded surface contaminants. The aspect of skipping in stylus measurement of film-steps is neglected for this reason.

III. EXPERIMENTAL

In order to compare the film profiles as measured by the observation of colors and with the spectrophotometer with those determined by ellipsometry and stylus and interference step height measurements, solid, dielectric films were formed on flat, vacuum-deposited, opaque metal substrates. Vacuum deposition yielded clean, reproducible substrate surfaces. The metal was deposited on glass slides. The optical constants of the metals were determined ellipsometrically. The effect of variations in the optical constants of both the film and substrate on the ellipsometric parameters was considered. Tests for anisotropy in the dielectric films were also made as an off-axis depositing scheme was used to prepare dielectric wedges.

White, polarized light interference was used to measure film profiles. Light reflected from the films was measured in three separate ways: (1) the color was recorded photographically, and the profile estimated from the colors and color transitions, (2) the interference spectrum was measured at discrete film positions with a spectrophotometer, and (3) the spatial distribution of selected wavelengths was measured along the film. The first two methods were used by Turney and Muller.[1,2]

The advantage of using white-light over monochromatic light for film thickness measurement is that different interference orders can be distinguished since the colors are non-repetitive.

For a wedge shaped, transparent film, white light yields maxima and minima at several wavelengths which depend on the film thickness.

Absolute intensity measurements were inaccurate because external fluctuations caused the instrument calibration to wander. Relative intensity measurements cancel out external fluctuations such as those of the light source and instrument. By scanning for maxima and minima of the intensity ratio, calibration of the spectrophotometer is eliminated. Therefore, the techniques of scanning the visible spectrum and scanning the film at fixed wavelength for maxima and minima of relative intensities were used.

Polarized light was used to create well defined phase change conditions, since the phase change in reflection depends on polarization. Above Brewster's angle δ_s and δ_p differ by 180° for dielectric reflection. This difference in phase results in approximately complimentary colors for the two polarizations at a given film thickness.

Film profiles were determined using an ellipsometer also. A monochromatic light beam was elliptically polarized by introducing a quarter-wave phase retardation and reflected from the dielectric-metal ensemble. The change in the state of polarization upon optical reflection was such that the reflected beam was linearly polarized. Azimuth measurements of the polarizer and analyzer rotation around the optic axis were made automatically using Faraday cells. The film thicknesses were then calculated from the measured values of the optical constants of the bare substrate, and the ellipsometric parameters, ψ, and Δ of the film-covered surface.

A profilometric determination of the film thickness was also made. In order to determine the film depth, traces of the stylus tip were taken over a step separating the film from the substrate.

Tests were made to determine the seismic limitations of step-measurements. Traces were taken at discrete film positions. Uniformity of film thickness across the film (in the x direction) was a criterion of this technique. Since films prepared by thermal evaporation from a point source exhibit circular interference fringes, it was, therefore, necessary to limit the amount of fringe curvature to a tolerable level. This was done by adjusting the deposition distance and by masking the substrate. Therefore, the step height measured profilometrically along the edge of the film and the film thickness across the film were nearly the same.

Lastly, film thickness was measured using a Zeiss-Linnik Interferometric Microscope. In order to use this technique, a reflecting coating had to be applied to the dielectric film-metal substrate combination in order to equalize reflectivity and phase change on both sides of the step. Step height was then measured at discrete film locations by measuring the displacement of monochromatic interference fringes.

A. Film Preparation

1. Selection of Materials

The choice of film and substrate was based on both their respective optical properties and their joint optical effects. Selection began with the choosing of the substrates such that a wide range of relative phase change, δ_1, was realized simultaneously with a wide range of reflection modulus, $|r_1|$. This insured a large variance in available reflectances. Figures 6 and 7 show several bare metal and semimetal positions on $|r_1| - \delta_1$ plots. The reason a wide range of metal reflectances was desired was to determine: (1) capability of resolving colors on high reflectance substrates, (2) comparison of color series

Figures 6 and 7
Identification of circled numbers.

Number	Material	n	k	λ(nm)	Reference
1	Ag	0.08	3.40	546.1	45
2	Al	0.81	5.47	546.1	11
3	Cr	2.11	1.55	589.0	46
4	Si	4.14	0.03	546.1	47
5	Ni	1.80	3.29	546.1	48
6	Sn	1.48	3.54	589.0	49
7	Mn	1.83	3.17	546.0	50
8	Be	2.66	2.36	546.1	51
9	Ti	2.41	3.24	589.0	52
10	W	3.90	3.15	546.0	53
11	Ta	3.30	2.30	546.1	54
12	Mo	3.59	3.41	546.0	11
13	Nb	3.60	3.60	-----	55
14	Fe	3.35	1.15	546.1	56
15	Ge	5.20	2.10	546.1	57
16	InSb	4.18	1.94	564.0	58
17	FeSi	2.661	1.29	589.3	59
18	GaAs	4.00	0.31	546.1	60
19	InAs	4.32	0.56	563.0	61
20	InP	3.47	0.36	563.0	62
21	GaP	3.65	0.001	520.0	63

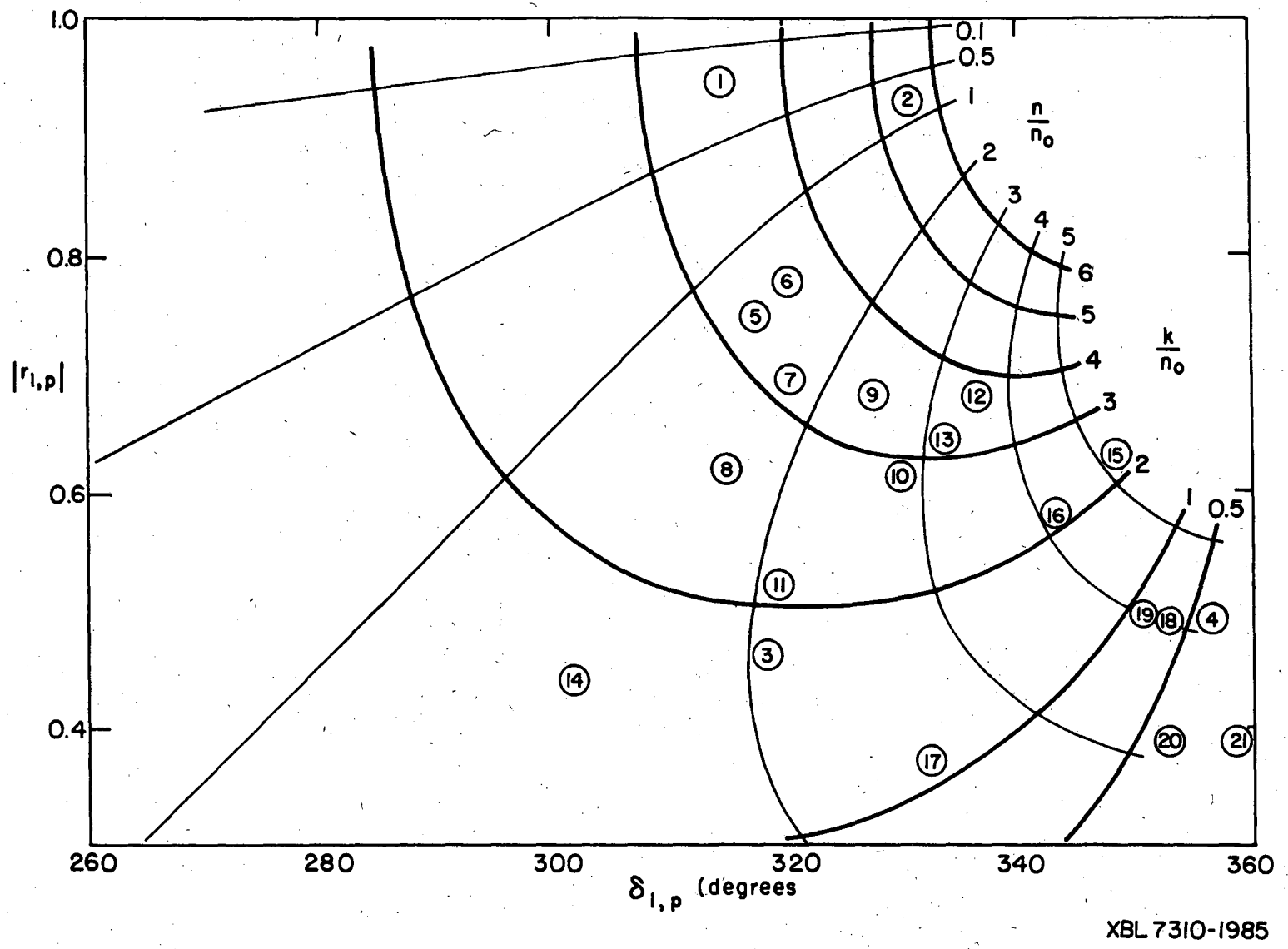

Fig. 6. Absolute phase change, δ, and modulus $|r|$ (amplitude) of reflection coefficient for reflection from a bare metal substrate of refractive index $n_c = n - ik$. Angle of incidence 45°, p-component. Materials identified on p. 29.

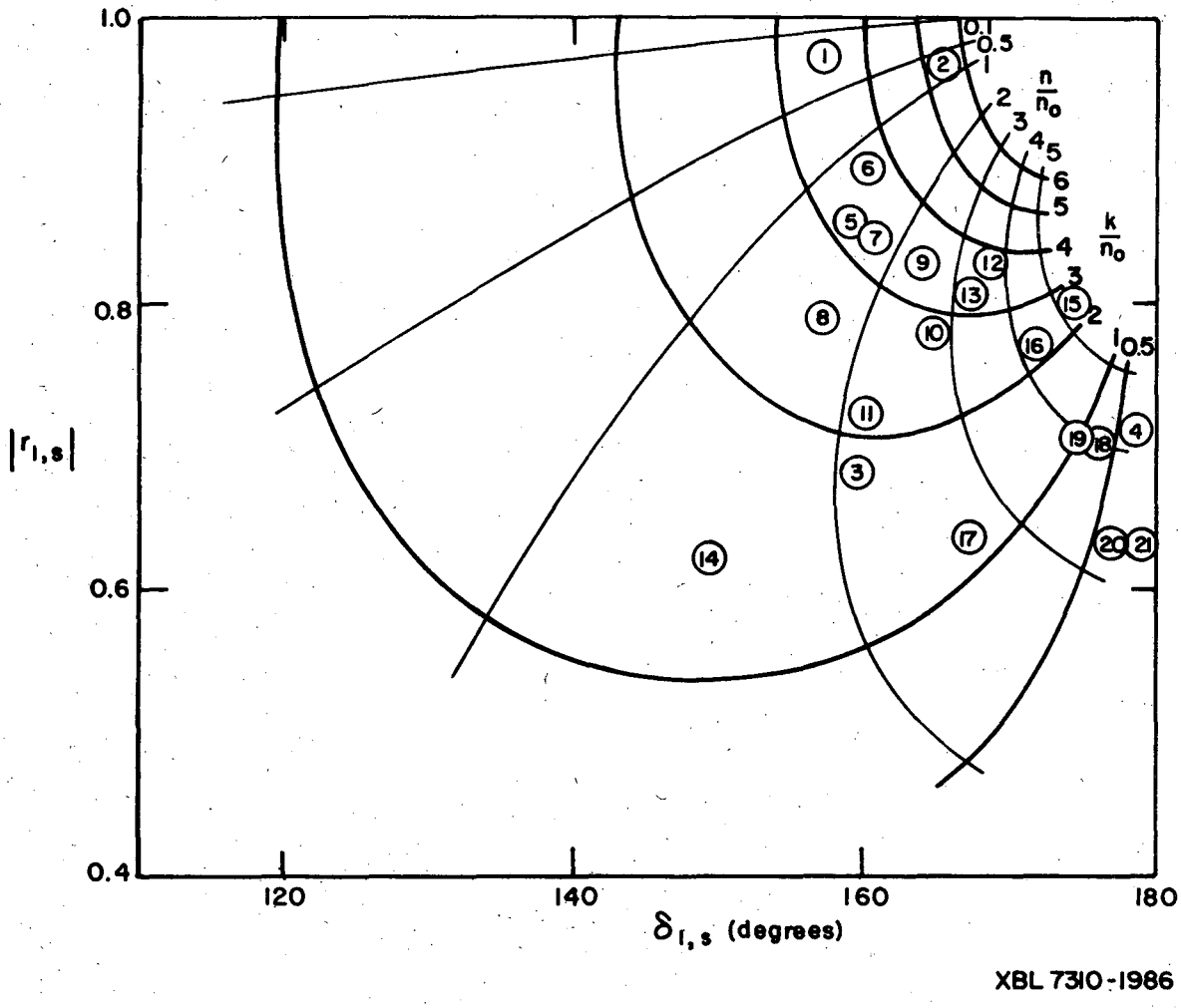

Fig. 7. As Fig. 6, s-component.

with predicted series for medium reflectance substrates and (3) comparison of color series with predicted series for dielectric or low reflectance substrates. (Index values are for deposited metals in some instances.) Hence, the range of possible color series extends to several color charts (each chart is valid for a specified reflectance modulus).

Since δ_1 is dependent on the index of refraction of the film, the choice of the film materials was based on obtaining the widest range of δ_1 for each substrate. This insures the widest range of δ_{TOT} for the film-substrate pair. A wide range of δ_{TOT} at any particular value of modulus of reflection provides a sampling of color-series in different portions of the color chart. Since the phase behavior of s- and p-light is different, color series for s- and p-polarizations are associated with different values of δ_{TOT}. Figures 8 through 13 show plots of δ_{TOT} vs angle of incidence for the film-substrate pairs selected. The pairs are not only the result of a selection of the basis of optical effects, but are the result of considerations of chemical and mechanical stability.

The optimum angle of incidence, corresponding to observation of fringes with the best contrast, was based on numerical computation of the Michelson fringe visibility of 584 nm incident light wavelength.

Figures 14 through 18 are plots of fringe visibility vs angle of incidence for each film-substrate pair. The angle of incidence selected for observing intefference colors was chosen both on the basis of these figures and on the basis of the area of film surface sampled by the fiber probe at the angle. In the case of large values of optimum angle, the area of film surface available for sampling was much less than the elliptical area sampled by a fiber-probe, so a compromise was made between

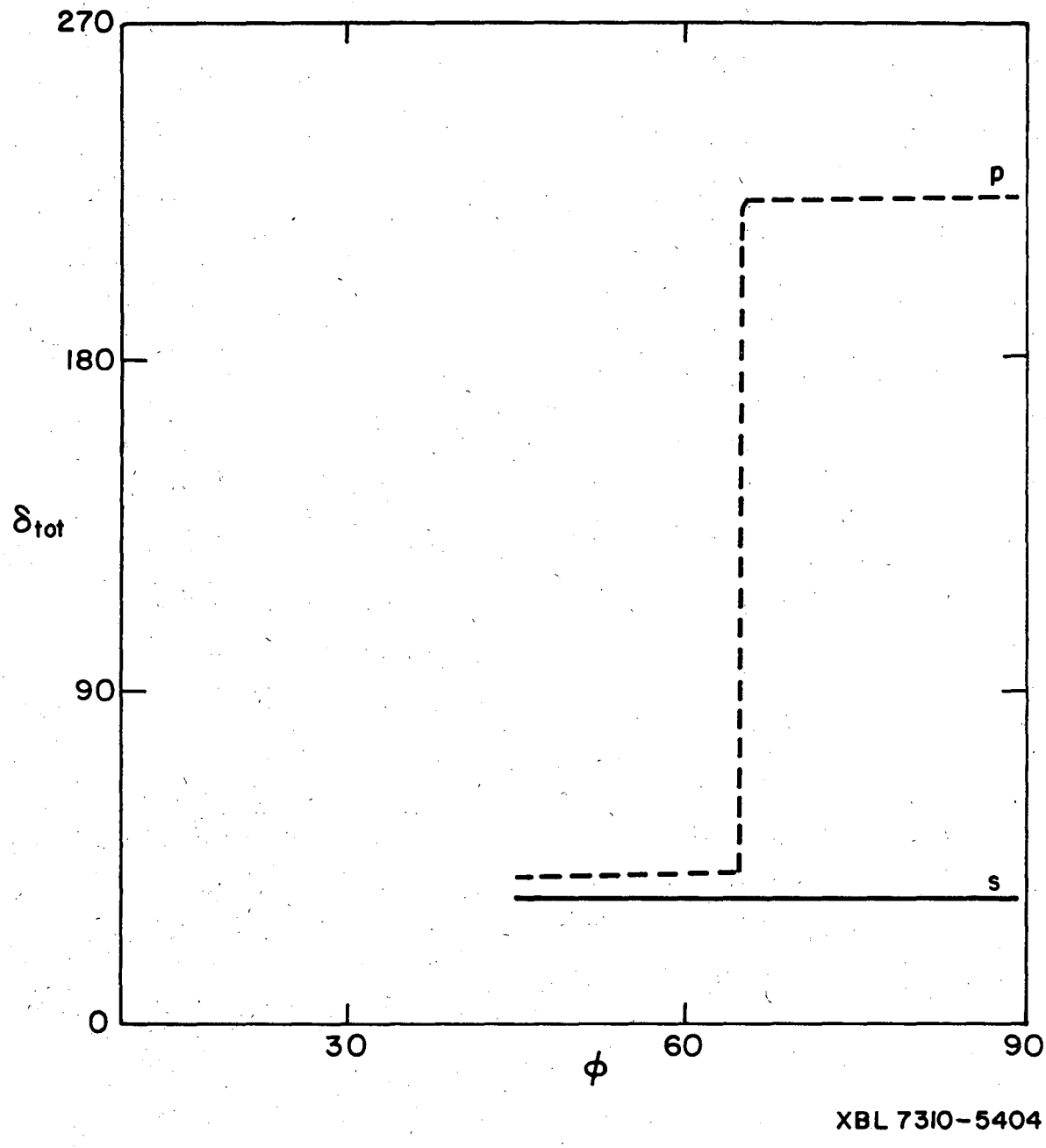

Fig. 8. Total phase change, δ_{TOT}, vs angle of incidence at the dielectric film-air interface. ZnS film on aluminum substrate. Incident light at λ=546.1 nm n_{ZnS}=2.30, $n_{aluminum}$=0.82-5.4i

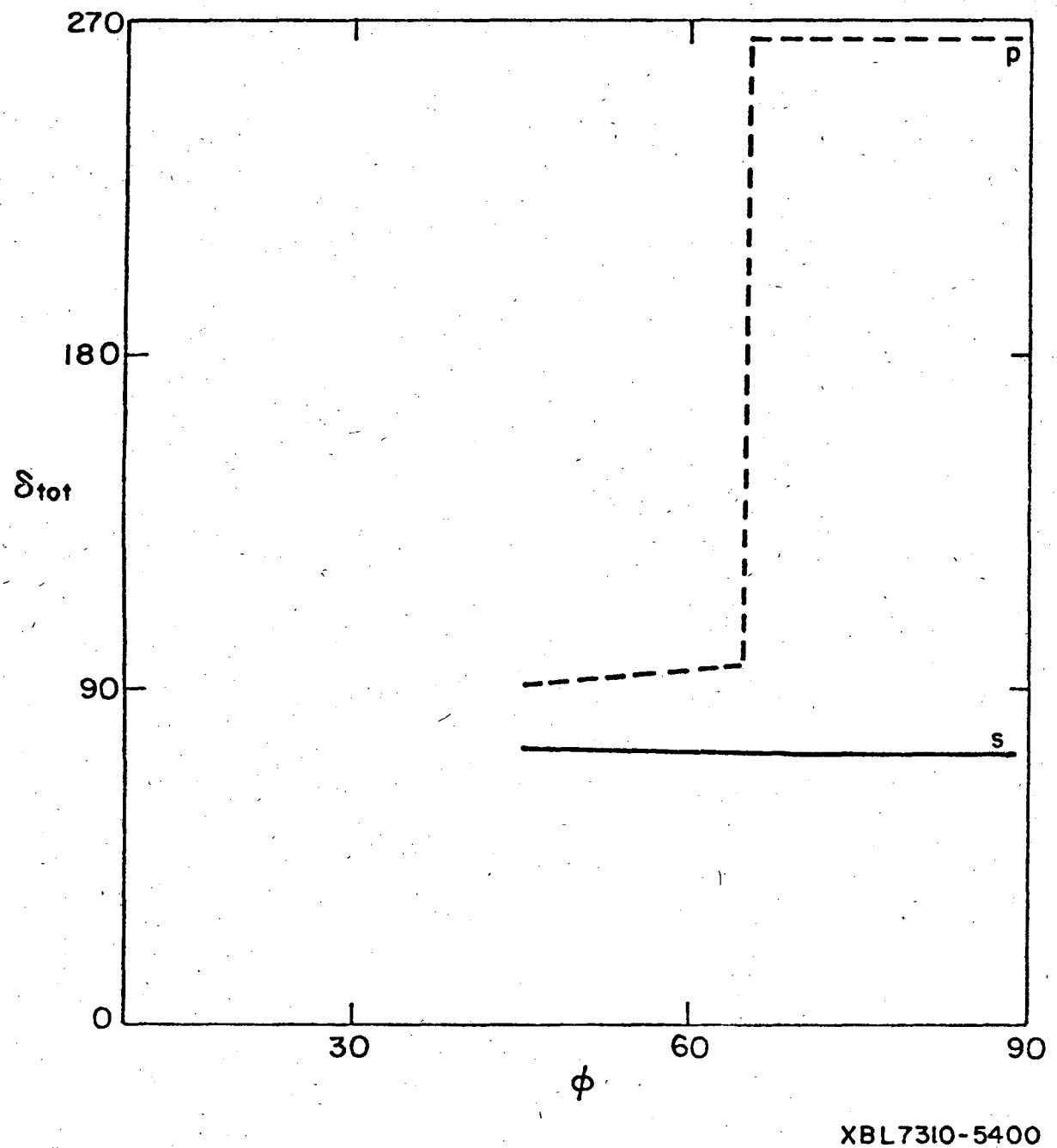

Fig. 9. As in Fig. 8. ZnS film on chromium substrate. $n_{ZnS}=2.30$, $n_{chromium}=2.11-1.55i$

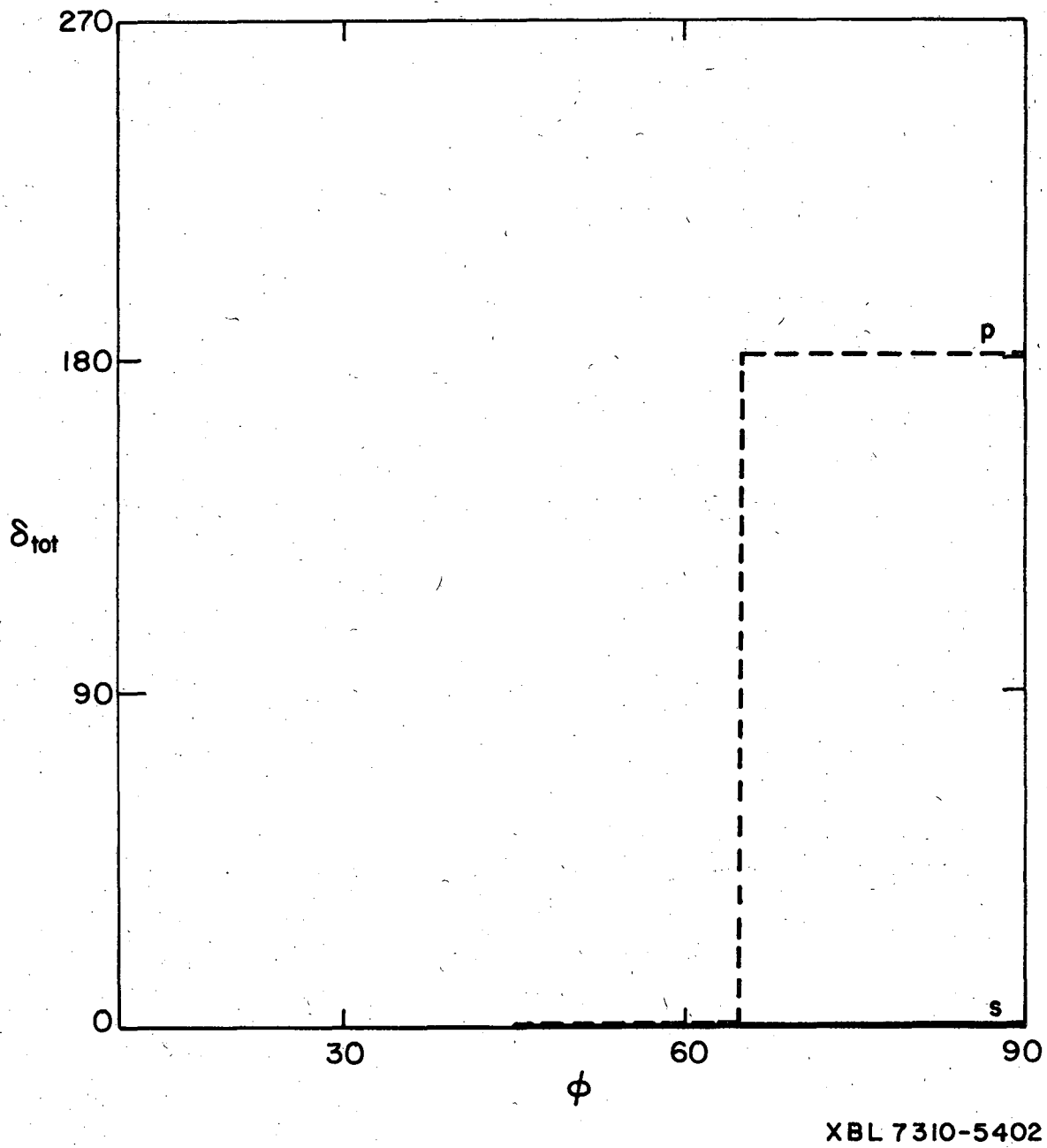

Fig. 10. As in Fig. 8. ZnS film on silicon.
$n_{ZnS}=2.30$, $n_{silicon}=4.14-0.03i$

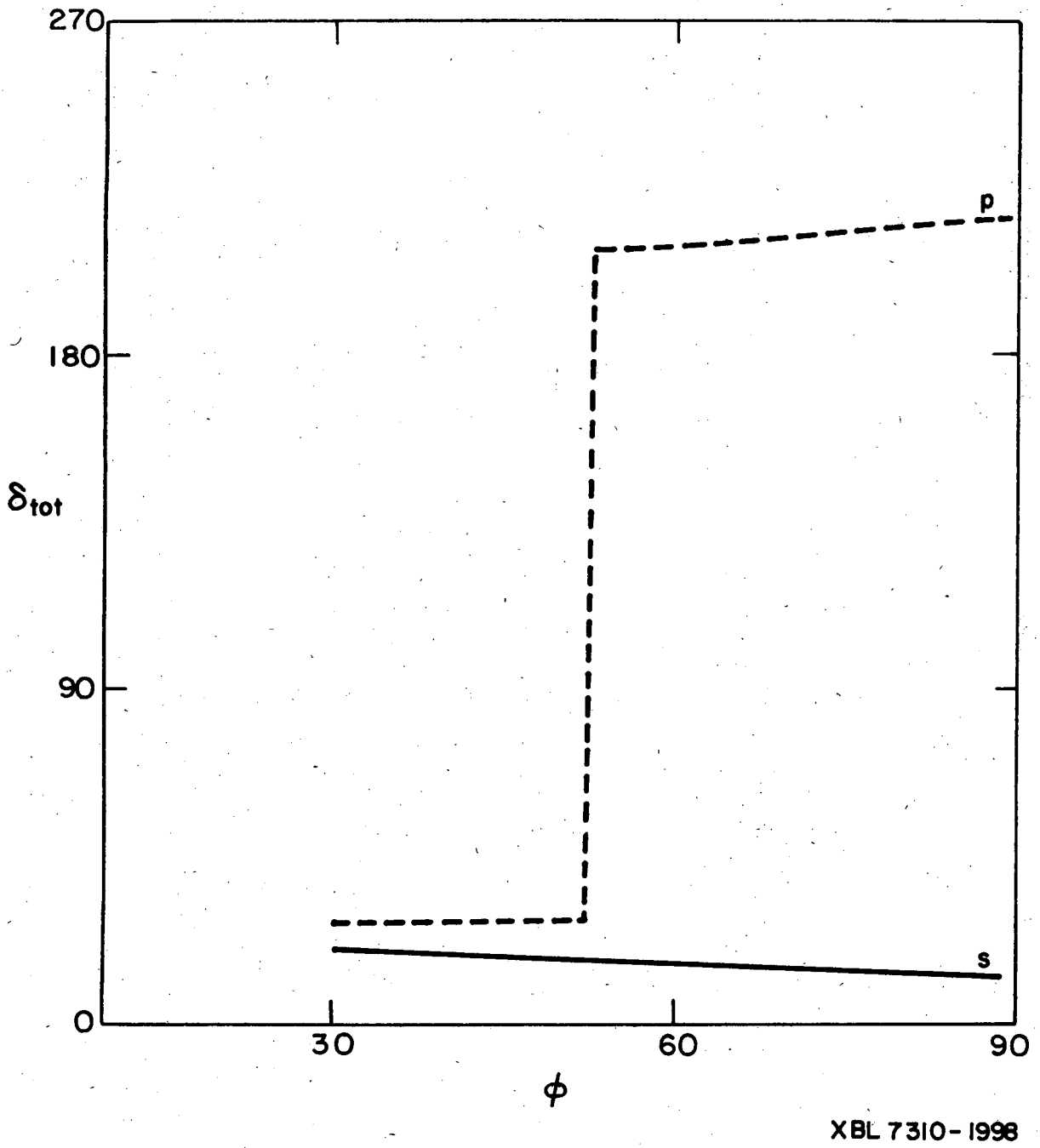

Fig. 11. As in Fig. 8. Cryolite film on aluminum substrate. $n_{cryolite}=1.30$, $n_{aluminum}=0.82-5.40i$

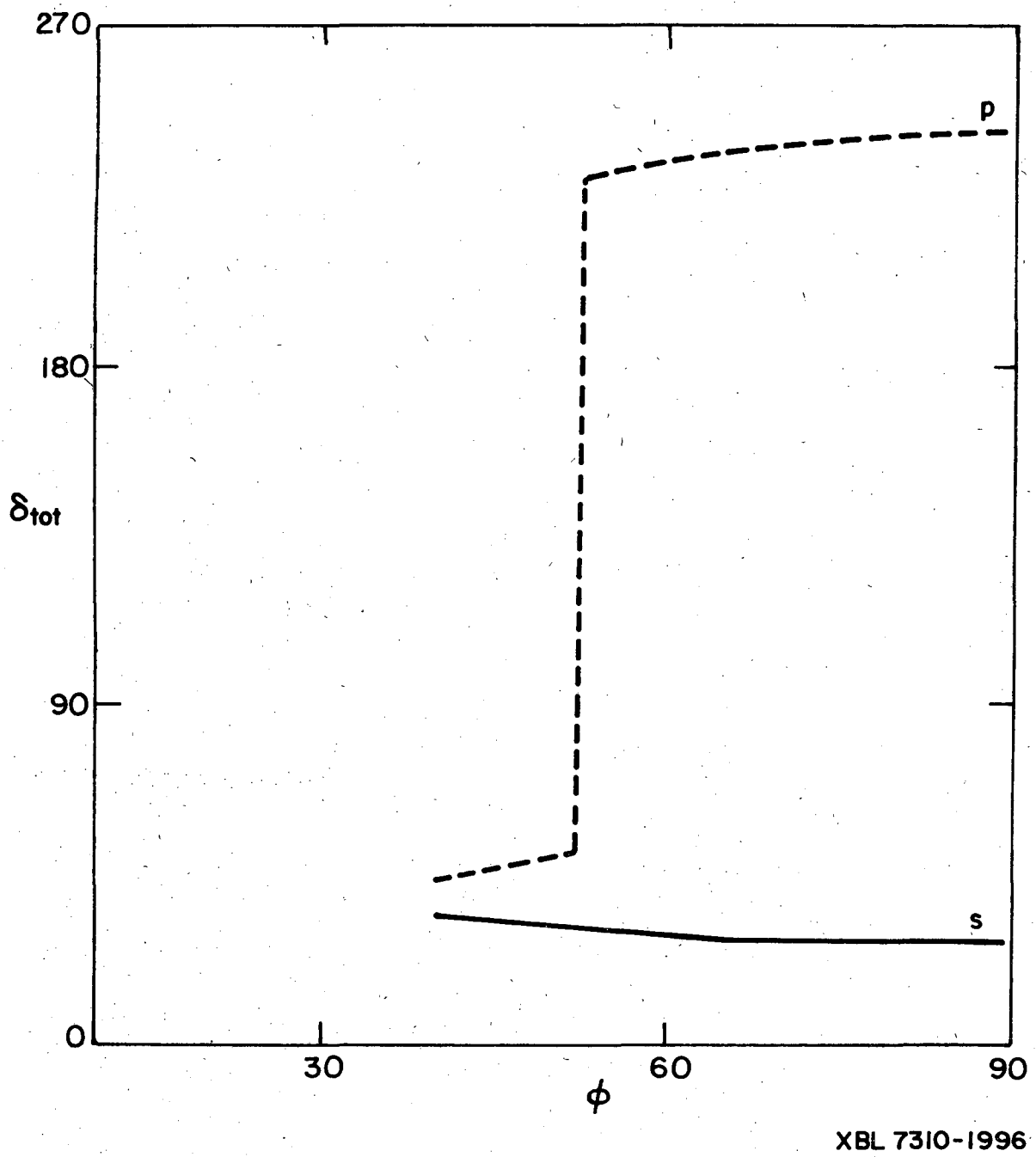

Fig. 12. As in Fig. 8. Cryolite film on chromium substrate. $n_{cryolite}=1.30$, $n_{chromium}=2.11-1.55i$

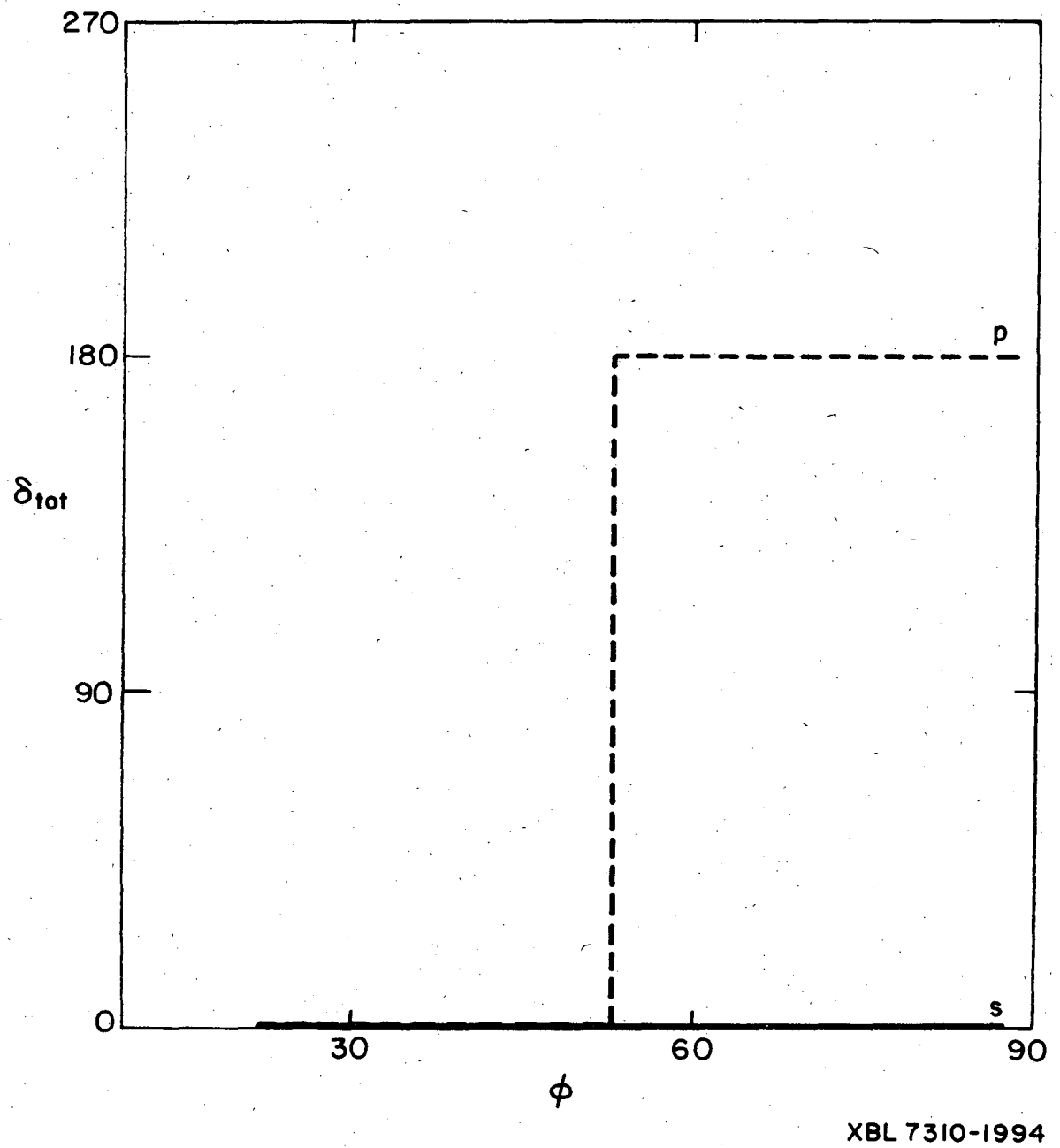

Fig. 13. As in Fig. 8. Cryolite film on silicon substrate. $n_{cryolite}=1.30$, $n_{silicon}=4.14-0.03i$

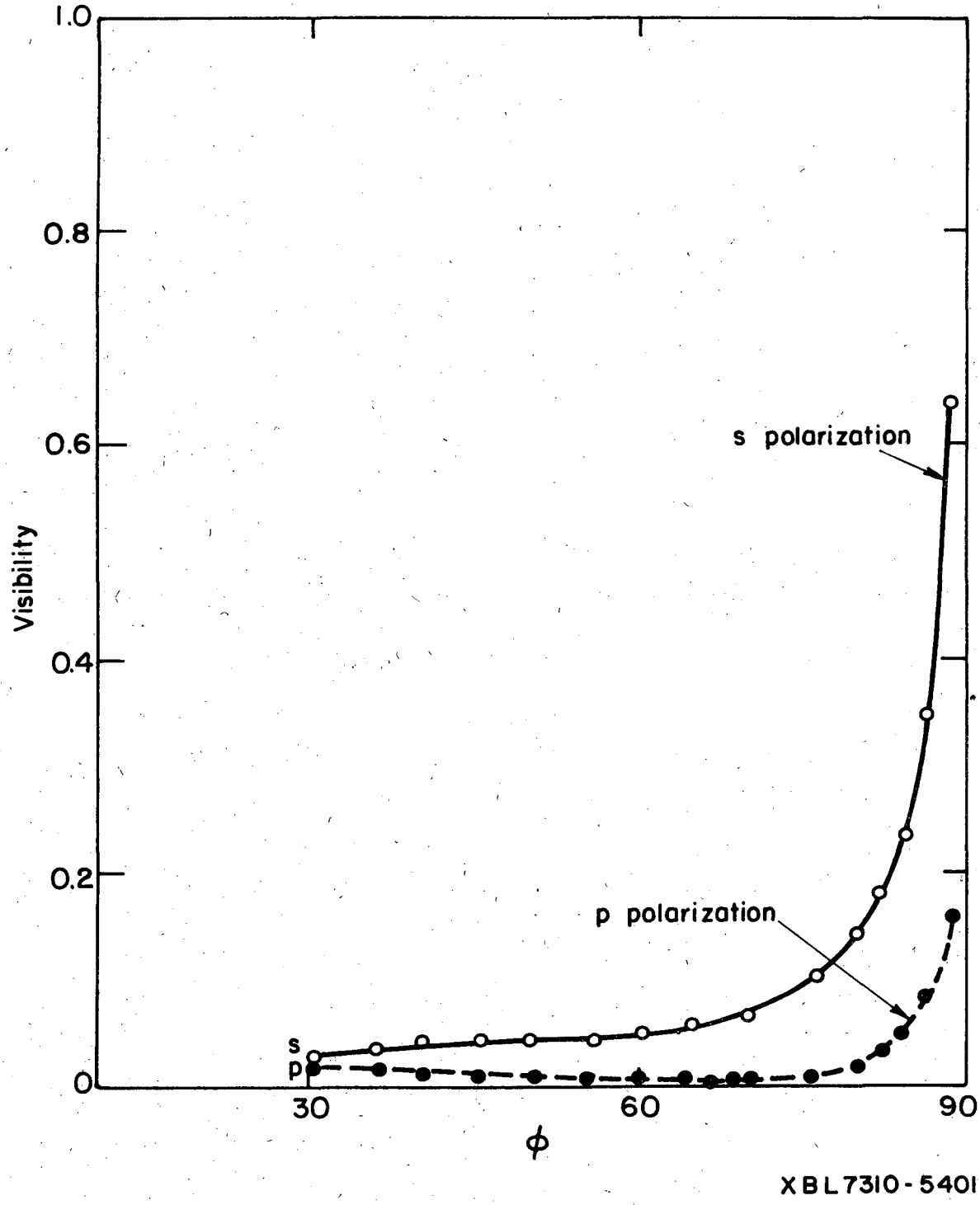

Fig. 14. Michelson fringe visibility vs angle of incidence at the dielectric film-air interface. Incident light wavelength, λ=546.1 nm. At the optimum angle of incidence the fringe visibility is one. ZnS film on chromium substrate.

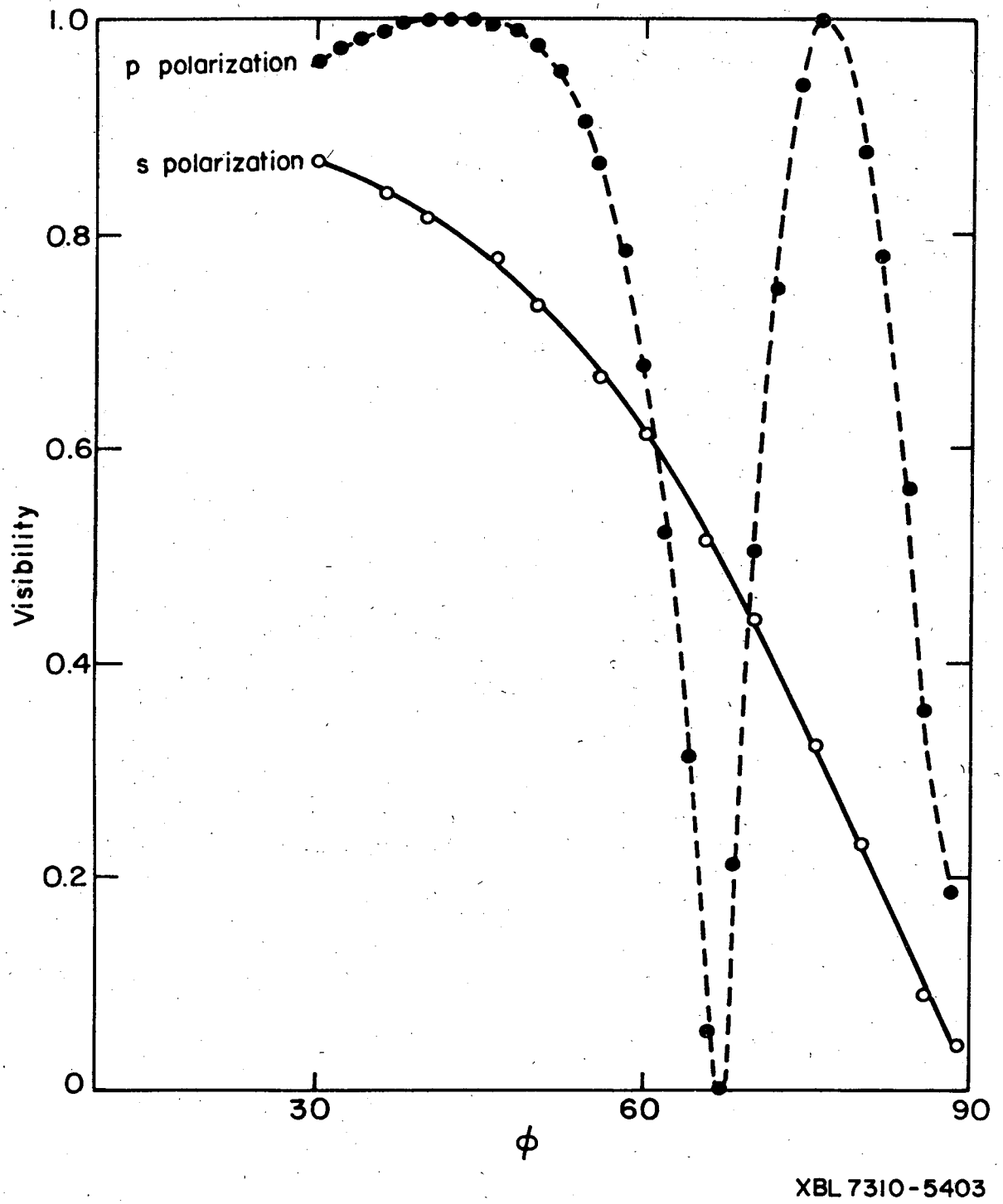

Fig. 15. As in Fig. 14. ZnS film on silicon substrate.

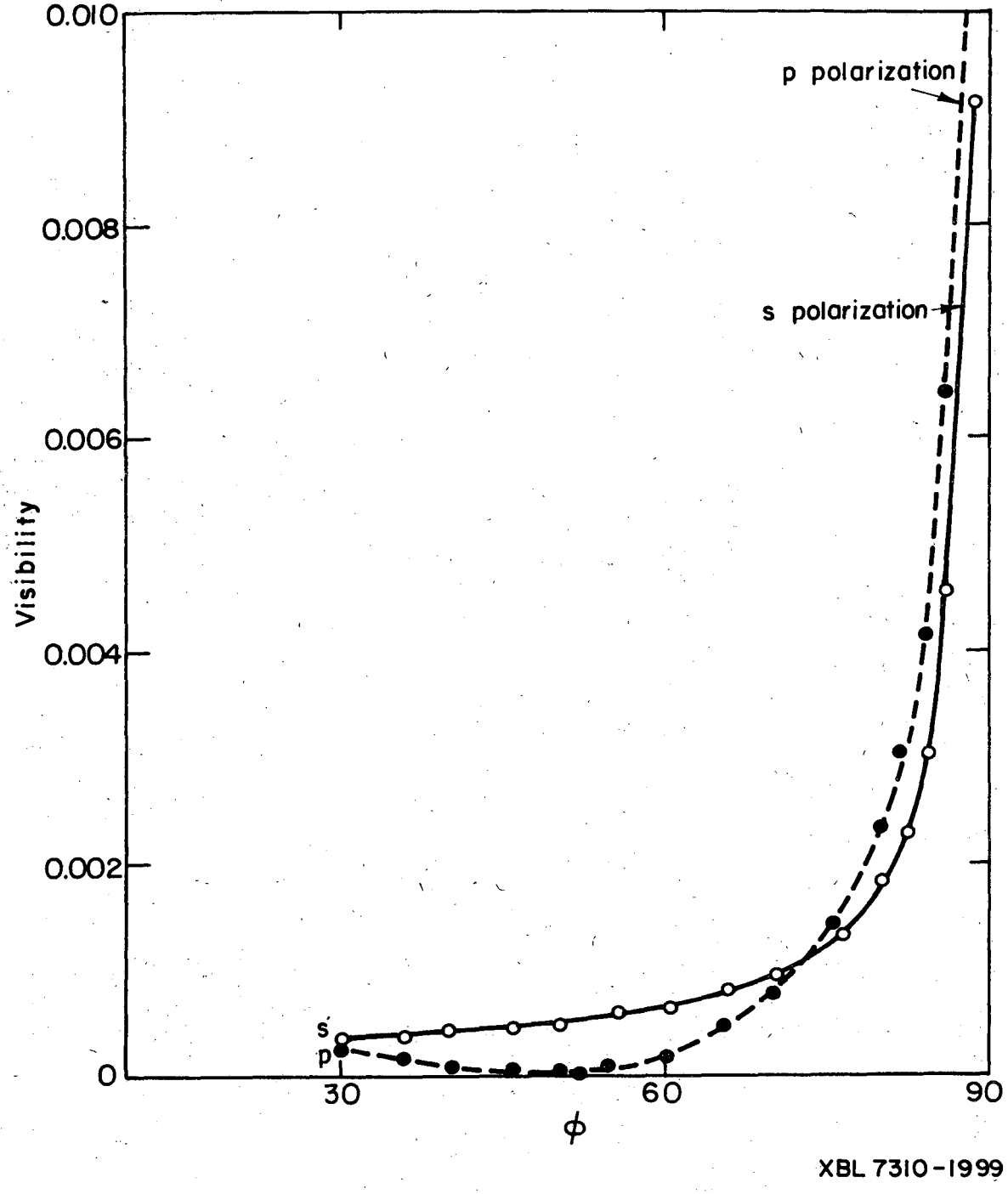

Fig. 16. As in Fig. 14. Cryolite film on aluminum substrate.

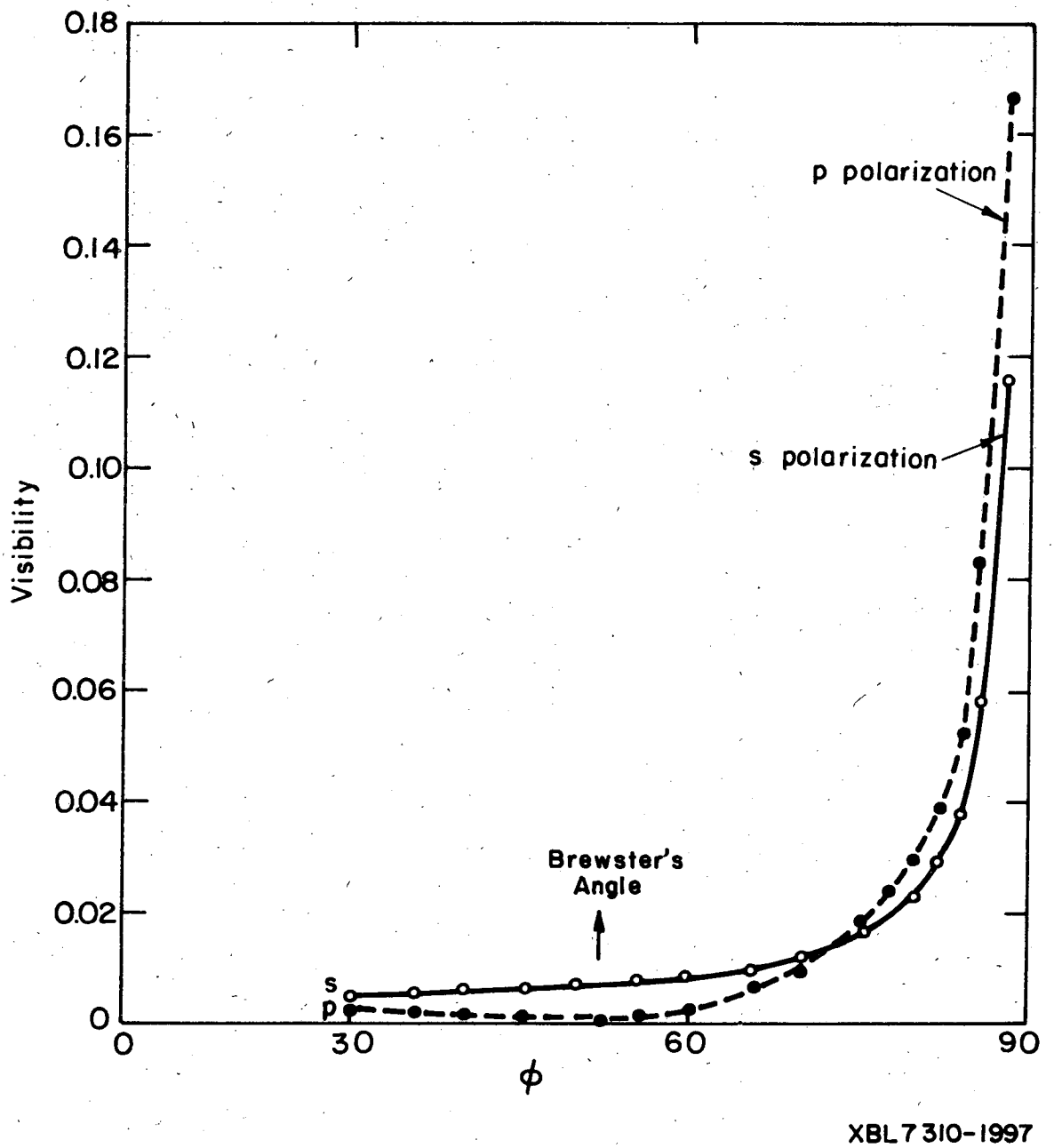

Fig. 17. As in Fig. 16. Cryolite film on chromium substrate.

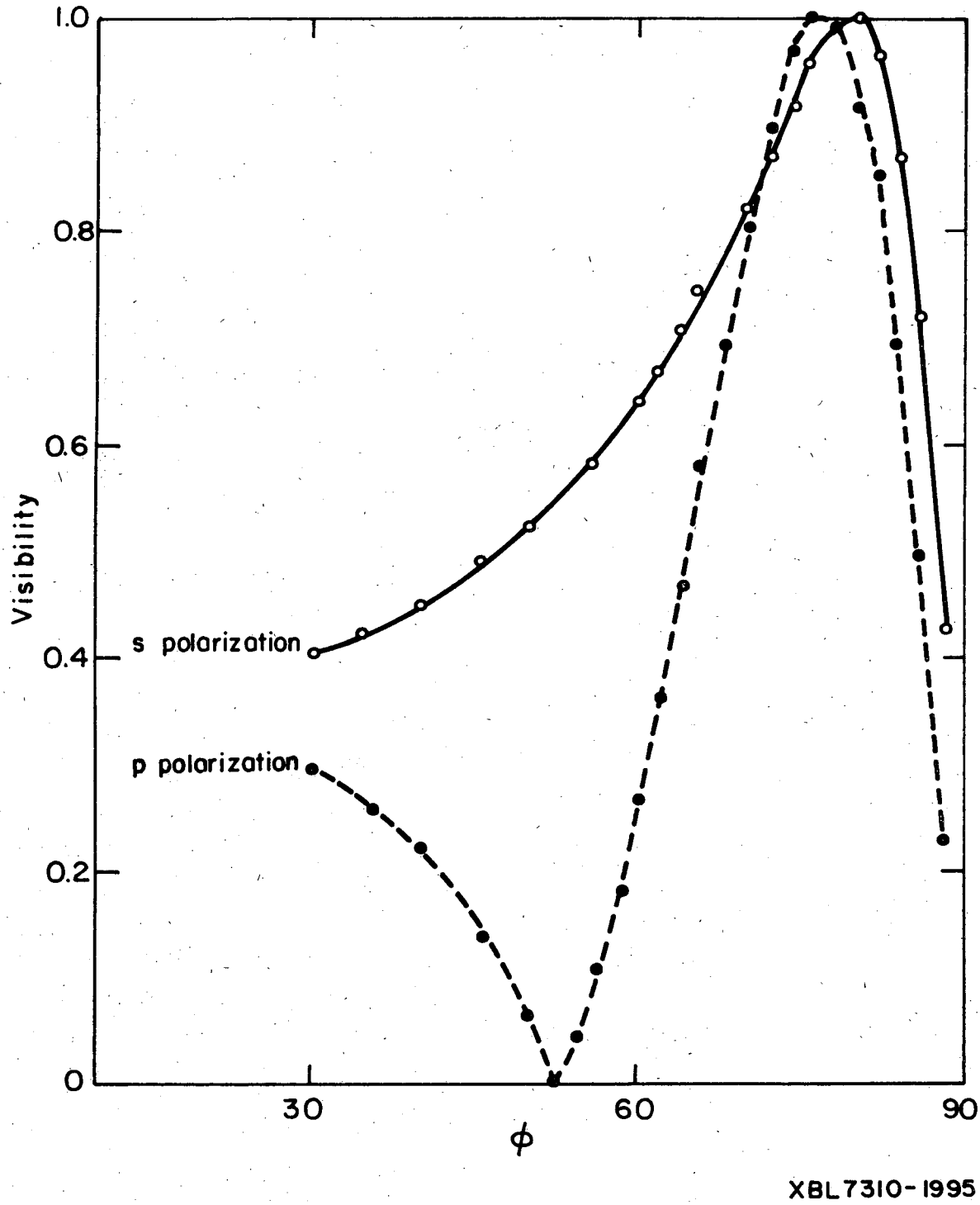

Fig. 18. As in Fig. 14. Cryolite film on silicon substrate.

maximum fringe visibility and minimum allowable sample space. For dielectric-aluminum pairs, this meant observing fringes at 80 degrees angle of incidence instead of at the optimum angle of incidence of 88°. All chromaticity computations were made for the observation angle.

2. Cleaning of the Substrates

The purity of substrates is vital to obtaining smooth, optically uniform, mechanically sturdy thin films in vacuum by a thermal deposition preparation.[30] The substrates for deposition of metal films were polished, 3 by 1 in., glass microscope slides. The slides were bathed in an aqueous solution of potassium dichromate and sulfuric acid at 150°F for 4-5 hours after a thorough detergent cleaning. Then, the slides were rinsed with cold distilled water and immersed in hot distilled water for an additional hour. These washings were done to remove contaminant molecules such as grease and heavy metals. The slides were rinsed again in a stream of distilled water and quickly transferred to a desiccator for 24-hour drying. Precautions were taken to avoid contamination by the desiccant, Drierite, in that shielding was placed between the substrates and desiccant. Adhesion of deposited metal films was satisfactory.

Instead of depositing silicon from a vapor phase containing 10^{-6} Torr of residual gases (O_2, N_2, CH_4, H_2, H_2O), silicon wafers 3-inch in diameter and 20 mils thick were used. The silicon surface was highly polished with surface irregularities (roughness) of 300Å determined profilometrically. To clean the wafers, a two-step procedure was used. First, the silicon was immersed in a concentrated (48%) solution of

hydrogen fluoride. Having been thoroughly rinsed in a distilled water stream, the wafer was then immersed in an equal-weight solution of hydrogen peroxide and hydrogen chloride. The first cleaning removed light metal contaminants, while the second cleaning removed heavier contaminants.[31] The wafers were bathed in hot distilled water and transferred to a desiccator.

In order to leave exposed strips of bare substrate by masking, deposited chromium and aluminum films were removed from vacuum before dielectric films were deposited. Oxide layers of indeterminate thickness formed so that independent measurements of the substrates' optical properties were required. The effect of a ±20% variation in both refractive index and extinction coefficients is discussed in Section 7.

3. Deposition Apparatus

In order to prepare the dielectric-metal pairs, a thermal deposition method was employed. To achieve high vacuum, an automatic vacuum apparatus (Mikros, Automatic Vacuum Evaporator, Model VE-10) equipped with feed-through electrodes was used. Mechanical and diffusion pumps evacuated a 10 in. by 12 in. cylindrical bell jar within 10 minutes to a pressure of 0.1 micron. Within a half-hour the absolute pressure was 10^{-6} Torr. Four 5/16 in. O.D. current feed throughs rated at 100 amps-50 volts were provided together with a rotary specimen holder. Pt, 10% Rh thermocouples were installed to monitor evaporant source temperatures. Feed through and holder were both O-ring and teflon sealed while the thermocouples were epoxy-sealed. Both a Pirani transducer system and a discharge vacuum meter indicated pressure in the bell jar. Adjustable copper electrodes were built to position the sources.

A turntable mount for the specimens was constructed which premitted both angular and vertical adjustments. The specimen was firmly clamped to a special holder which permitted a separate rotation of the specimen about its center axis. The specimen could be either moved past the vapor stream or maintained in a stationary position during deposition.

Attempts were made to deposit at normal incidence by moving the substrate in a linear fashion past the source axis, but control of the planetary rotation of the specimen was not adequate to produce a slowly tapering wedge film. Therefore, an off-axis deposition arrangement was used for wedges. Advantage was taken of the cosine squared material distribution at the substrate for condensate vaporized from a point source evaporator. Although the actual source used was an extended source evaporator, the material distribution with respect to deposition angle (the angle made between a ray in the plane of the substrate and a ray from the evaporant source to a point on the substrate) differed negligibly from that of a point source.

The evaporant source for powdered materials is described in Fig. 19. The "boat" crucibles were constructed from 10-mil thick sheet molybdenum, tantalum and tungsten. The crucible in the center of the boat reaches temperatures above 1200°C. This high temperature is due to the reduced area for current flow resulting in high local current densities and resistive heating. Tapering the fins allows a greater current to pass through the crucible and results in higher source temperatures. Other source designs[30,32] are possible, but few require as little machining or yield as high temperatures for the same current loads.

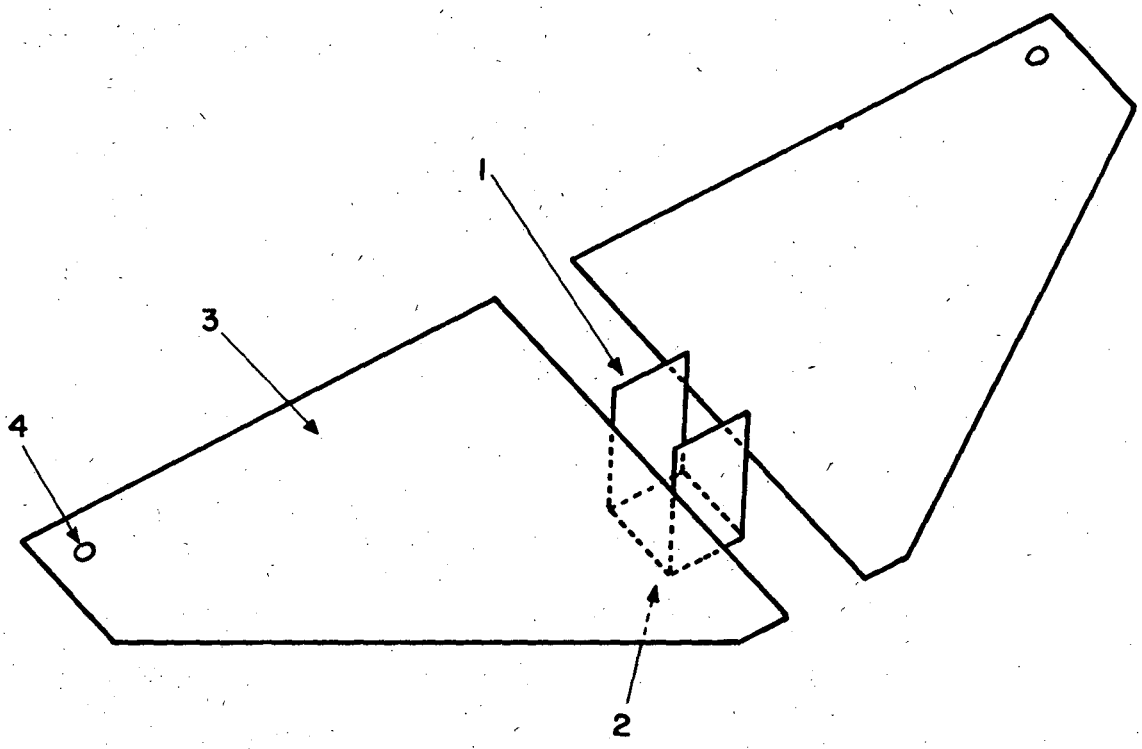

XBL7310-1987

Fig. 19. Diagram of evaporant source for powdered materials. 1. baffles, 2. crucible, 3. fins, 4. screw holes (for electrical connection).

A helical tungsten "basket" evaporator was used to evaporate aluminum wire. The source was constructed by winding 20 mil tungsten wire into a spiral. Small sections of evaporant wire were hung onto the "basket" and, then, melted so that the evaporant evenly wetted the tungsten coil. The wetted evaporant could then be vaporized by raising the coil temperature.

4. Preparation of Metal Substrates

The selected substrate materials were aluminum, chromium and silicon. The substrates were prepared by thermal deposition in the first two instances while p-type, boron doped silicon wafers were used in the latter case.

Aluminum substrates were prepared by vaporizing aluminum from tungsten coils. Aluminum wire, 15 mil in diameter by 1/8 in. in length, wetted the tungsten at 960°C. At 960°C the vapor pressure of aluminum is 8×10^{-5} Torr.[33] The substrate, a microscope slide chemically cleaned[33] to remove contaminants, was then centrally positioned 10 cm above the source axis (normal to the center of the source). Residual gas pressure as indicated by the vacuum discharge tube transducer was 10^{-6} Torr. The coil was then heated resistively to about 1500°C at which temperature aluminum has a vapor pressure of 2×10^{-1} Torr. According to the kinetic theory, the number of aluminum atoms striking unit area of the substrate at normal incidence is 3.4×10^{9} atoms $cm^{-2}sec^{-1}$.[10] The area of a single adsorbed aluminum atom is about $6.54Å^2$ so that a monolayer deposits in 2.2×10^{-6} sec. Hence, a micron thick film forms in about a second assuming total adsorption.

The minimum allowable film thickness of aluminum was based on the value of the penetration depth for light. The penentration depth, -y, is defined as the distance into the metal film at which the square of the electric field amplitude (a measure of light intensity) decreases by a factor 1/e. Light at 650 nm incident normally onto an aluminum film (having an extinction coefficient of 6.51) dissipates by a factor 1/e at a thickness of 97Å. Deposition occurred at near normal incidence by planetary rotation of the specimen through the vapor stream.

The glass slides were masked with molybdenum sheet masks in order to provide an exposed strip of glass for step measurement of the metal film. Average step-height values for aluminum films on glass, obtained by profilometry, were in the range of 400 angstroms for a deposition duration of 5 seconds. At this film thickness, the aluminum film is impenetrable to all spectral wavelengths at all angles of incidence.[34]

A check of the film's impenetrability to light from a white gas-discharge lamp (fluorescent) confirmed that the aluminum films were opaque.

Chromium films on glass were prepared by resistively heating electronic-grade (99.999% pure), powdered metal from tungsten and Ta sheet metal boats. Although the recommended material for constructing an evaporator for chromium is tungsten,[30,32] tantalum boats were suitable. Tungsten sheet boats became extremely brittle upon heating and fractured frequently. Tantalum, although a lower-melting material than tungsten, could be cut more easily and was more resistant to thermal stress. Boat temperature was 1200°C during vaporization. At this temperature the vapor pressure of chromium was 4×10^{-5} Torr. Deposition duration was 15 min

after which time a measured film of 700Å was formed. The penetration depth for light for chromium films (of extinction coefficients 1.55) is 350Å.

To test for pinholing, the metal films were inspected under a high-resolution, white light microscope. The homogeneity of a deposited metal film depends on the ratio of the evaporator temperature and the substrate temperature as well as on the condition of the substrate.[35,39] Since the substrate was at room temperature at the beginning of condensation, homogeneous films of aluminum and chromium were anticipated.[36,38] However, the substrate temperature during condensation could not be controlled so that tests of the homogeneity of the metal films were required. Negligible pinholing was observed for either metal film.

Mechanical stability and adhesiveness to the glass were tested using a strip of tape. Films damaged by rapidly removing a strip of adhesive are considered mechanically unsuitable for use as solid films.[37] Both metal films passed this test.

The silicon wafers were masked before mounting in the vacuum chamber to expose a trapezoidal area of substrate 1 1/2 cm at the widest point by 7 cm long. The silicon was not evaporated because of its high chemical reactivity with residual oxygen and nitrogen. In general, the reactivity of residual gases is of minor importance at chamber pressures of 10^{-6} Torr or below for thermal deposition techniques. For plasma methods, however, residual gas partial pressures of even this vanishing magnitude constitute a major problem of reactivity.[40] The optical properties of thermally deposited silicon are sensitive to oxide and nitride formation even at concentrations produced in

vacuum-chamber atmospheres.[41,43,37] The formation of the mono and di-oxide mixtures may result in changes in the metal index of refraction as well as the color of the material.

5. Preparation of the Dielectric Wedges: Test for Anisotropy

The dielectric materials selected to coat the metals were cryolite (Na_3AlF_6) (Matheson, Coleman and Bell Chemicals Co.) and zinc sulfide (Research Chemicals Co.). Besides satisfying the optical requirements, these materials are industrially used for optical coatings. The indices of refraction of cryolite and zinc sulfide are 1.30±0.01 and 2.30, respectively.[10] The index of refraction of ZnS is independent of wavelength for the visible spectrum while it is also independent of film thickness for films thicker than 900Å.[9] The effect of variation in the film indices on the ellipsometric parameters ψ and Δ is considered in Section 7.

In order to produce wedge films in the range of film thickness from 0.05 to 1 micron, several wedges of each pair had to be prepared in some instances. Successive wedges were deposited at increasing durations so that their thickness profiles overlapped.

The substrates, which were deposited film in the cases of aluminum and chromium, were masked with molybdenum sheet prior to mounting in the vacuum chamber. This was done to provide a strip of exposed metal at the edge of the dielectric for step-height measurement to the metal surface. Wedges were obtained by directional deposition at a source to substrate (edge) distance of 10.5 cm. Tapering followed roughly a cosine squared distribution with respect to the deposition angle. Only half the distribution was used in the depositing scheme

employed. The minimum inclination of the vapor stream with respect to the substrate normal was 34°.

At this large inclination of the incident vapor stream, oriented films were anticipated.[43] This orientation would result in optical anisotropy which distorts the interpretation of colors from white light interference. To determine the effect of orientation, pairs of dielectric wedges were deposited on glass so that the thickness profiles of the members of a pair, a pair being characterized by a common dielectric, overlapped with the same thickness produced at different inclinations. The films were spectrophotometrically scanned continuously with respect to film position for maxima and minima at discrete wavelengths in the visible spectrum. Their step-height profiles were measured using a profilometer and an interference microscope. The position of maxima and minima was then compared for the portions of the films belonging to a pair having the same range of thickness, Figures 20(a), (b) and 21(a), (b) show the results of the tests for anistropy of the ZnS and cryolite wedges.

A difference of 300Å was observed between the thickness of the films at the same maxima or minima. With regard to the measurement techniques, however, the difference is close to the resolution of the instruments. Therefore, no pattern could be distinguished between the degree of orientation, indicated by the value of the deposition angle, and the anisotropy as determined by profile differences at spectral maxima or minima.

Films produced in this manner showed wide fringes, 0.25 in. in width, with no appreciable curvature. Curvature of the fringes using an extended evaporator, such as the one used, is elliptical rather

Figures 20

Comparison of mechanically established film thickness for wedge films of cryolite deposited on glass slides at positions of spectroscopic maxima and minima identified in Fig. 20a using p-polarized light for two samples.

Max. Min.	Film Thickness (Å)		Deposition Angle (Degree)	
	Sample 1	Sample 2	Sample 1	Sample 2
0	2750	---	26.0°	---
1	2950	---	25.8°	---
2	5300	5500	18.5°	29.6°
3	6000	6100	14.8°	27.5°
4	6900	6900	9.5°	25.5°

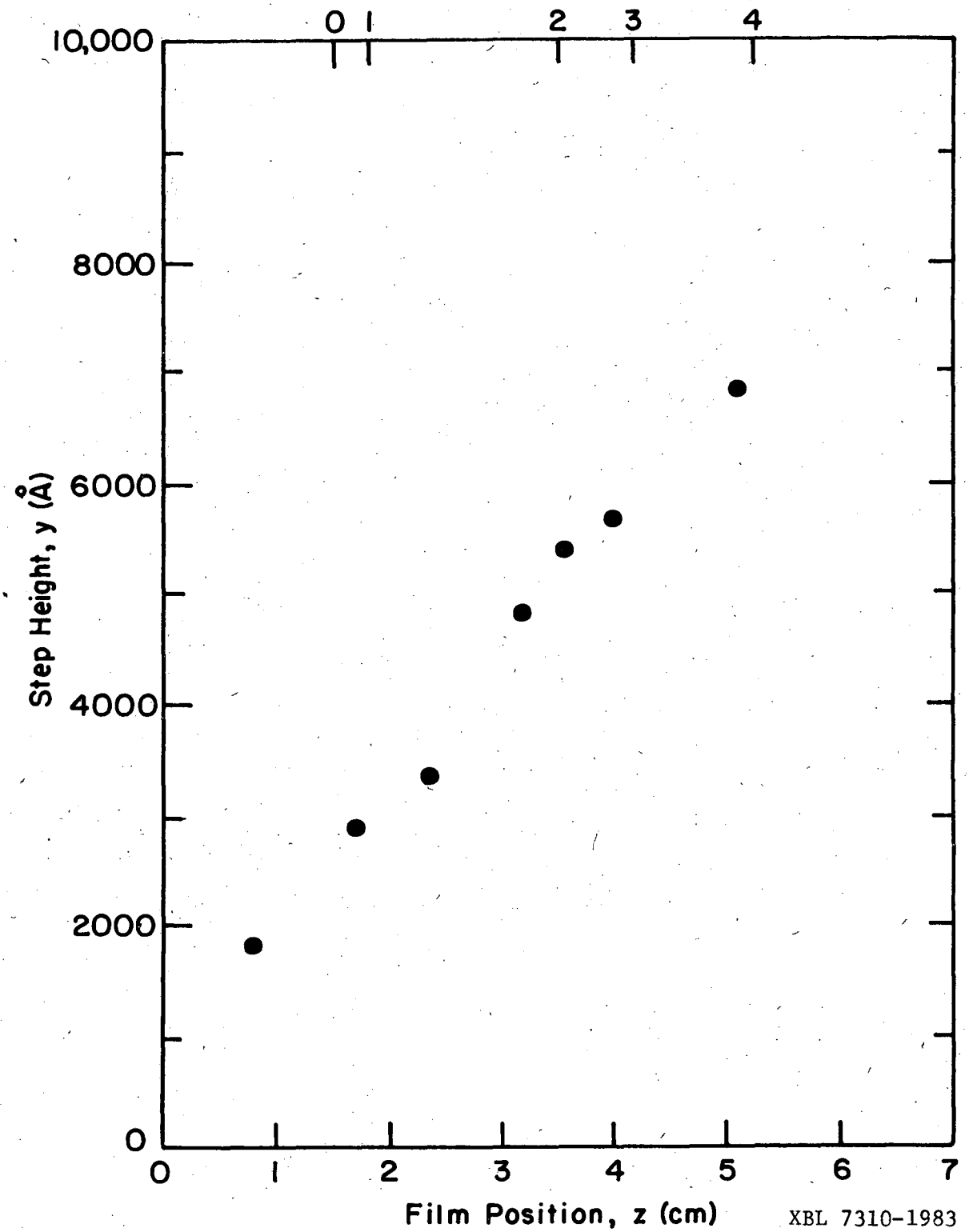

Fig. 20a. Anistropy. Film profile of sample 1 of cryolite film on glass determined by mechanical step-height measurement. Selected maxima and minima of intensity are indicated on the top. The numbers correspond to: 0 minima at 600 nm, 1 minima at 650 nm, 2 maxima at 650 nm 3 maxima at 470 nm, 4 minima at 650 nm.
• Mechanically measured step height.

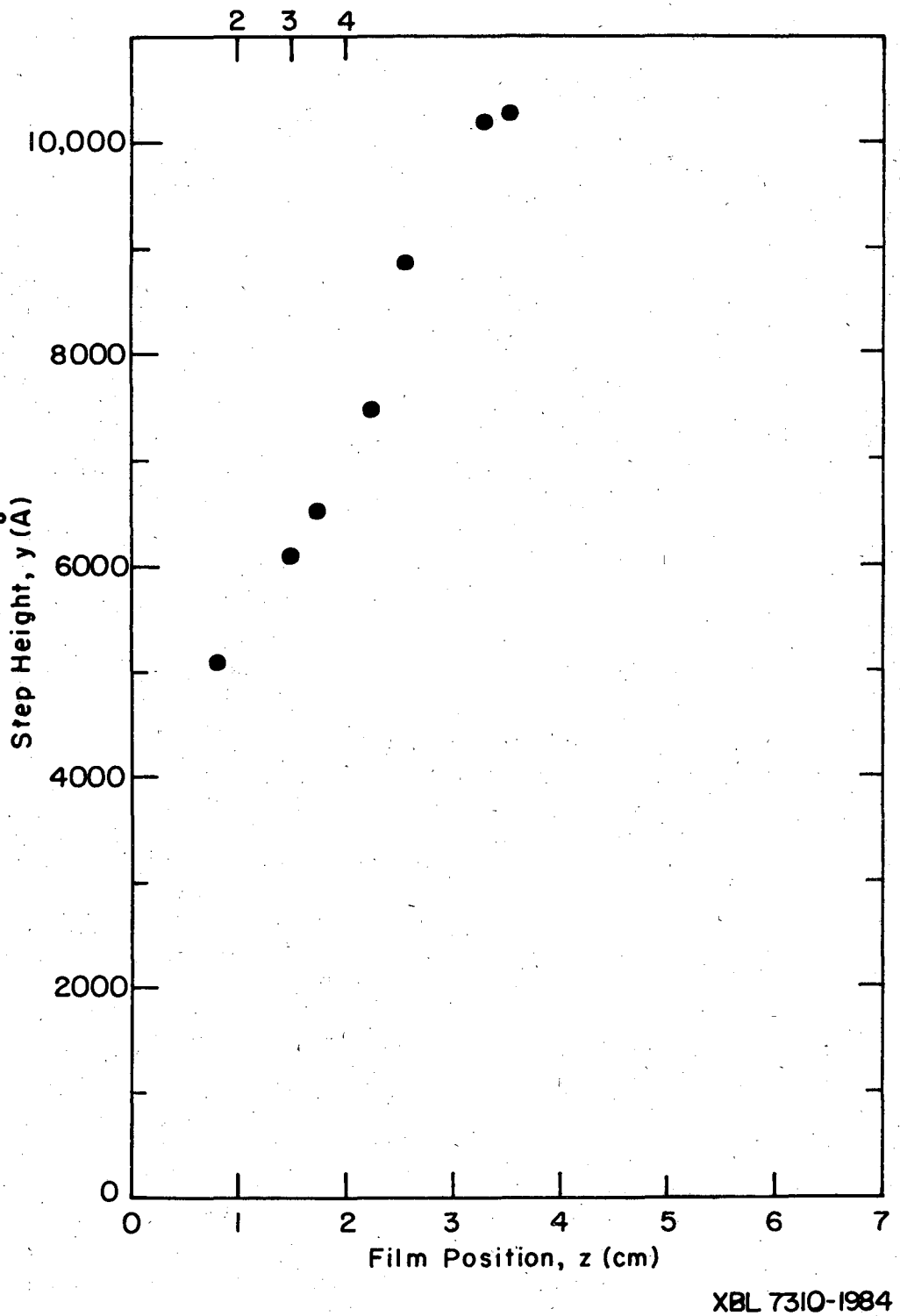

Fig. 20b. As in Fig. 20a. Sample 2 of cryolite film on glass.

Figures 21

Comparison of average* film thickness for wedge films of zinc sulfide deposited on glass slides at positions of spectroscopic maxima and minima identified in Fig. 21a using p-polarized light.

Max.	Min.	Film Thickness (Å)		Deposition Angle (Degrees)	
		Sample 1	Sample 2	Sample 1	Sample 2
	0	510	---	34.8°	---
1		650	710	29.0°	28.0°
	2	1020	1100	15.4°	19.8°
	3	1160	1360	9.2°	18.5°
	4	1250	1500	5.1°	14.4°
	5	----	1670	---	2.7°

*Film thickness at a given film position was determined by taking the average of step-height measurements by interference microscopy and profilometry interpolated for the film-position of interference minima and maxima.

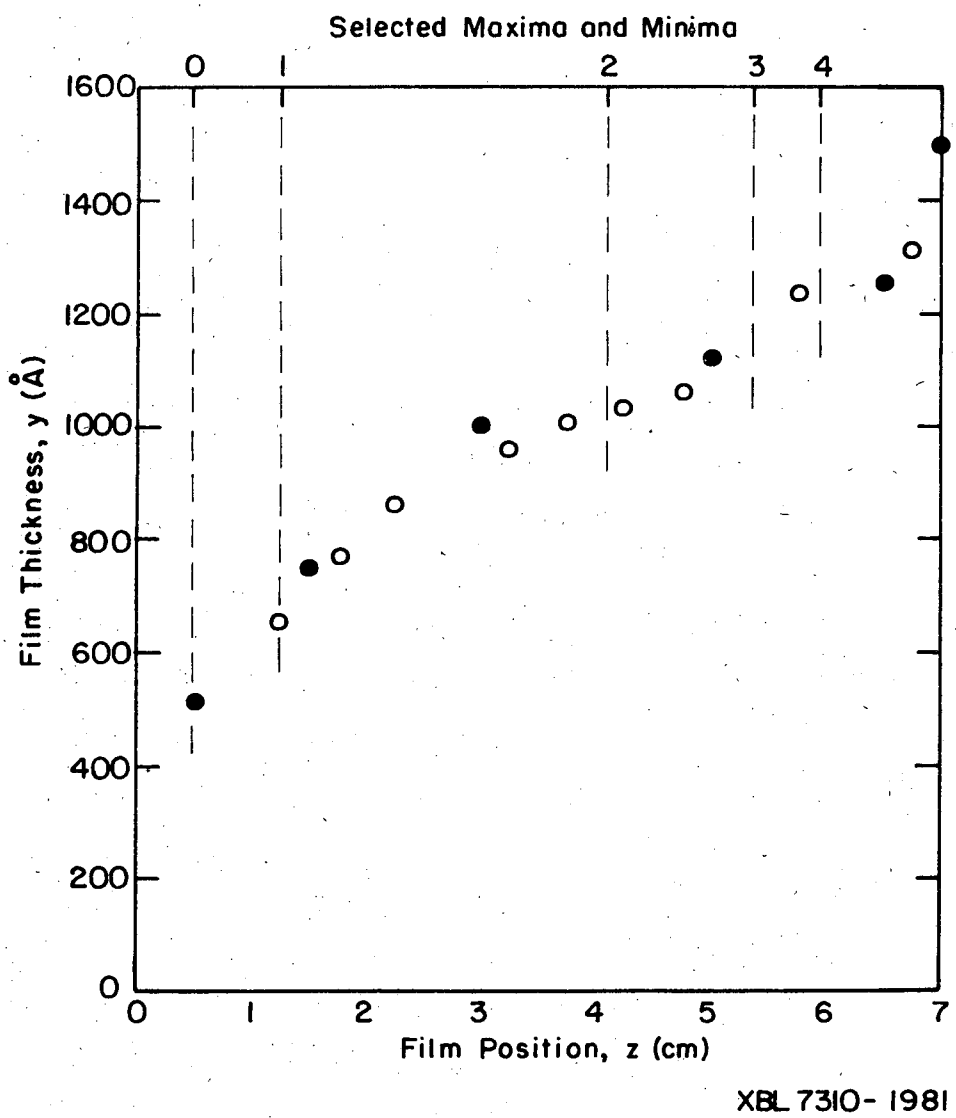

Fig. 21a. Anistropy. Film profile of sample 1 of zinc sulfide film on glass determined by mechanical and optical step-height measurements. Selected maxima and minima of intensity are indicated at the top. The numbers correspond to: 0-maxima at 520 nm, 1-maxima at 580 nm, 2-minima at 580 nm, 3-maxima at 470 nm, 4-minima at 580 nm, 5-maxima at 580 nm.
● Mechanically measured step height.
◯ Optically measured step height.

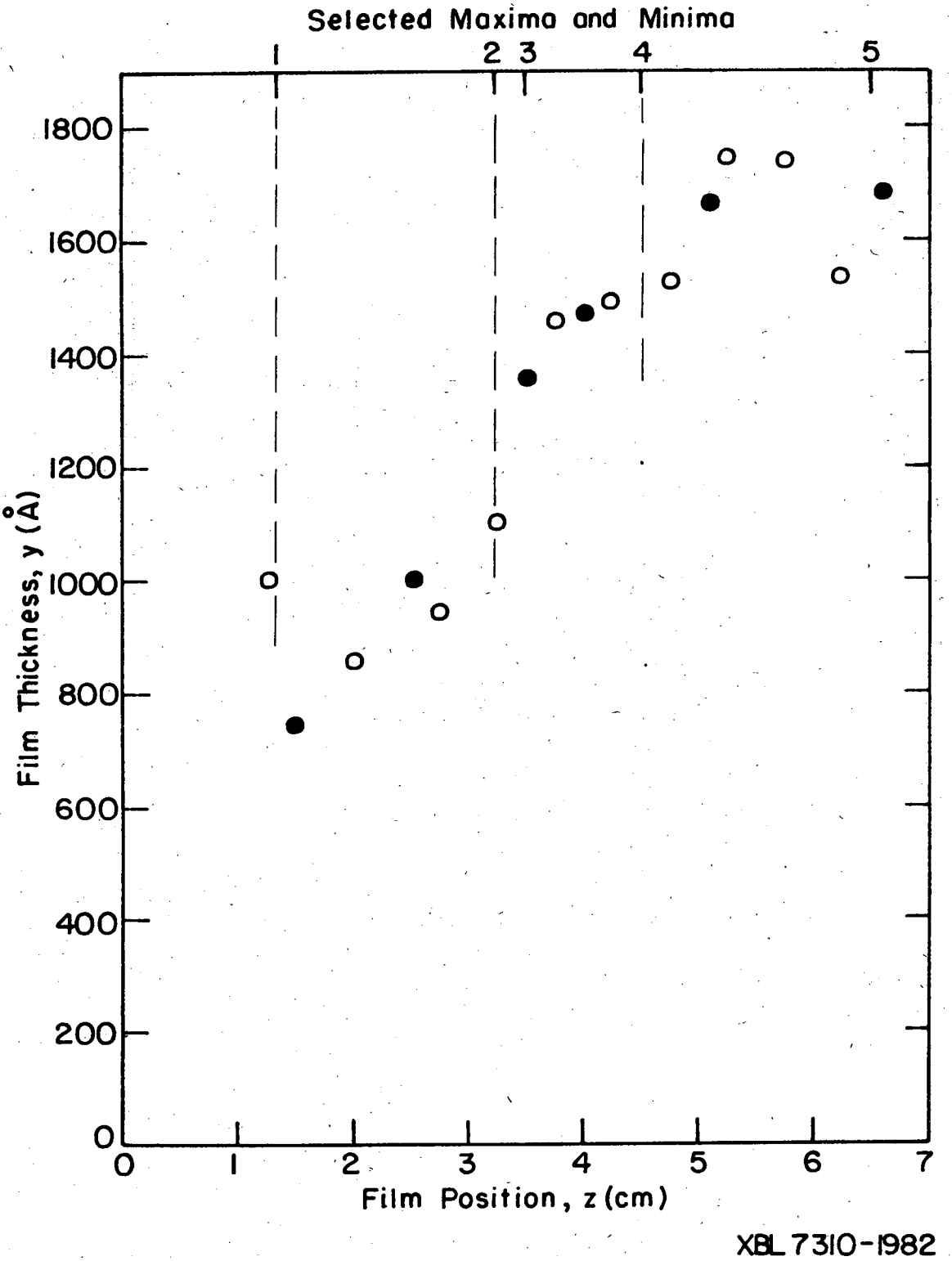

Fig. 21b. As in Fig. 21a. Sample 2 of zinc sulfide on glass.

than circular for a plane substrate. Hence, masking the substrate to eliminate regions of large curvature of the fringes results in straighter fringes.

6. Definition of Specimen Coordinates

Figure 22 shows the coordinate system used to locate film positions of interest. The origin of the z and x axes is at a corner of the glass-slide near the thin edge of the dielectric wedge. The direction of increasing z is the direction of increasing wedge thickness. This direction was chosen to facilitate orienting the film. Thick and thin edges of the taper were easily located since masking was trapezoidal. The wide edge of the trapezoid corresponded to the thick edge of the taper and vice versa.

Diamond scribe marks along the strip of exposed slide were cut along the z-axis. Uniformity of the film in the x direction was essential for sampling with the optics probe.

The origin of the y axis was the surface of the metallic substrate. The reason the real substrate surface was chosen was to eliminate the effect of possible variations in the thickness of the metal substrate. The +y direction is indicated by an arrow head.

7. Optical Constants

The literature values of the optical constants could not be relied upon due to possible surface adsorption and oxide formation on the substrate. In order to test the literature values, ellipsometer parameters at various film thicknesses for ψ and Δ were measured for

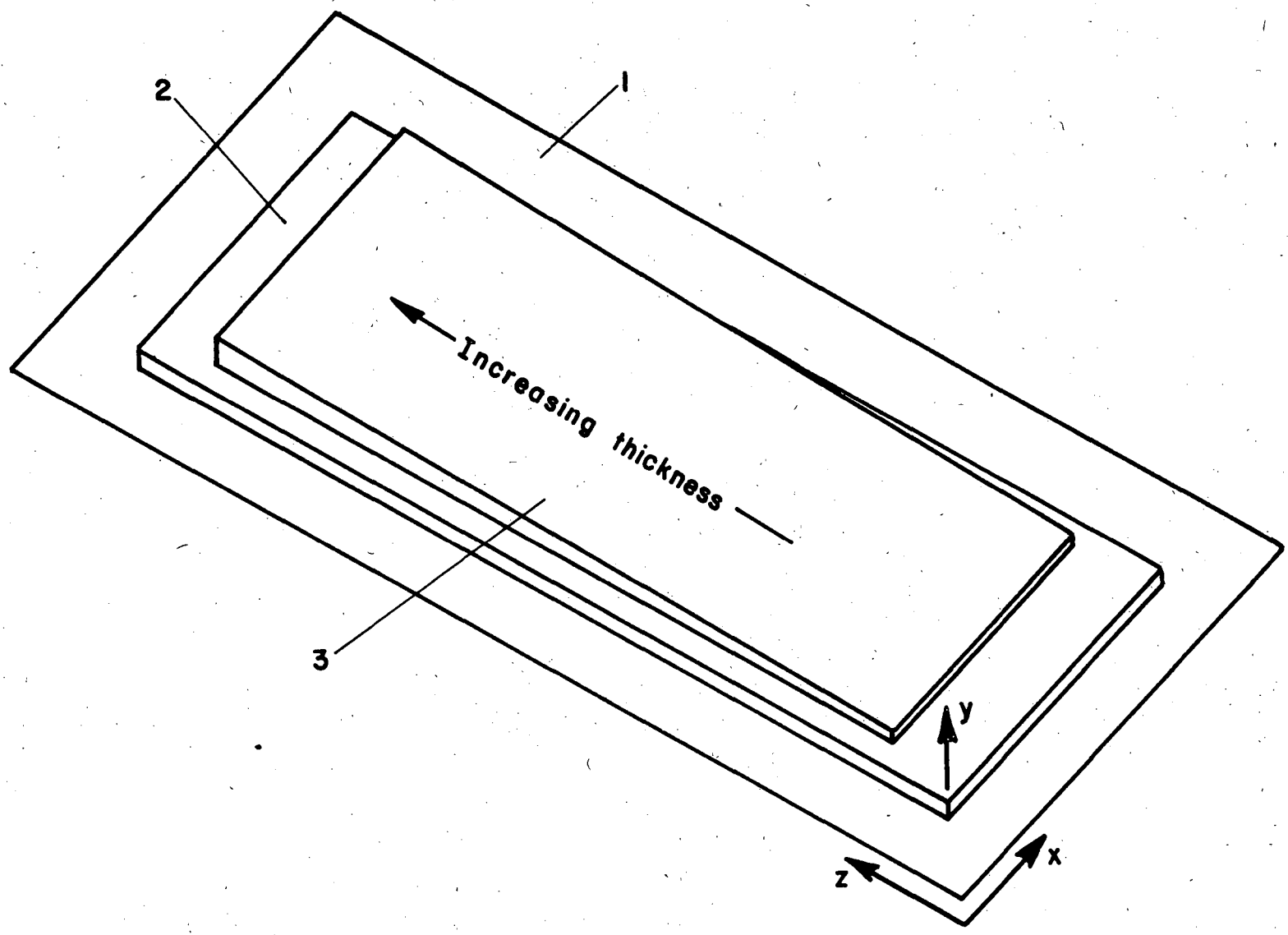

Fig. 22. Description of specimen coordinate system. 1. Glass slide. 2. Metal substrate layer. 3. Wedge-shaped dielectric layer.

each film-substrate pair and compared to computed values, assuming a variability of film and substrate indices of ±20%. The results are shown in Figs. 23 through 34. The plots indicate that selection of reported optical properties is satisfactory to within ±20% in all cases.

B. Thin Film Interference

1. Optical Bench

The optical bench used before by Turney is shown in Fig. 35. Three images were recorded simultaneously by the camera: a caption and two images of the surface.

The light sources were two microscope lamps focused on ground glass screens. The lights operated at 18 watts each. A pair of irisis (diam. 1/8 in.) were placed in front of the screens to define approximate point sources. A pair of positive lenses were used to provide parallel beams to reflect from the film surface. The two beams were polarized, using Polaroid filters, normal and parallel to the horizontal plane of incidence.

The collimating optical bench was mounted on a table which could pivot about a common axis with the surface. Thus, the angle of incidence could be varied to obtain the angle of best fringe contrast. A field lens placed near the film surface refocused the collimated, reflected beam. This lens focused the light to the diaphragm of the camera objective and allowed all the reflected light to be received by the camera.

The nominal angle of incidence, ϕ, is one half the reading on the track on which the movable optical bench rides. The separation between the p and s polarizations was 6°. The actual angles of incidence were $\phi+3°$ and $\phi-3°$, respectively.

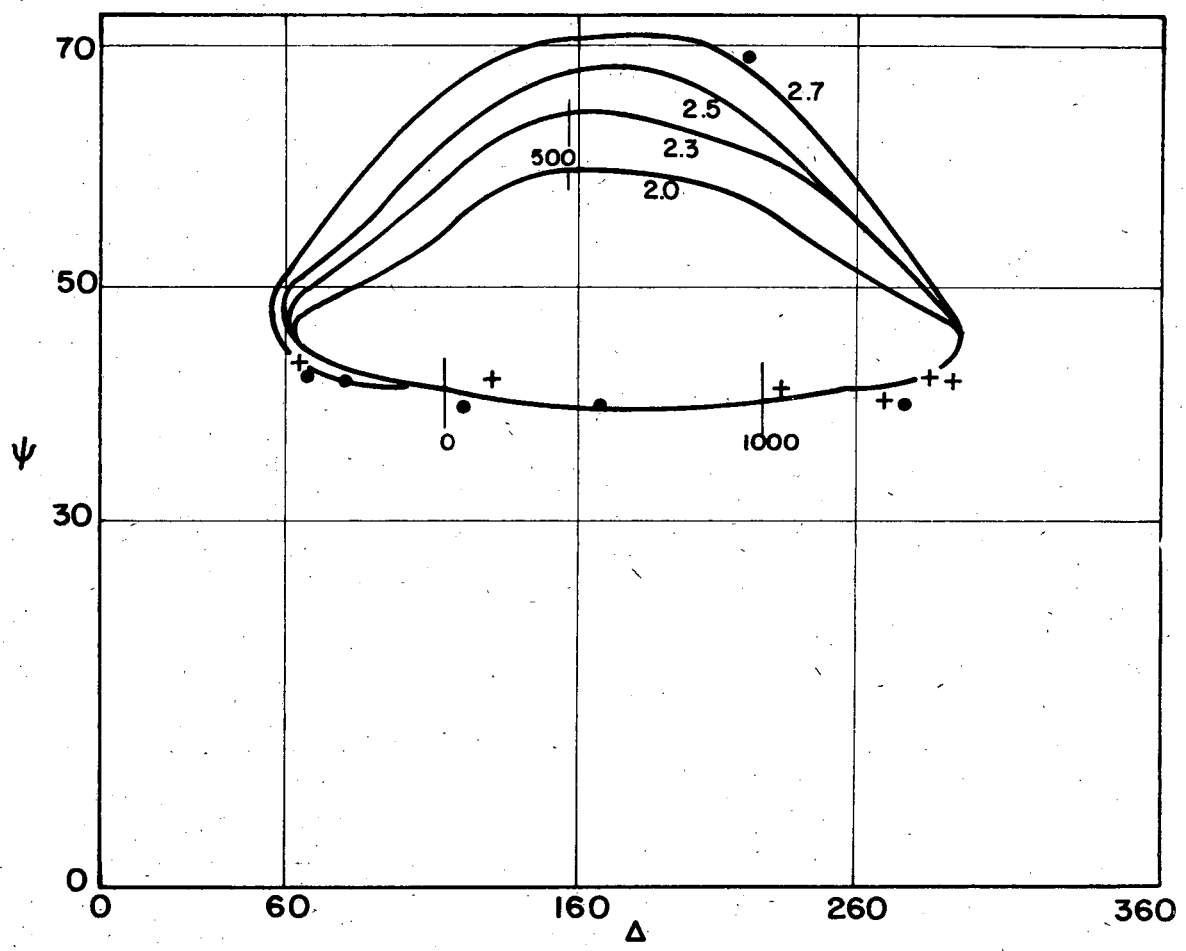

XBL 7310-5435

Fig. 23. Comparison of measured and computed ellipsometer quantities ψ (deg) and Δ (deg). ZnS film on aluminum substrate, ϕ=75°. Computed curves for fixed substrate refractive index, n_{Al}=0.82-5.41i, and film refractive index that varies about the literature value of 2.3. Vertical lines indicate film thickness in Å, + measured data for sample 1, • measured data point for sample 2.

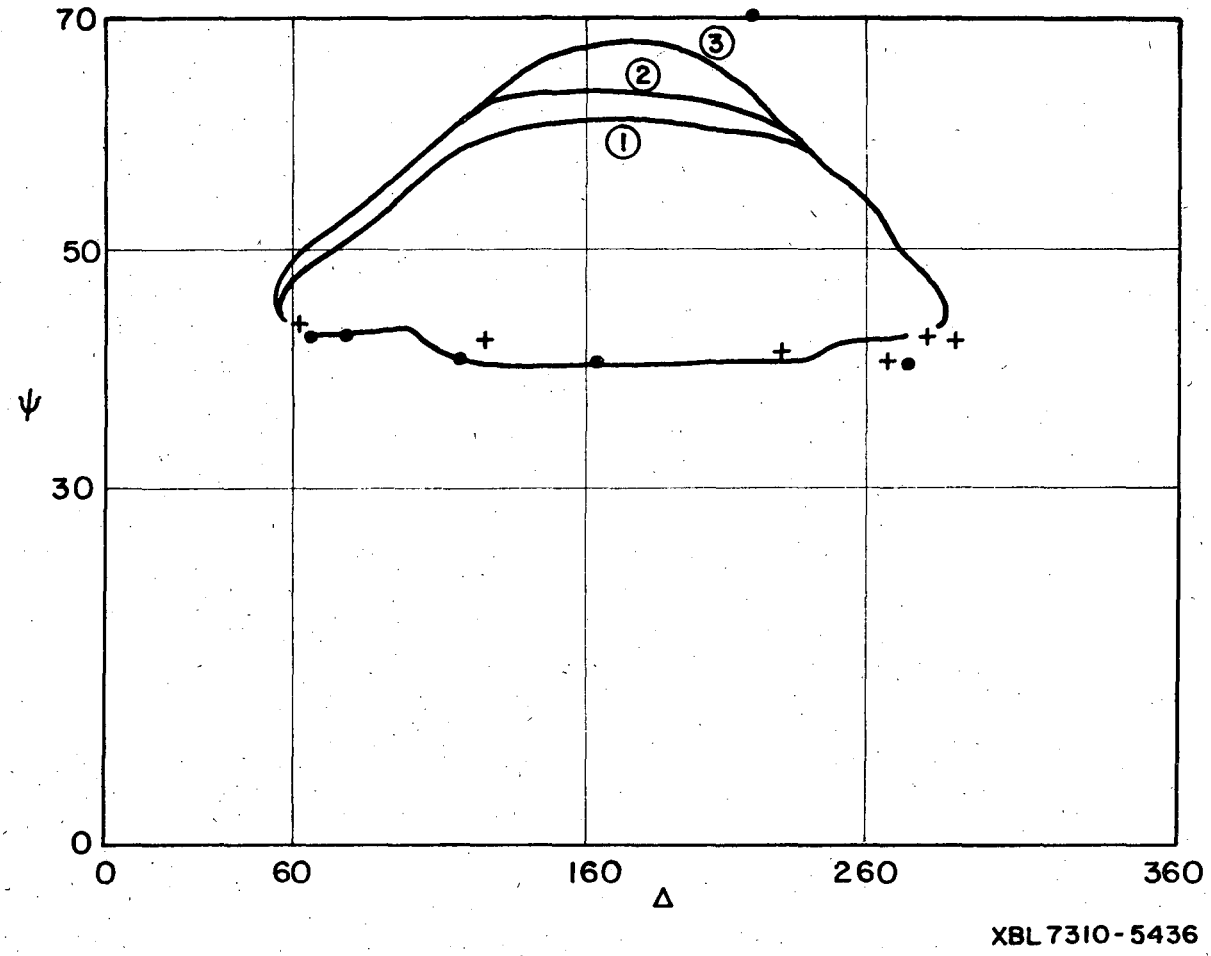

Fig. 24. As in Fig. 23. Computed curves for fixed film refractive index, $n_{ZnS}=2.3$, and variable metal index.

1. $n_{Al}=0.98-6.48i$
2. $n_{Al}=0.90-5.94i$
3. $n_{Al}=0.74-4.86i$

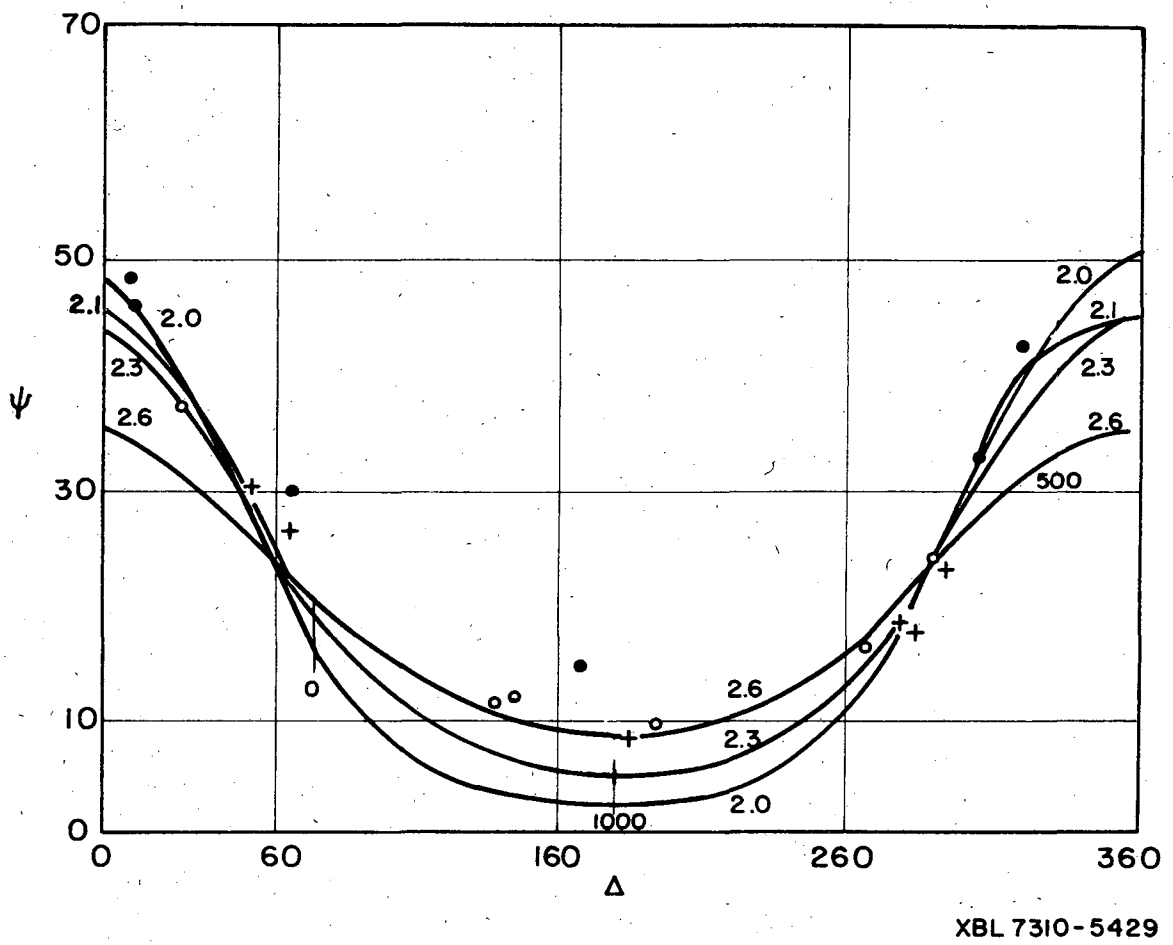

Fig. 25. Comparison of measured and computed ellipsometer quantities ψ (deg) and Δ (deg). ZnS film on chromium substrate, ϕ=75°. Computed curves for fixed substrate refractive index, n_{Cr}=2.11-1.55i, and film refractive index that varies about the literature value of 2.3. + is measured data of sample 1, • is measurement sample 2, and ◯ is sample 3.

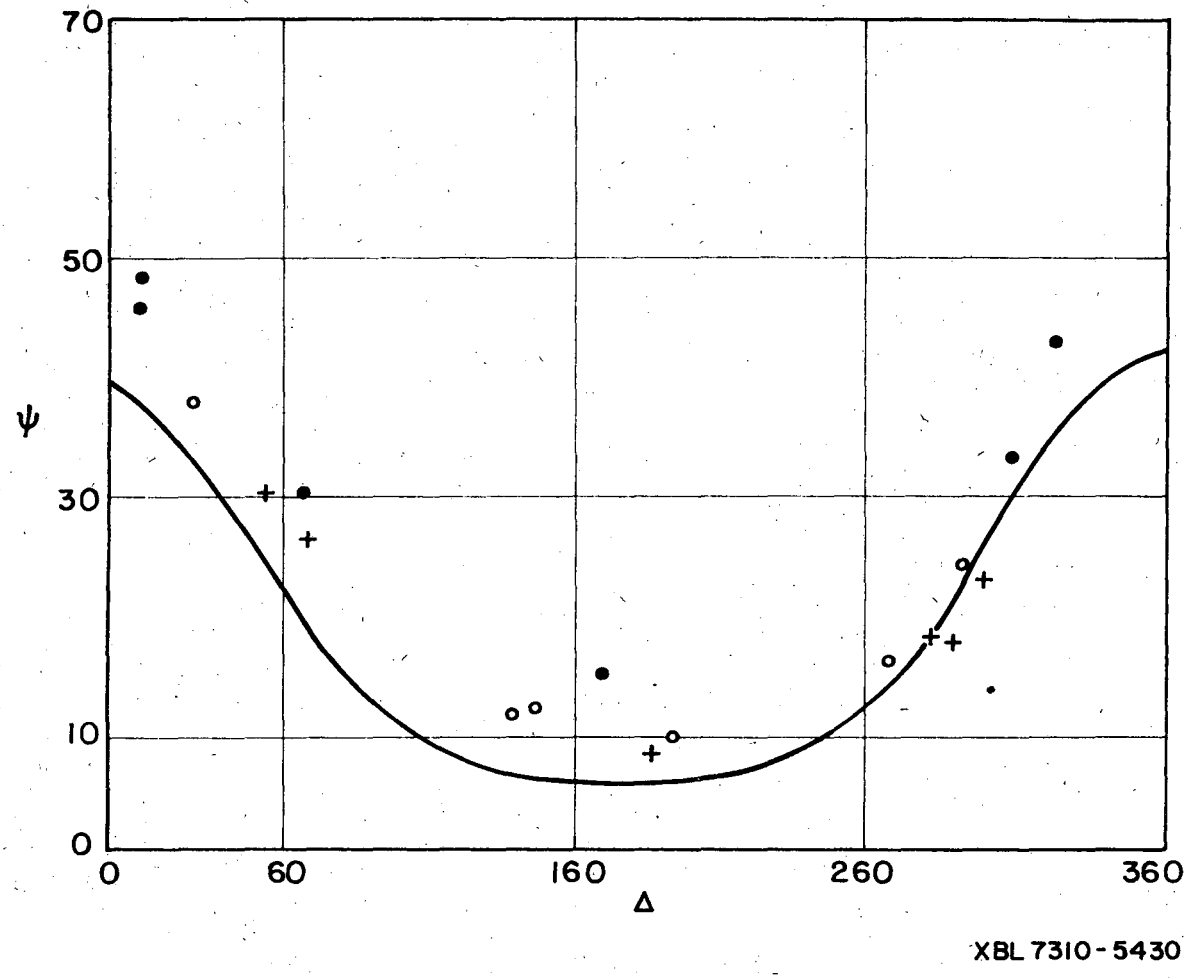

Fig. 26. As in Fig. 25. Computed curves for fixed film refractive index, n=2.3, and variable metal index. The single line encompasses a ±20% variation in N and K of the substrate.

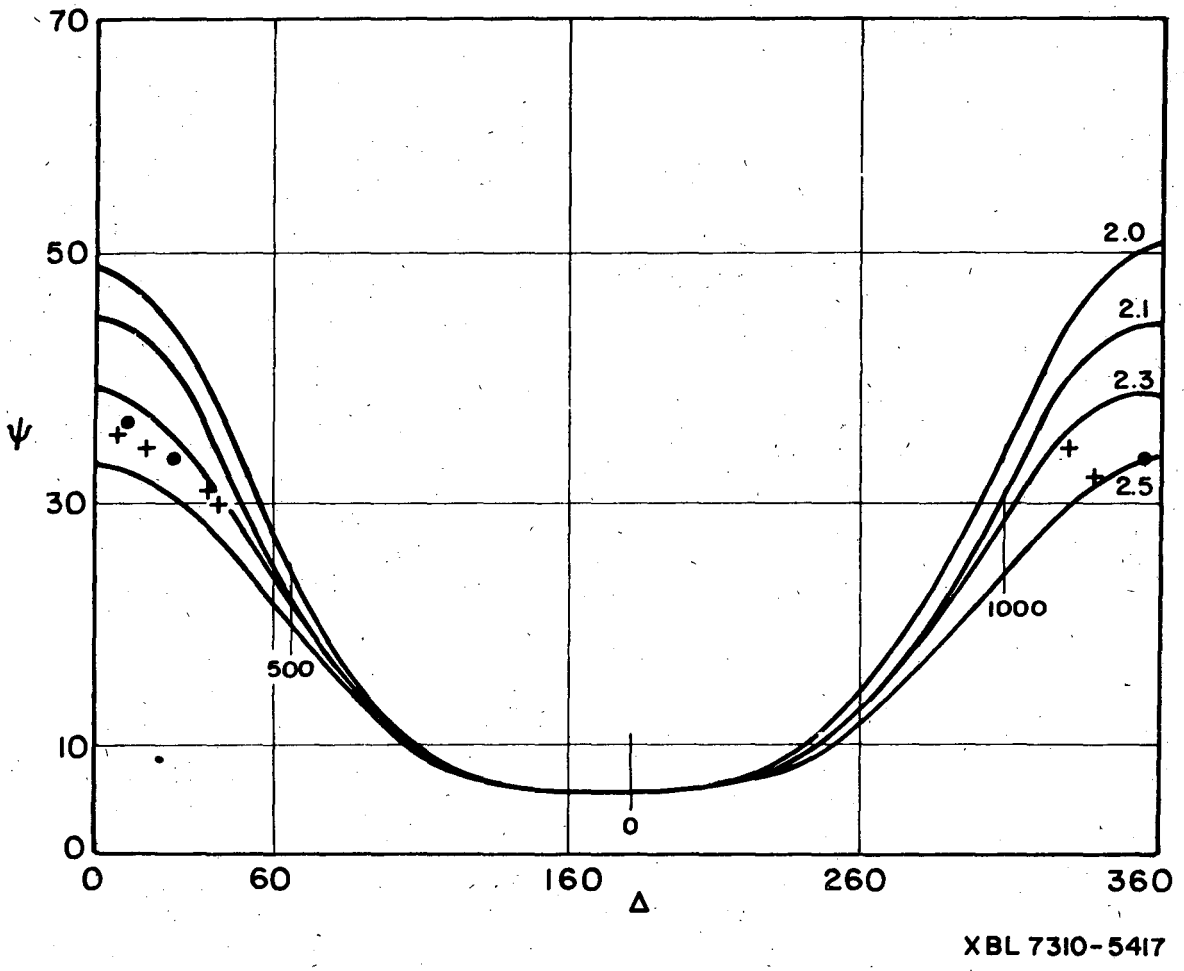

Fig. 27. Comparison of measured and computed ellipsometer quantities ψ (deg) and Δ (deg). ZnS film on silicon substrate, ϕ=7.5°. Computed curves for fixed substrate refractive index, n_{Si}=4.14-0.03i, and film refractive index that varies about the literature value of 2.3. + measured data point of sample 1, • measured data of sample 2.

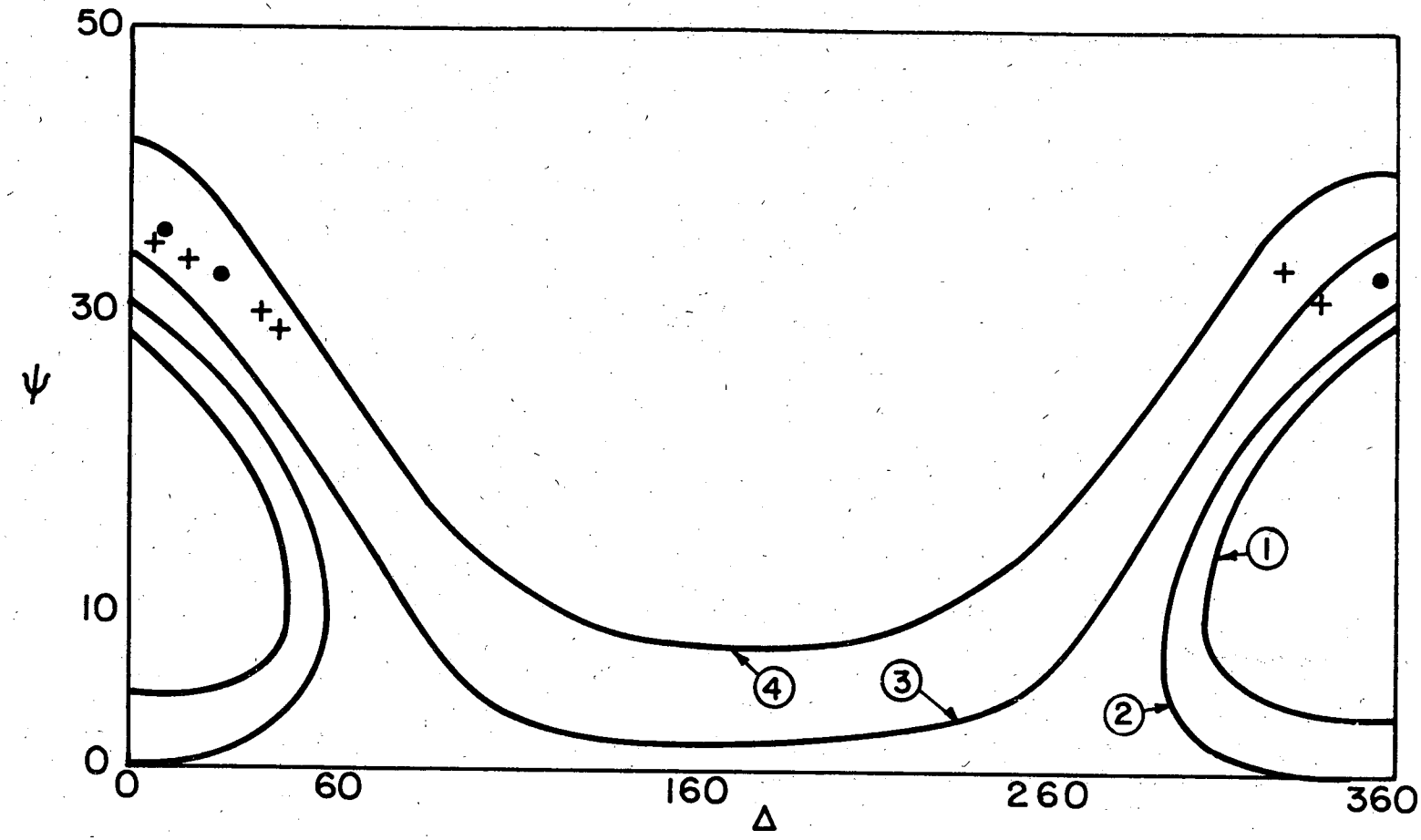

XBL7310-5418

Fig. 28. As in Fig. 27. Computed curves for fixed film refractive indes, $n_{ZnS}=2.3$, and variable metal index. 1. $n_{Al}=3.31-0.025i$, 2. $n_{Al}=3.50-0.026i$, 3. $n_{Al}=3.90-0.0285i$, 4. $n_{Al}=4.70-0.0345i$

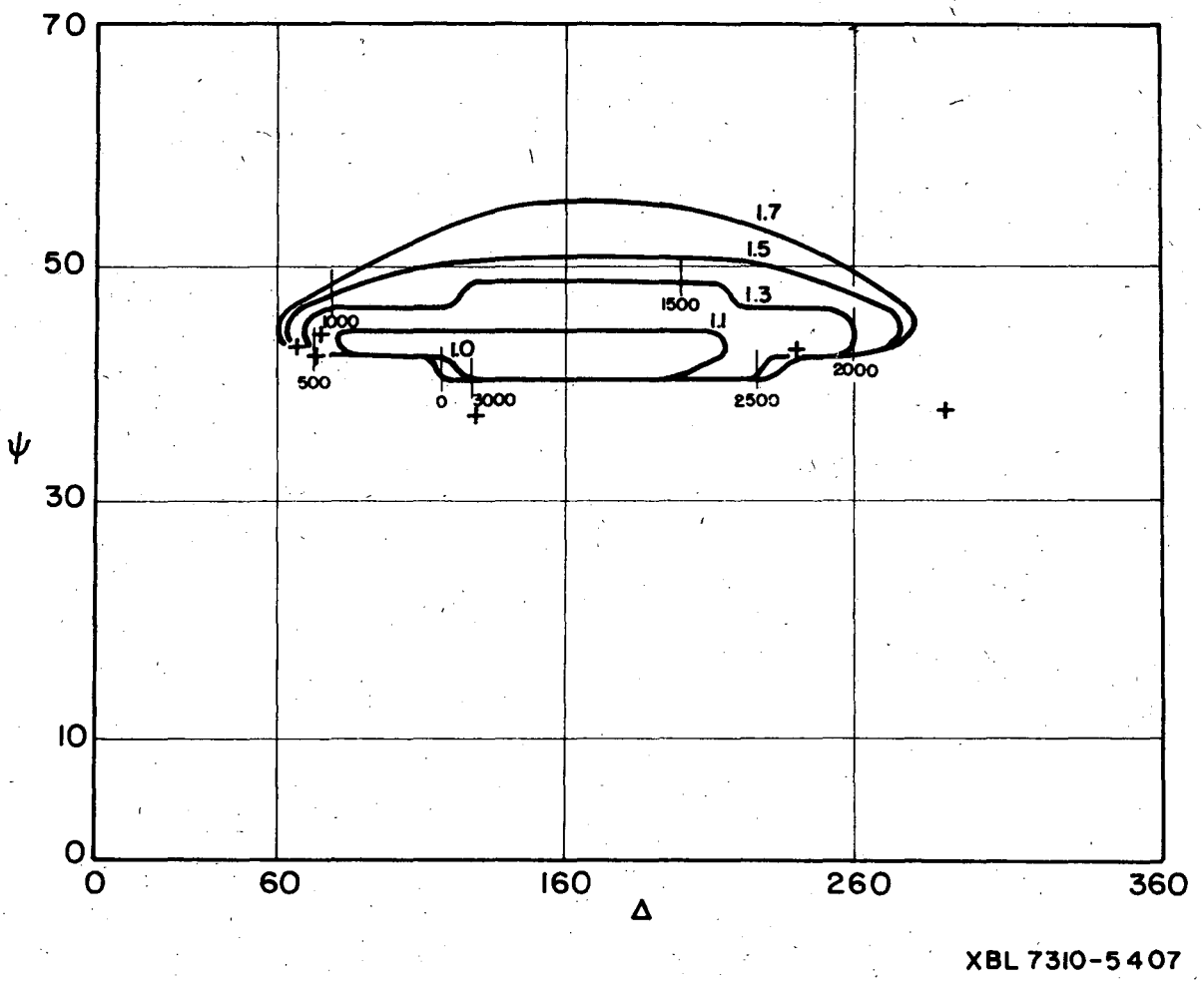

Fig. 29. Comparison of measured and computed ellipsometer quantities ψ (deg) and Δ (deg) . Cryolite film on aluminum substrate, ϕ=75°. Computed curves for fixed substrate refractive index, n_{Al}=0.82-5.40 , and film refractive index that varies about the literature value of 1.3. +'s are measured data points.

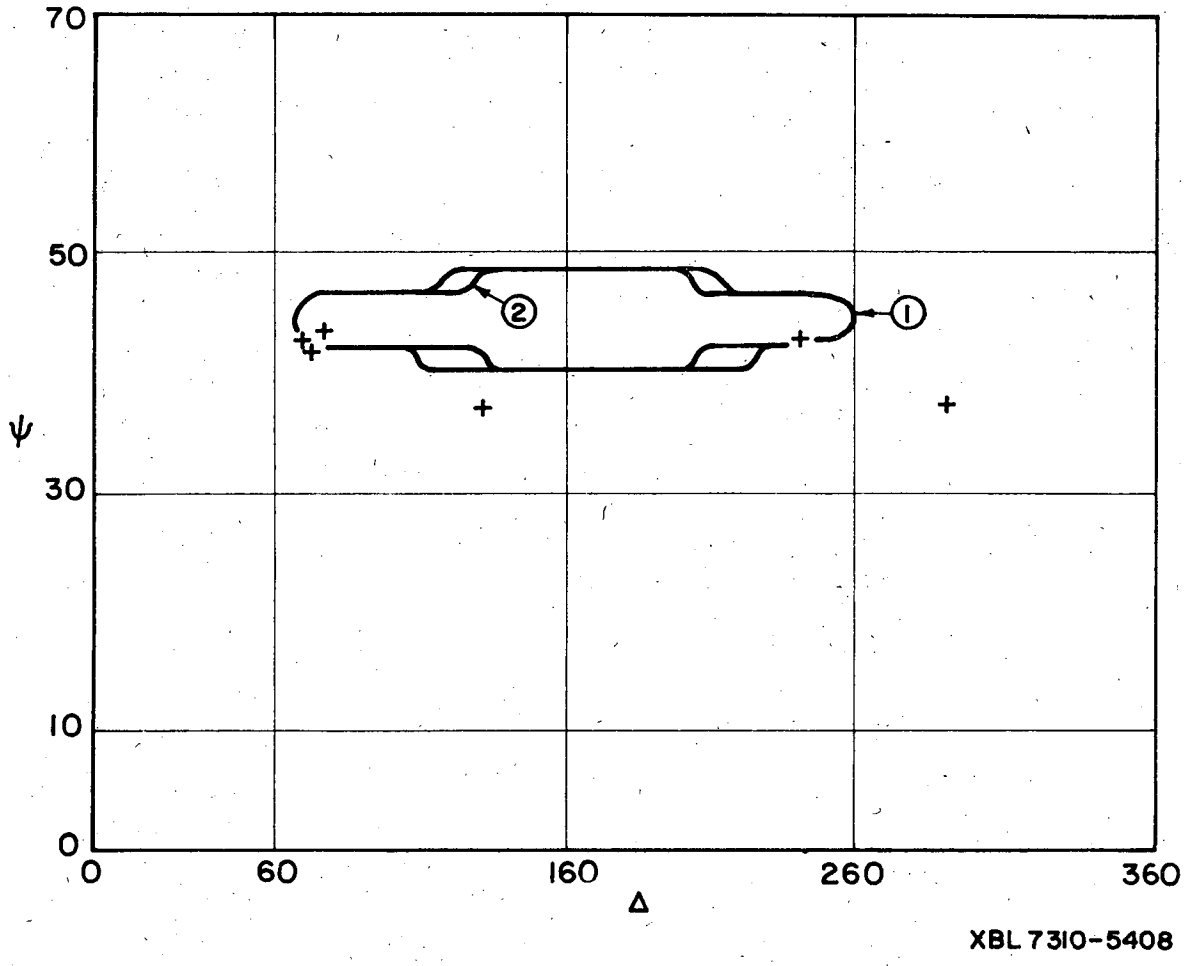

Fig. 30. As in Fig. 29. Computed curves for fixed film refractive index, n=1.3, and variable metal index. 1. $n_{Al}=0.74-4.86i$, $n_{Al}=0.98-6.40i$

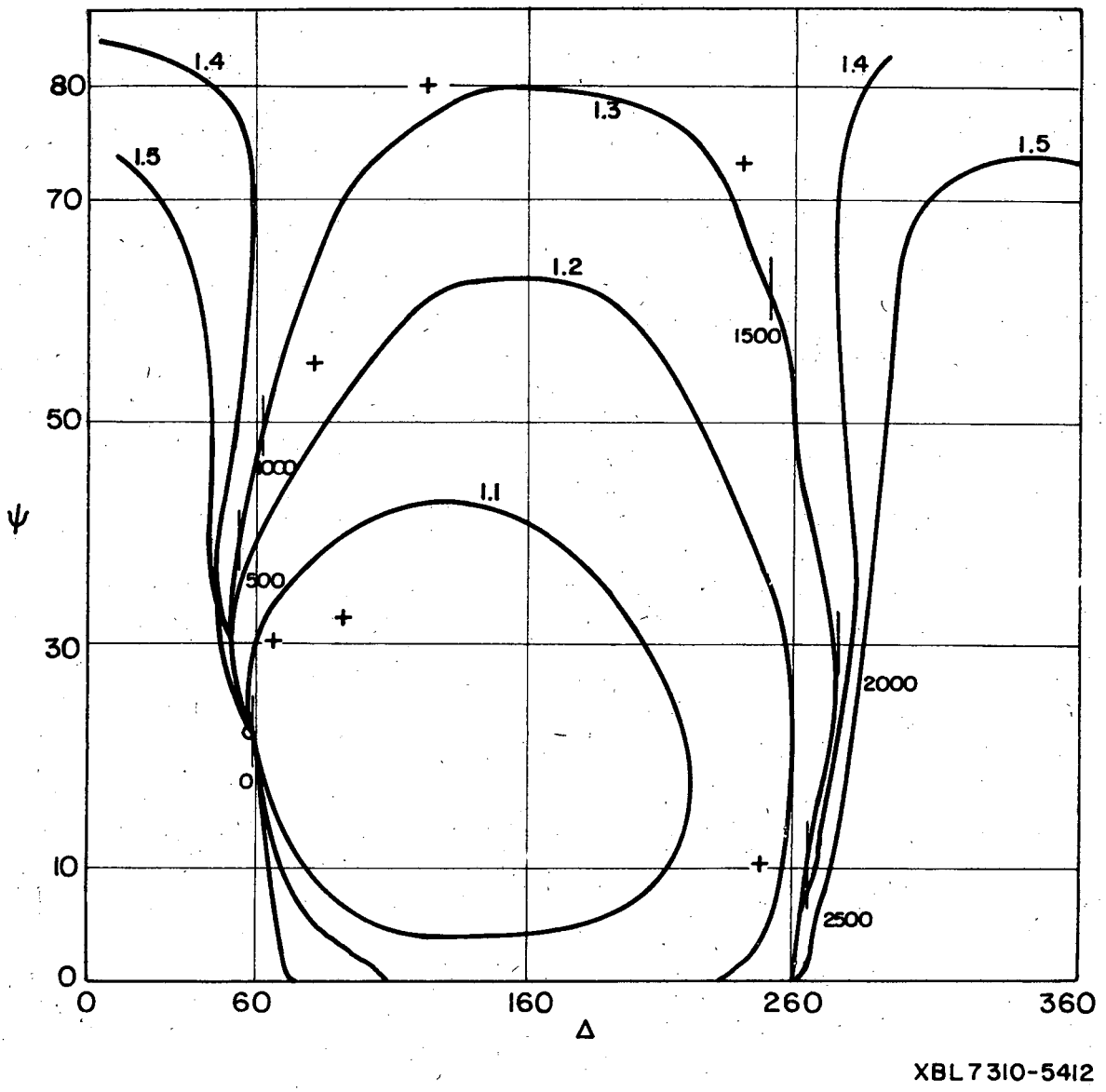

Fig. 31. Comparison of measured and computed ellipsometer quantities ψ (deg) and Δ (deg). Cryolite film on chromium substrate, ϕ=75°. Computed curves for fixed substrate refractive index, n_{Cr}=2.11-1.55i, and film refractive index that varies about the literature value of 1.30. + is measured data.

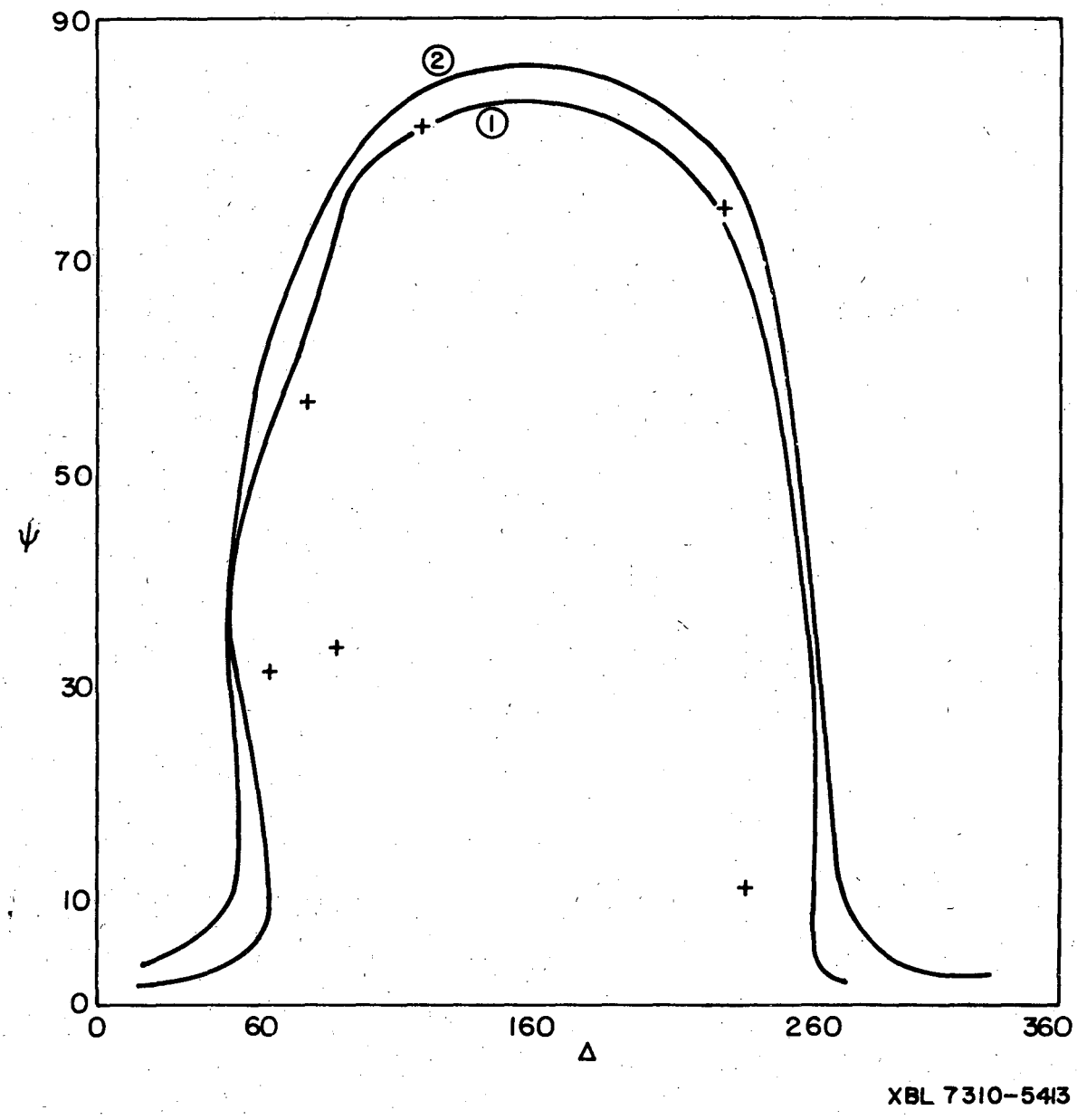

Fig. 32. As in Fig. 31. Computed curves for fixed film refractive index, n=1.30, and variable metal index. 1. $n_{Cr}=2.01-1.47i$, 2. $n_{Cr}=1.81-1.34i$

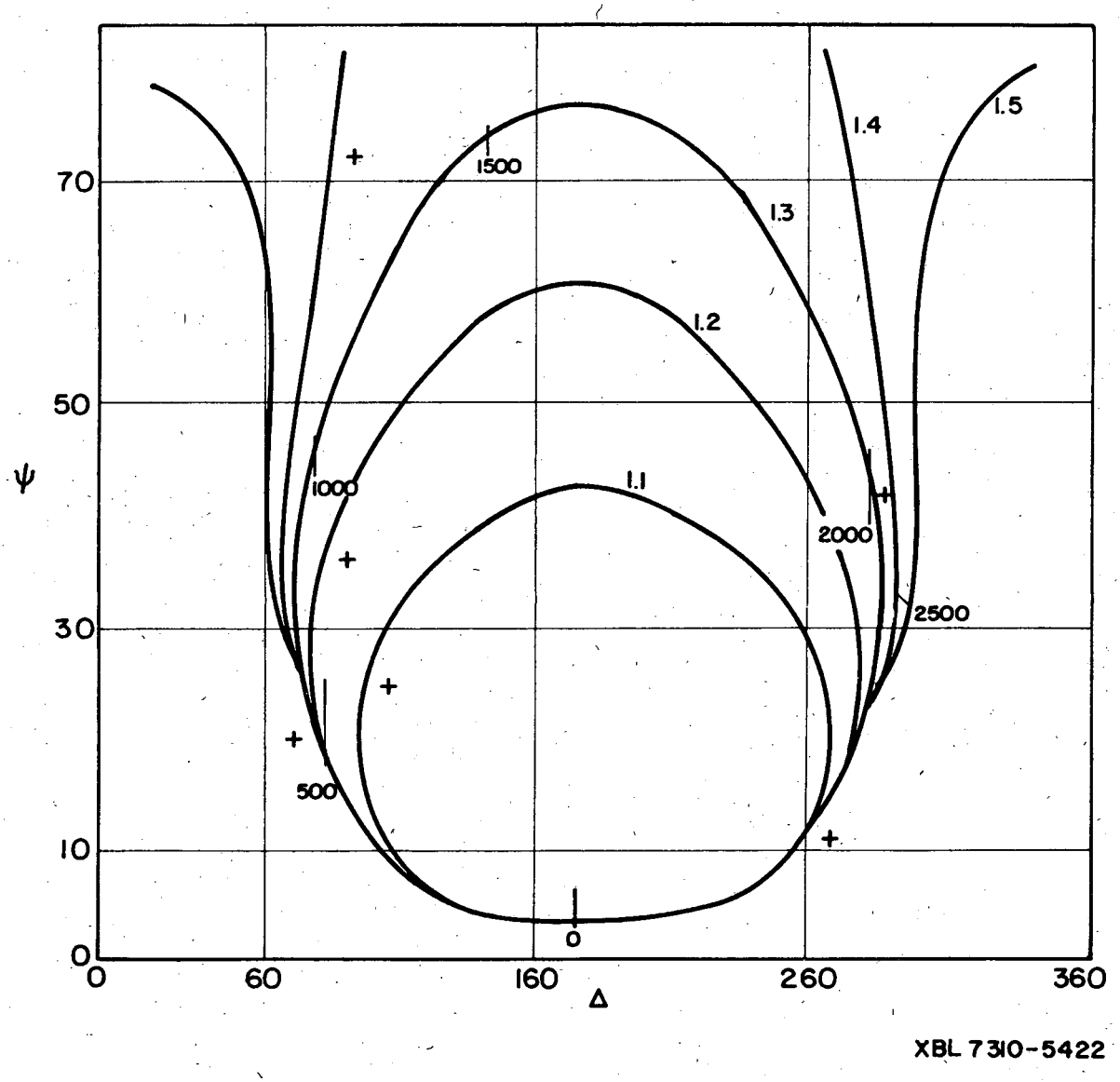

Fig. 33. Comparison of measured and computed ellipsometer quantities Ψ (deg) and Δ (deg). Cryolite film on silicon substrate, Φ=75°. Computed curves for fixed substrate refractive index, n_{Si}=4.14-0.03i, and film refractive index that varies about the literature value of 1.3ϕ. + indicates a data point.

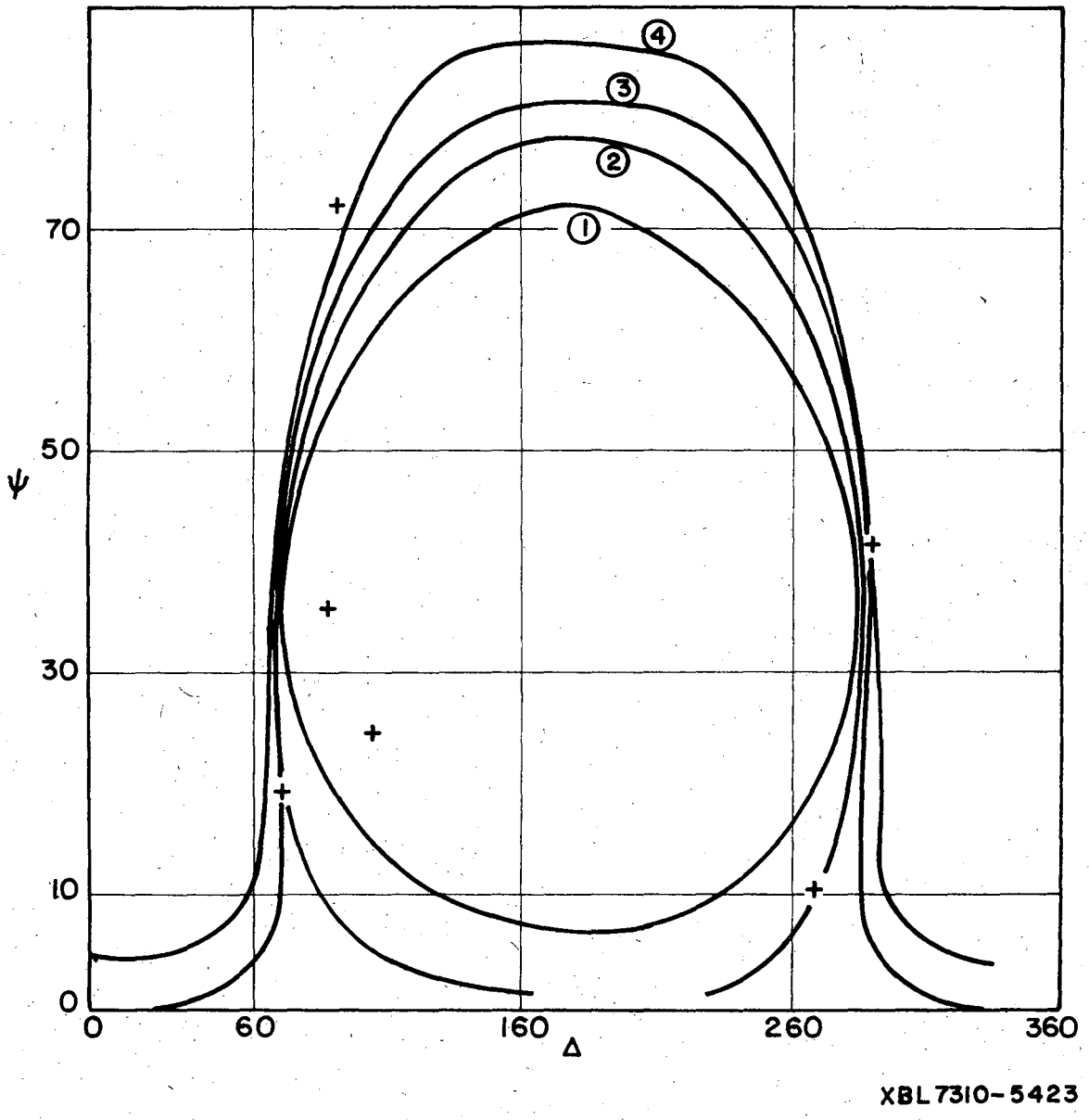

Fig. 34. As in Fig. 33. Computed curves for fixed film refractive index, n=1.3, and variable metal index. 1. $n_{Si}=4.74-0.084i$, $n_{Si}=3.91-0.029i$, 3. $n_{Si}=3.51-0.027i$, 4. $n_{Si}=3.30-0.024i$.

Figure 35

Schematic diagram of optical bench.

(1) Microscope lamps

(2) Neutral density step wedges

(3) Source iris with diffusing screen

(4) First surface mirrors for captions

(5) Collimating lenses

(6) Polarizing filter s-polarization

(7) Polarizing filter p-polarization

(8) Sample surface

(9) Field lens

(10) Stereo mirror system

(11) Camera objective

(12) Camera diaphragm

(13) Film plane

(14) Focusing lenses for captions

(15) Captions

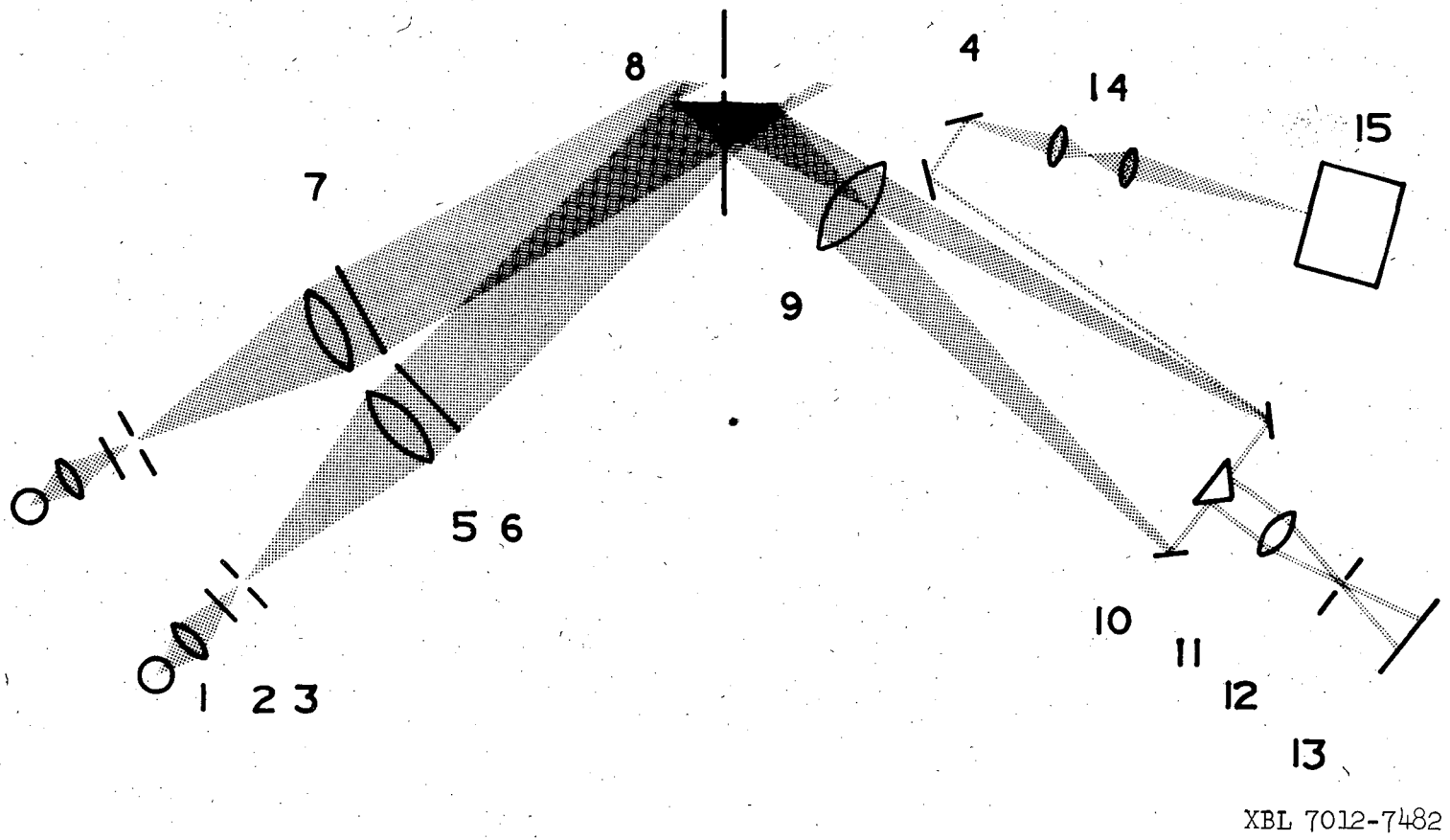

Fig. 35. Schematic diagram of optical bench.

A stero mirror system, placed ahead of the camera, was adjusted so that the two beams converged and crossed at the point where the source irisis were in focus. This is the point where the diameter of the beams is smallest. The diaphragm of the camera objective was placed at this point to prevent vignetting of the images.

The camera used was a Nikon F 35 mm body. This was used with a 400 nm objective formed by coupling two 800 mm achromatic, thin lenses. The camera and objective were mounted separately so that the camera could be removed to align the objective.

A gentle shutter release was necessary to prevent vibration from blurring the photos. A timer on the camera allowed 10 seconds to elapse between shutter release and setting the timer. The photographs were taken on Ektachrome color slide film balanced for 3200°K tungsten at 1/60 second exposure time.

To record the film-substrate combination, lettering that indicated the nominal angle of incidence, the sample number and the exposure setting was assembled on another optical bench as a caption. A system of mirrors and lenses brought the image of the caption in focus next to both images of the specimen surface.

The alignment procedures for the optical bench have been described by Turney.[2]

2. Chromaticity Values

Calculated chromaticity values* are shown in Figs. 36 through 47. For each film-substrate pair, there are two charts corresponding to s and p-polarizations of the incident light. The hue is purer the larger the displacement of a point on the curves from the region of white. Each point corresponds to a thickness of the dielectric film.

3. Color Series

From the chromaticity values, color series were determined at the angle of incidence of the observations. The observed and calculated color series are compared in Figs. 48 through 59. Film range is shown for the observed fringes. Color value derived from the Turney charts are also shown. The values of the optical path difference for passage of light through the film layer are indicated below the calculated and Turney color series. Interference colors from three different films are illustrated in Fig. 60.

The assumption of an interference order was made based on independent profile measurements. This was necessary to determine the range of ΔS which was applicable to the specimen.

C. Spectroscopy of Interference Colors

Figures 61 and 62 are diagrams of the spectrophotometer systems. Two photometers (Gamma Scientific Models 700 and 2020) were used. A fiber optics probe was place in the incident beam while the other was placed in the reflected beam. Only one source was used during a measurement.

*Fortran IV program Chrom was used. The value of δ_{TOT} calculated in this program is the same for the convention of electric field vector directions adopted at the Nebraska convention.

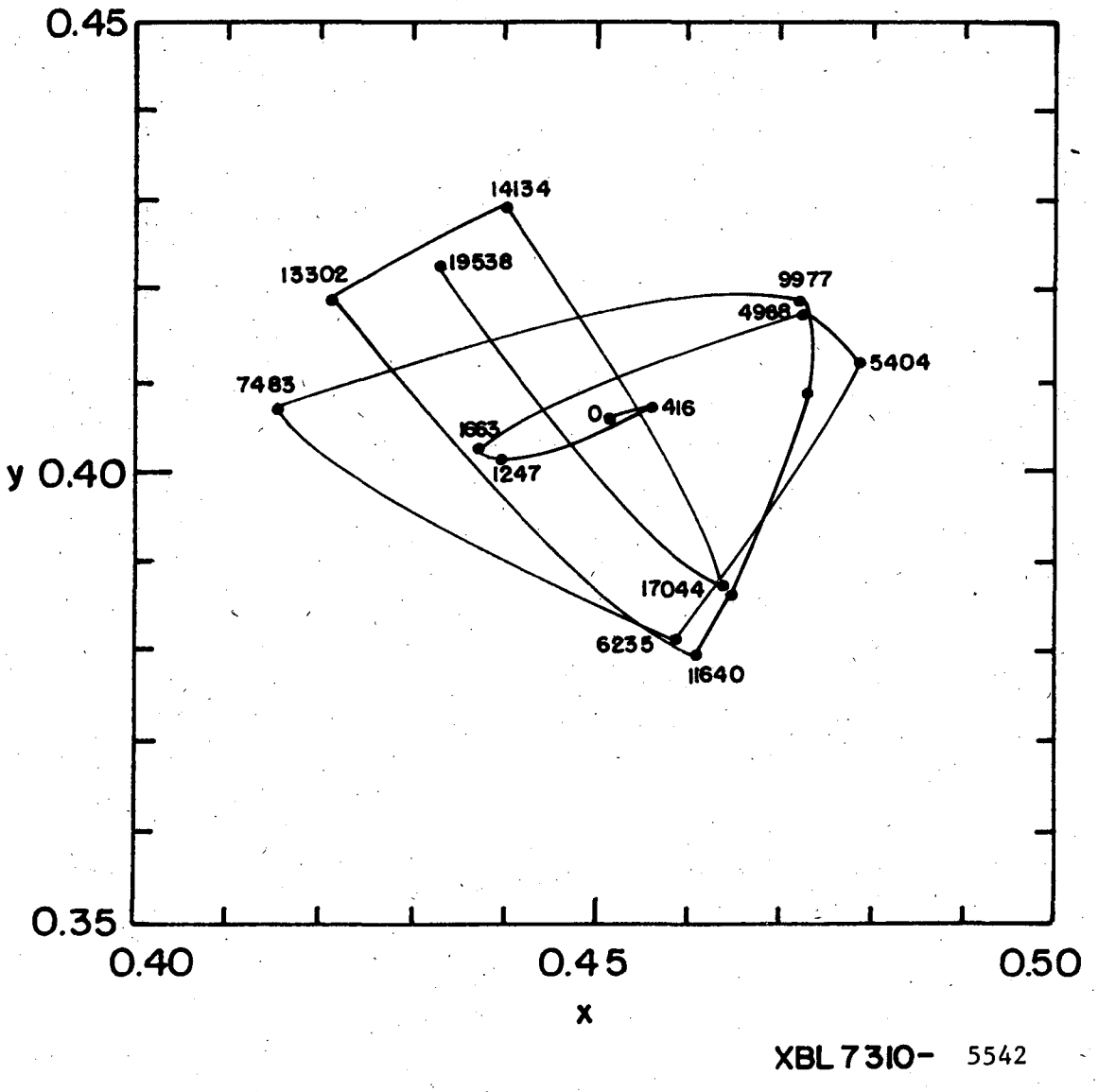

Fig. 36. Chromaticities of ZnS film on aluminum substrate for p-component of light. ϕ=80°, δ_{TOT}=240.00° and $r_{p,1}$=0.88. Points indicate the optical path difference, ΔS in Å.

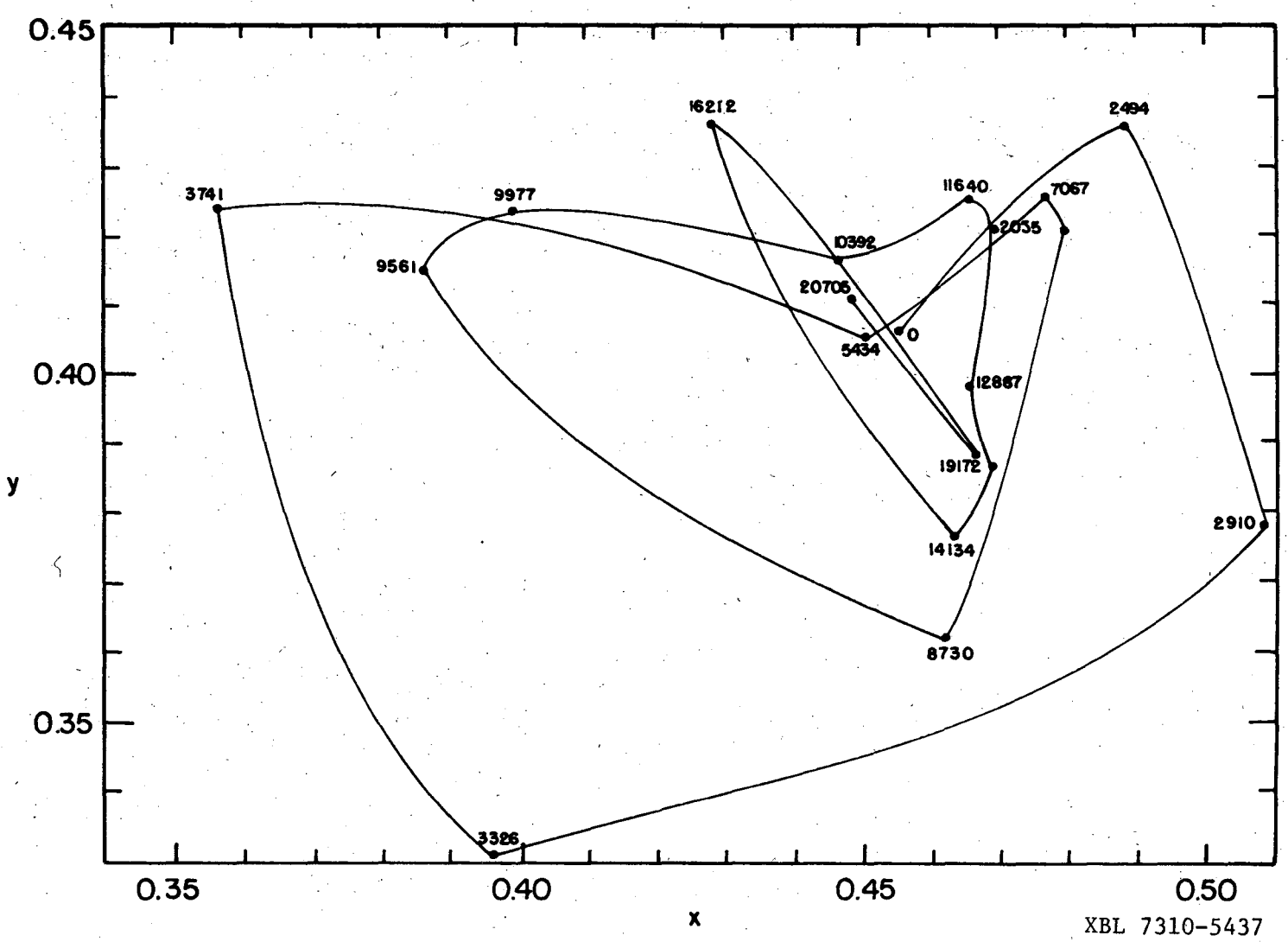

Fig. 37. Chromaticities of ZnS film on aluminum substrate for s-component of light. ϕ=80°, δ_{TOT}=30.00° and $r_{s,1}$=0.90.

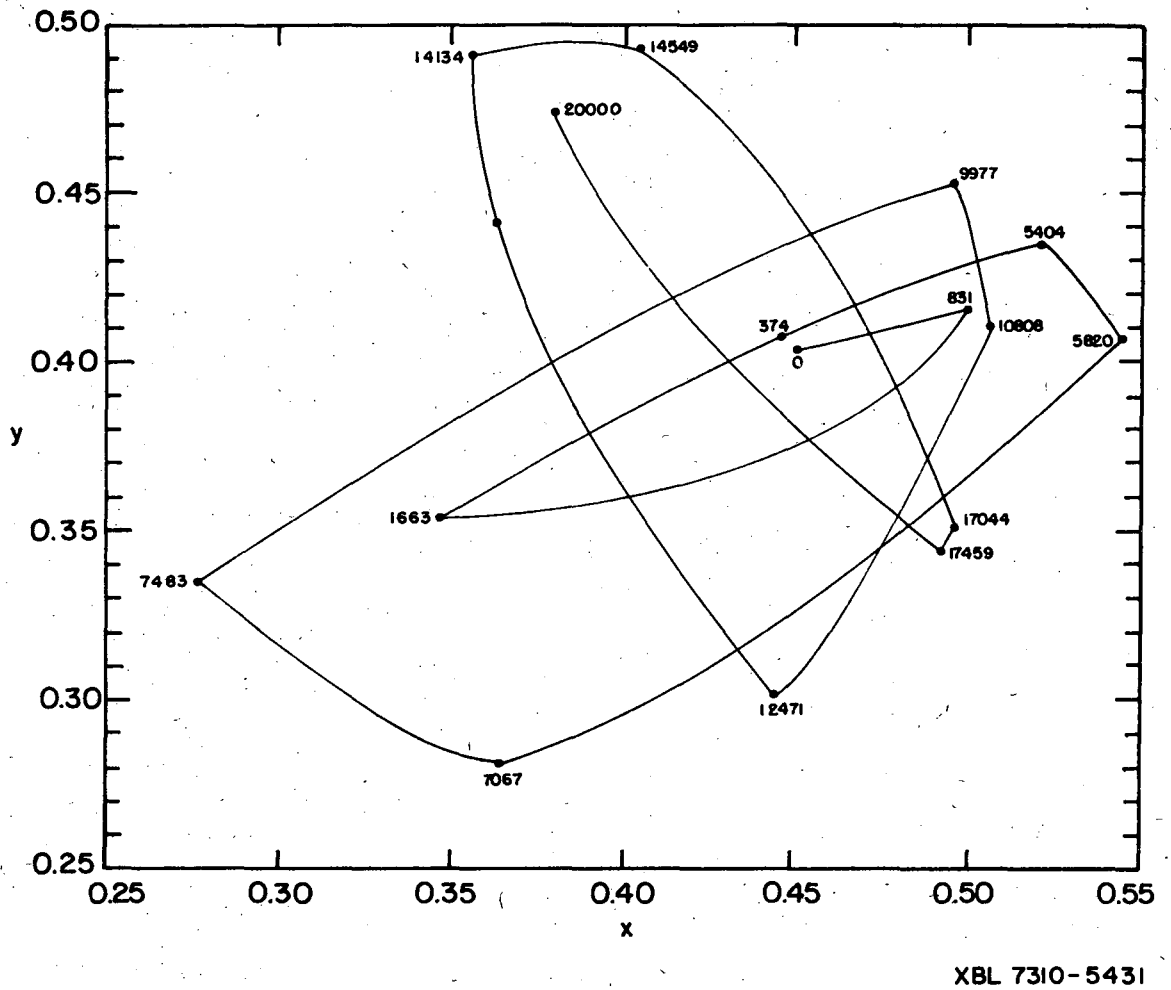

Fig. 38. Chromaticities of ZnS film on chromium substrate for p-component of light. ϕ=80°, δ_{TOT}=270.00° and r_{pl}=0.56.

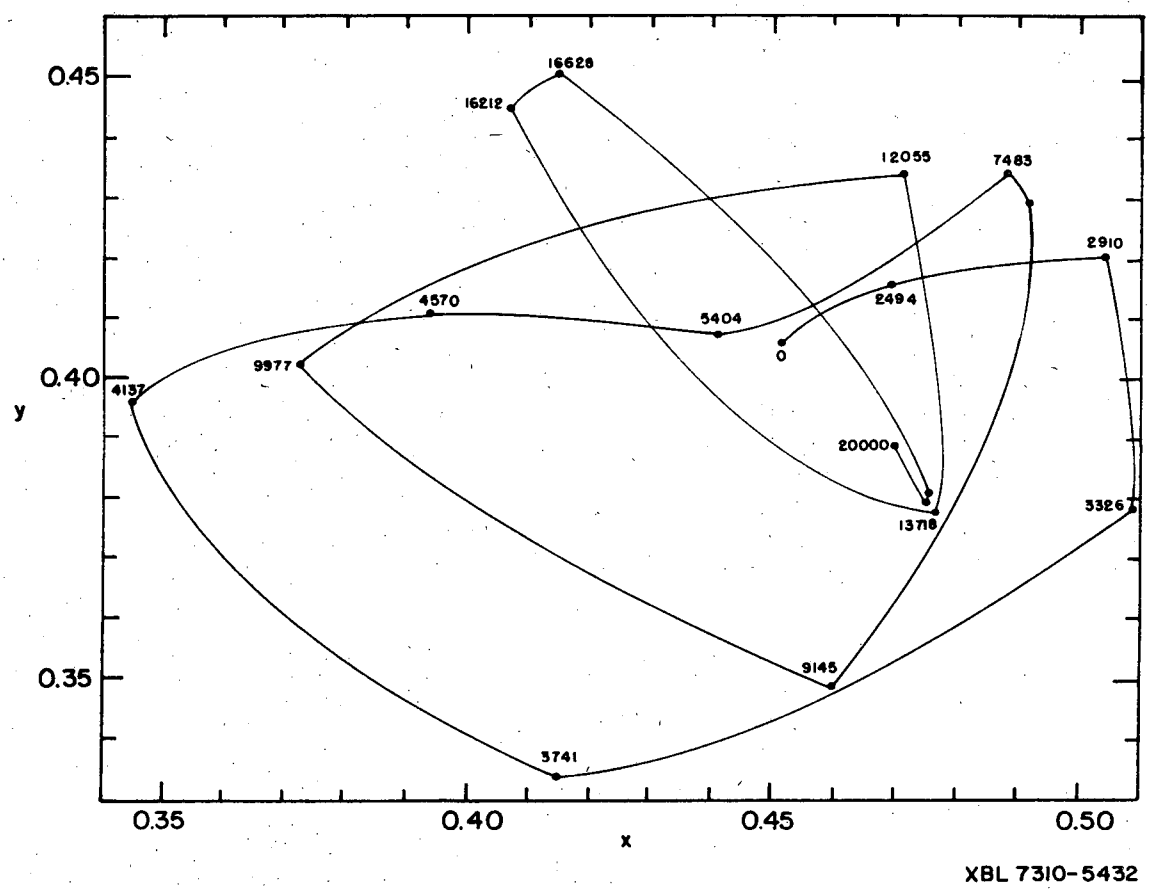

Fig. 39. Chromaticities of ZnS film on chromium substrate for s-component of light. ϕ=80°, δ_{TOT}=60.00 and r_{s1}=0.64

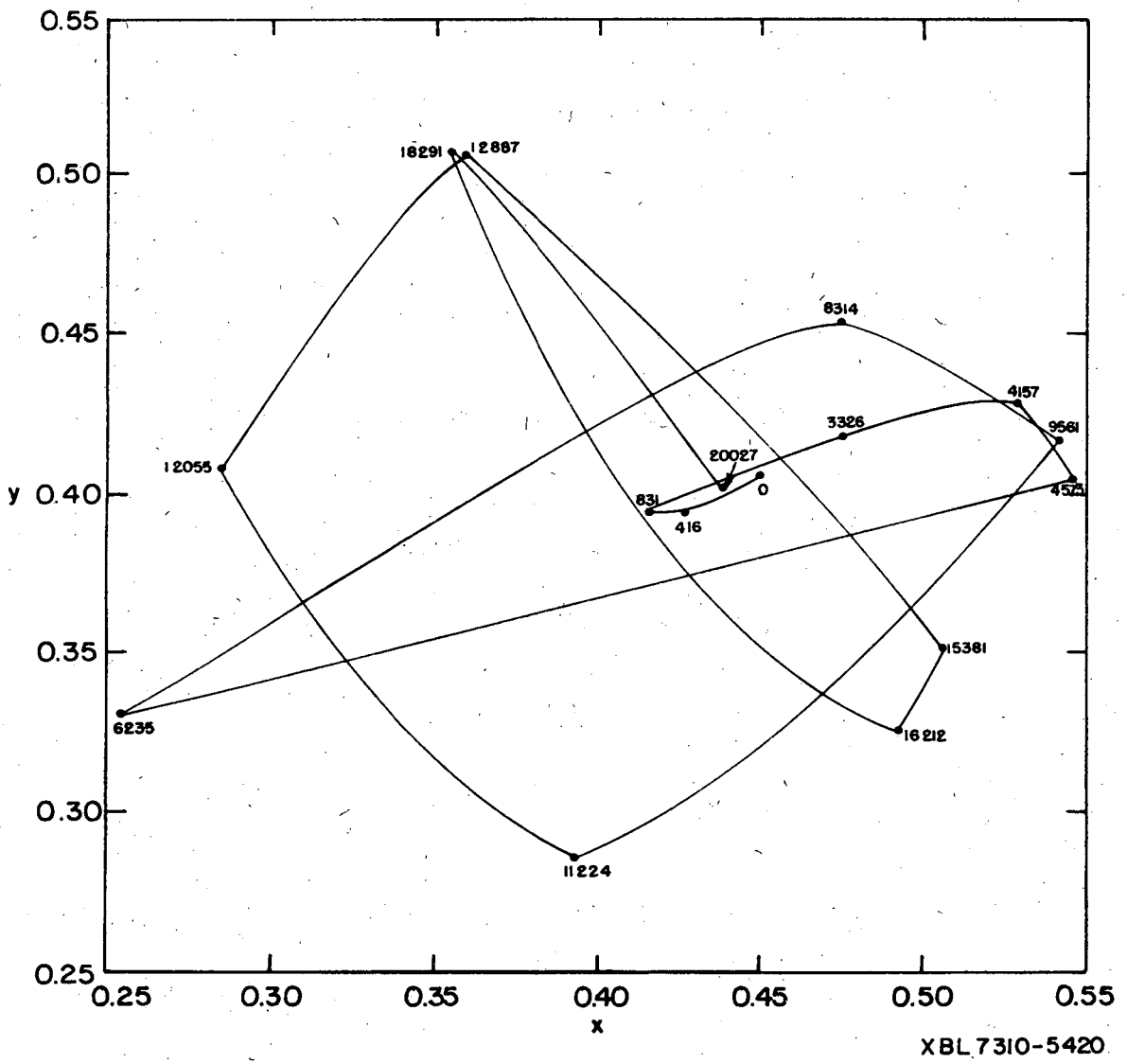

Fig. 40. Chromaticities of ZnS film on silicon substrate for p-component of light. ϕ=80°, δ_{TOT}=180.00°, r_{pl}=0.26.

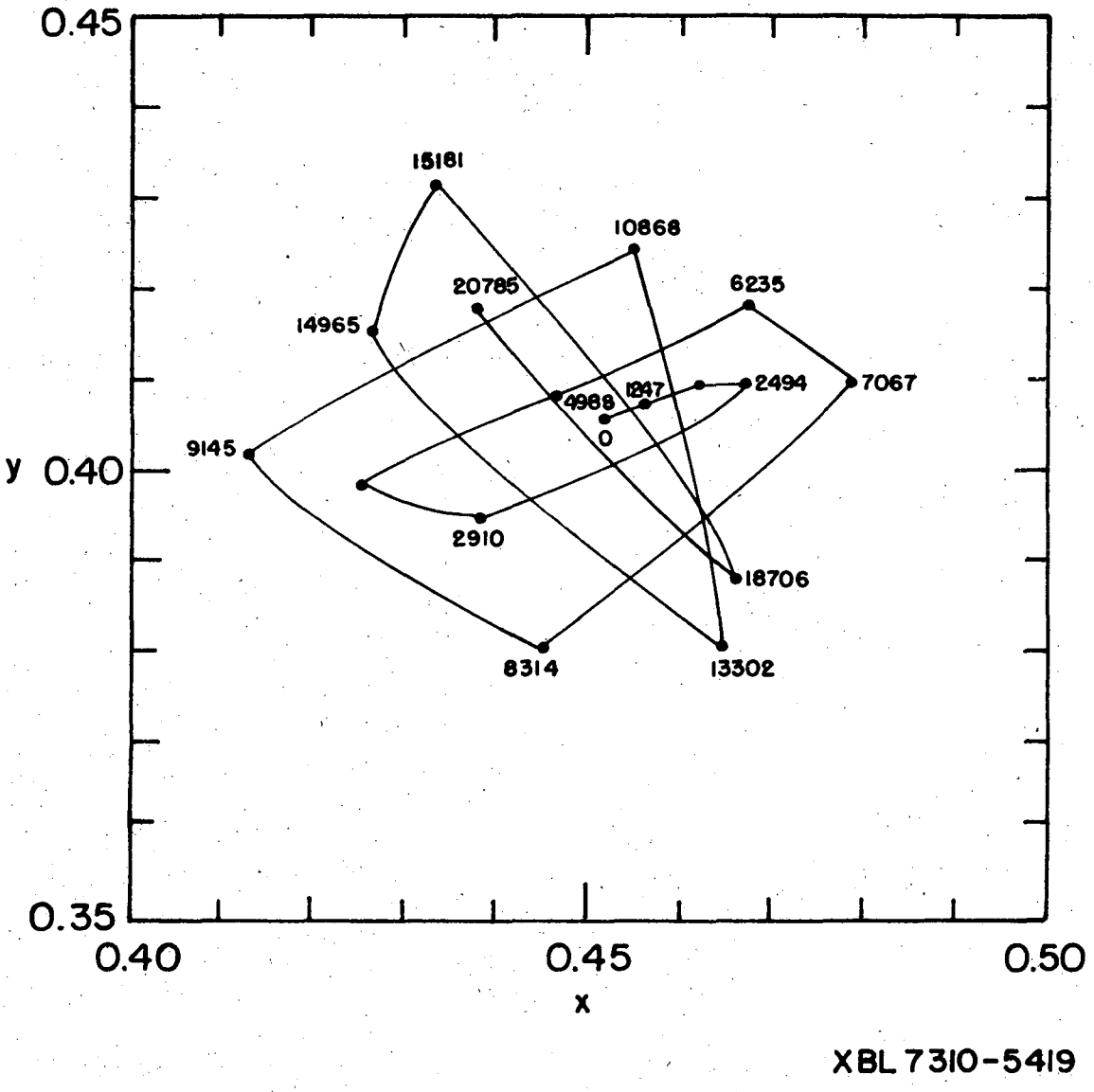

Fig. 41. Chromaticities of ZnS film on silicon substrate for s-component of light. ϕ=80°, δ_{TOT}=0.00°, r_{s1}=0.32.

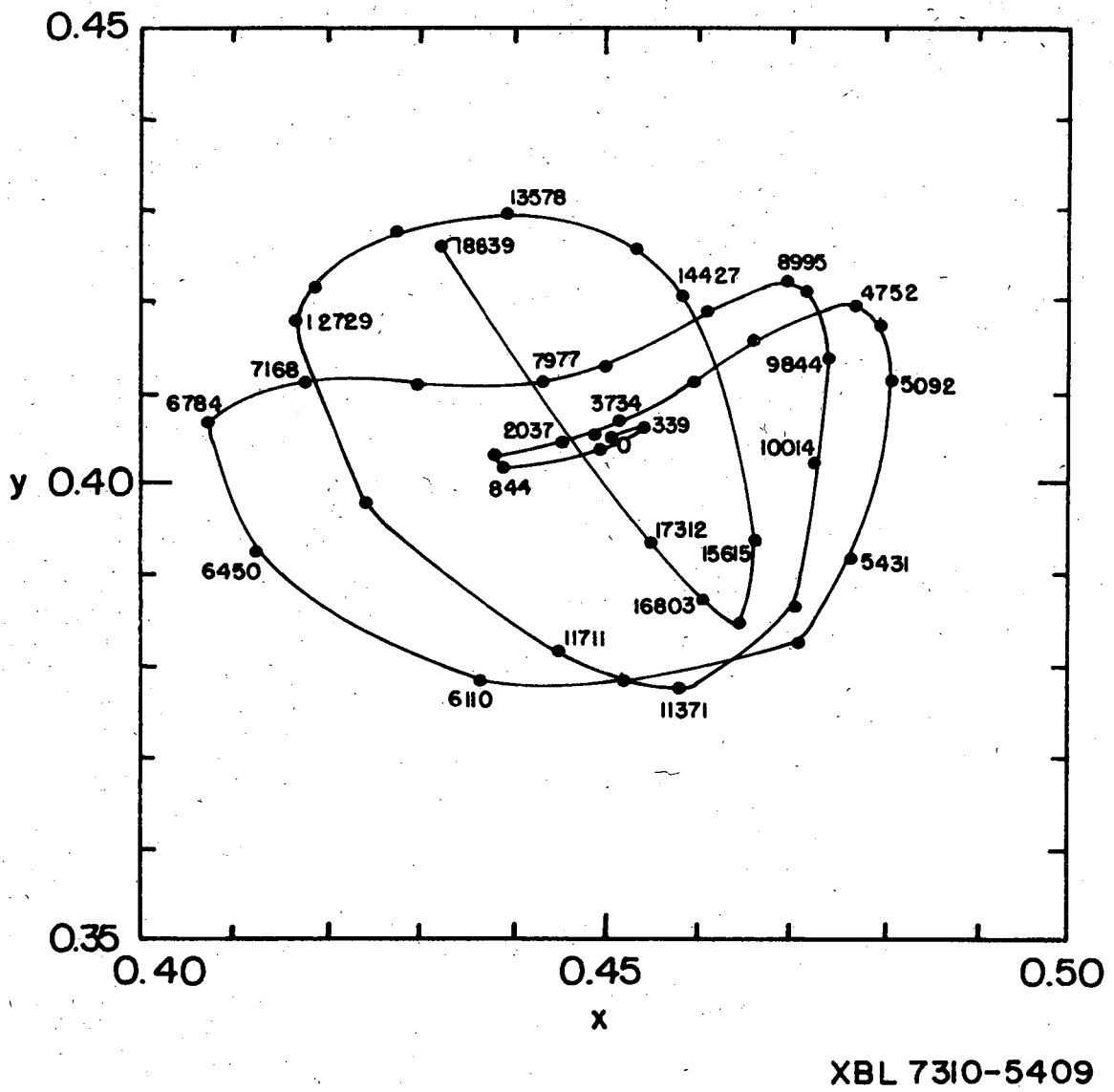

Fig. 42. Chromaticities of cryolite film on aluminum for p-component of light. ϕ=80°, δ_{TOT}=210.00°, r_{pl}=0.90.

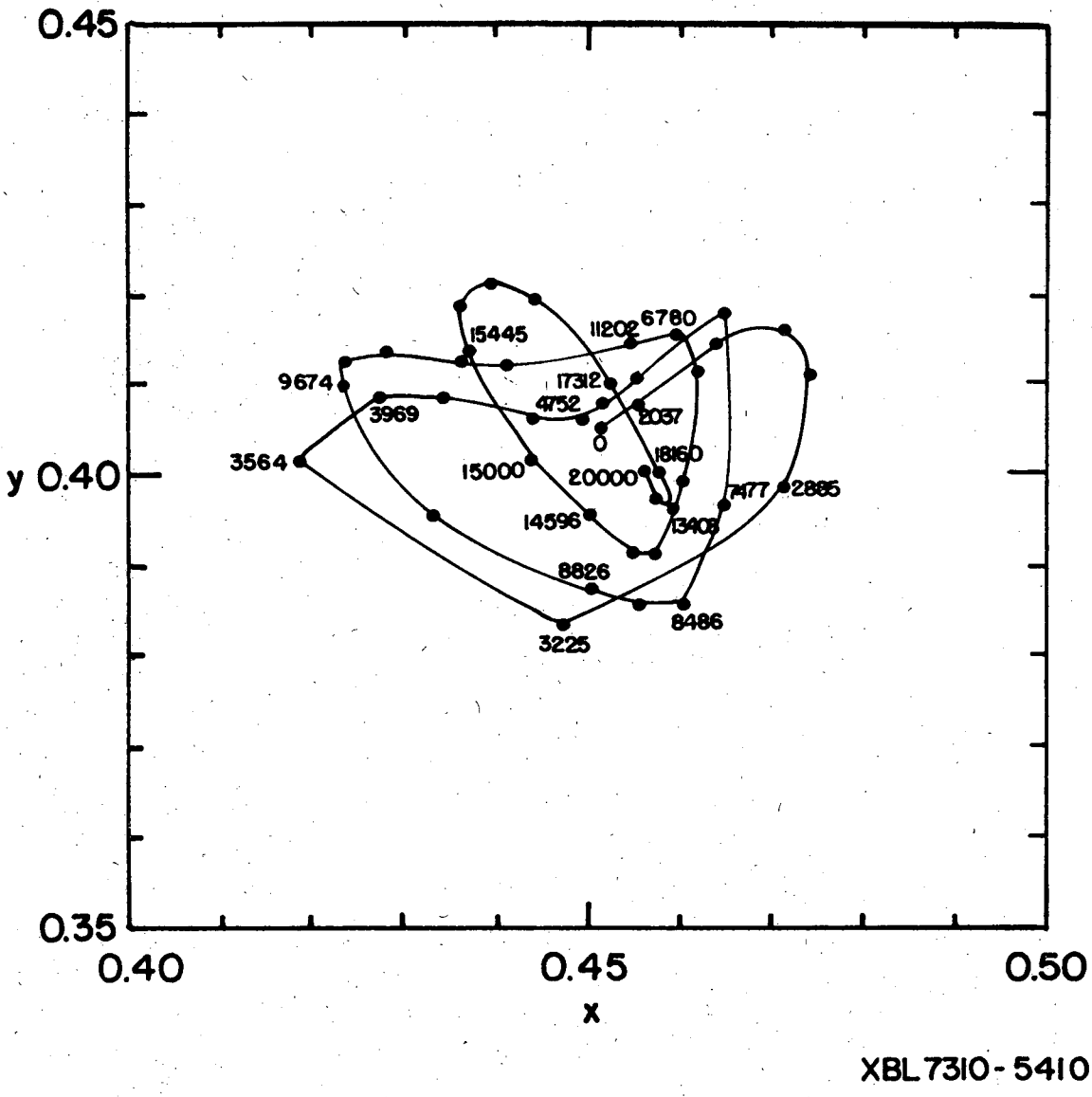

Fig. 43. Chromaticities of cryolite film on aluminum substrate for s-component of light. ϕ=80°, δ_{TOT}=30.00°, r_{sl}=0.95.

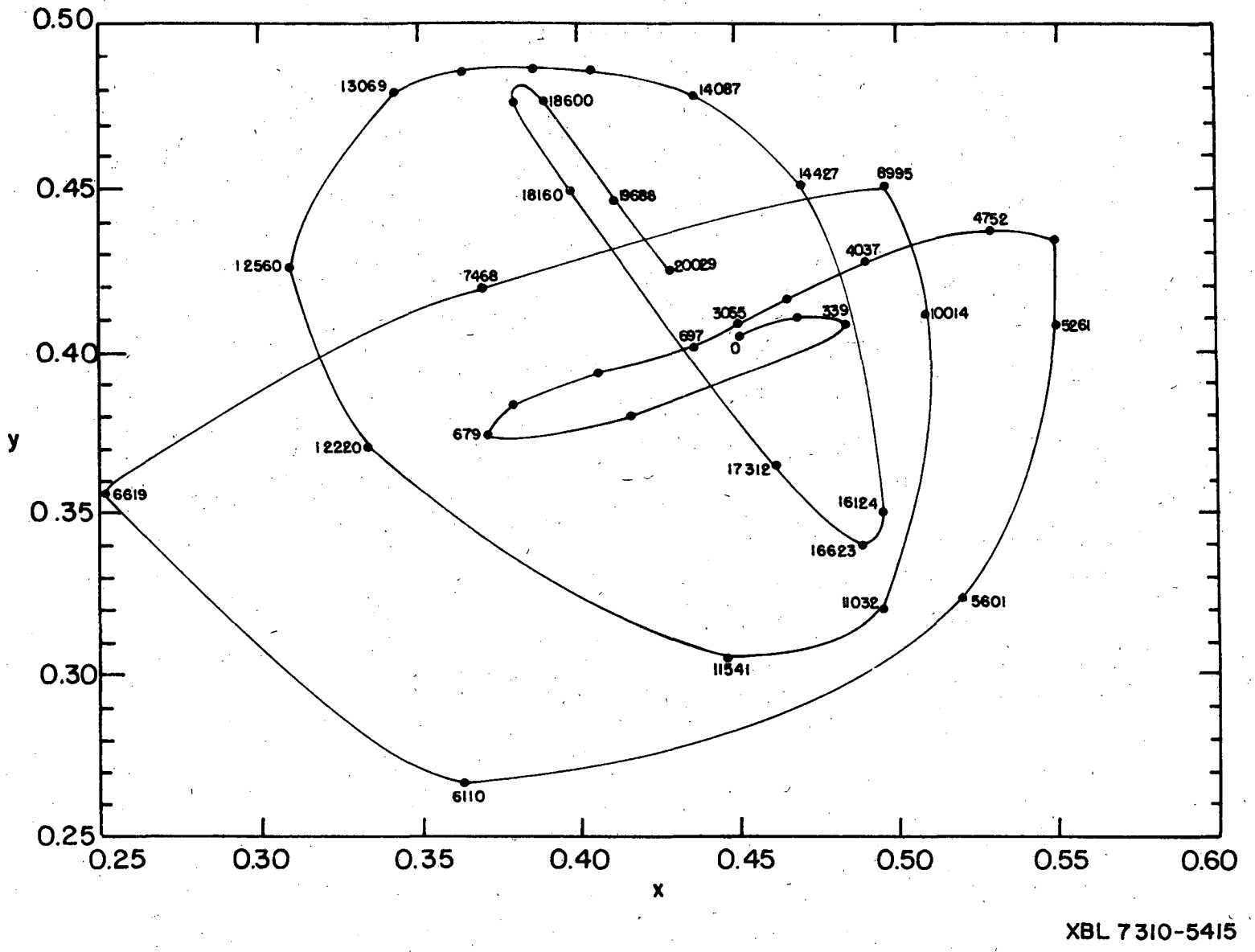

Fig. 44. Chromaticities of cryolite film on chromium substrate for p-component of light. $\phi=80°$, $\delta_{TOT}=210.00°$, $r_{pl}=0.61$.

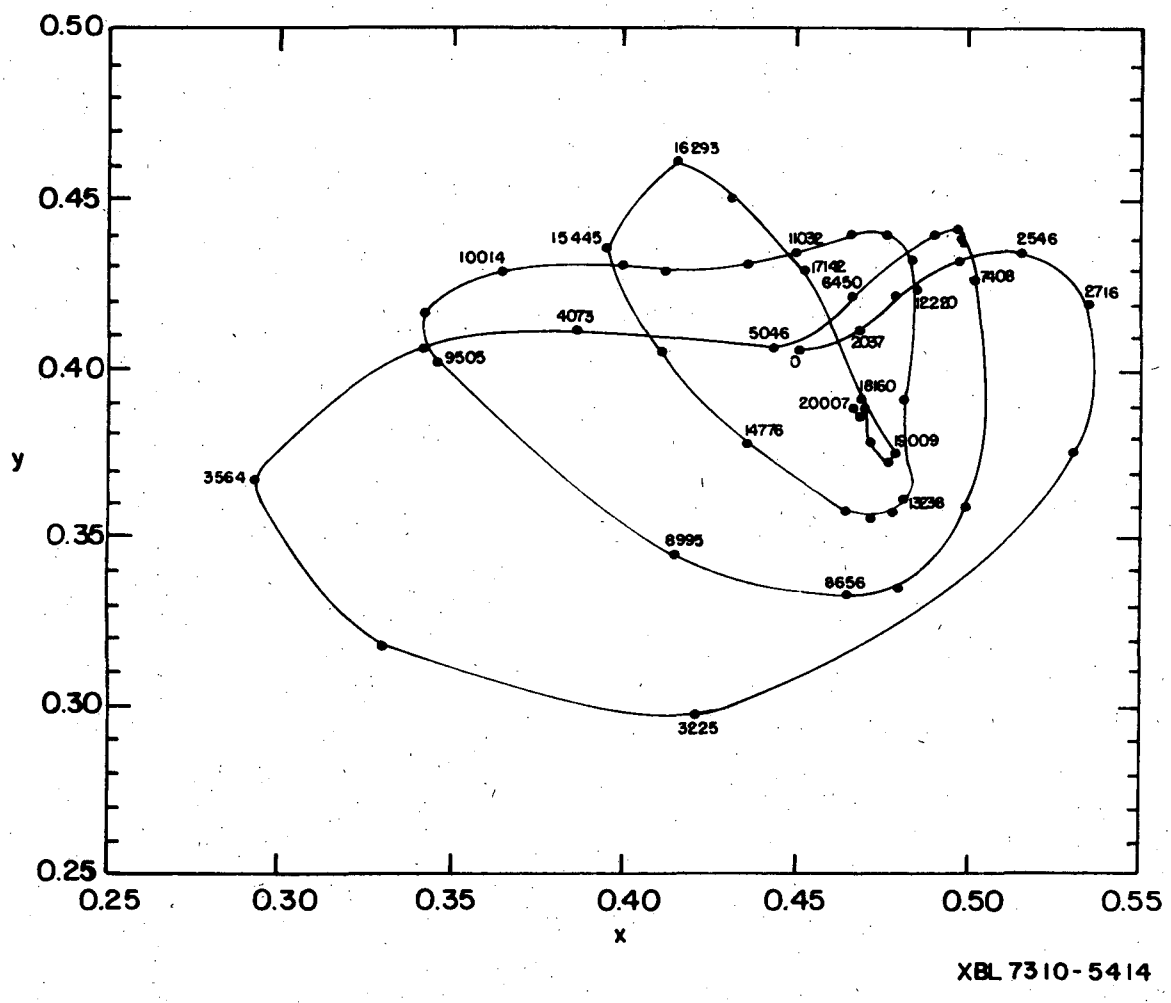

Fig. 45. Chromaticities of cryolite film on chromium substrate for s-component of light. $\phi=80°$, $\delta_{TOT}=30.00°$, $r_{sl}=0.81$.

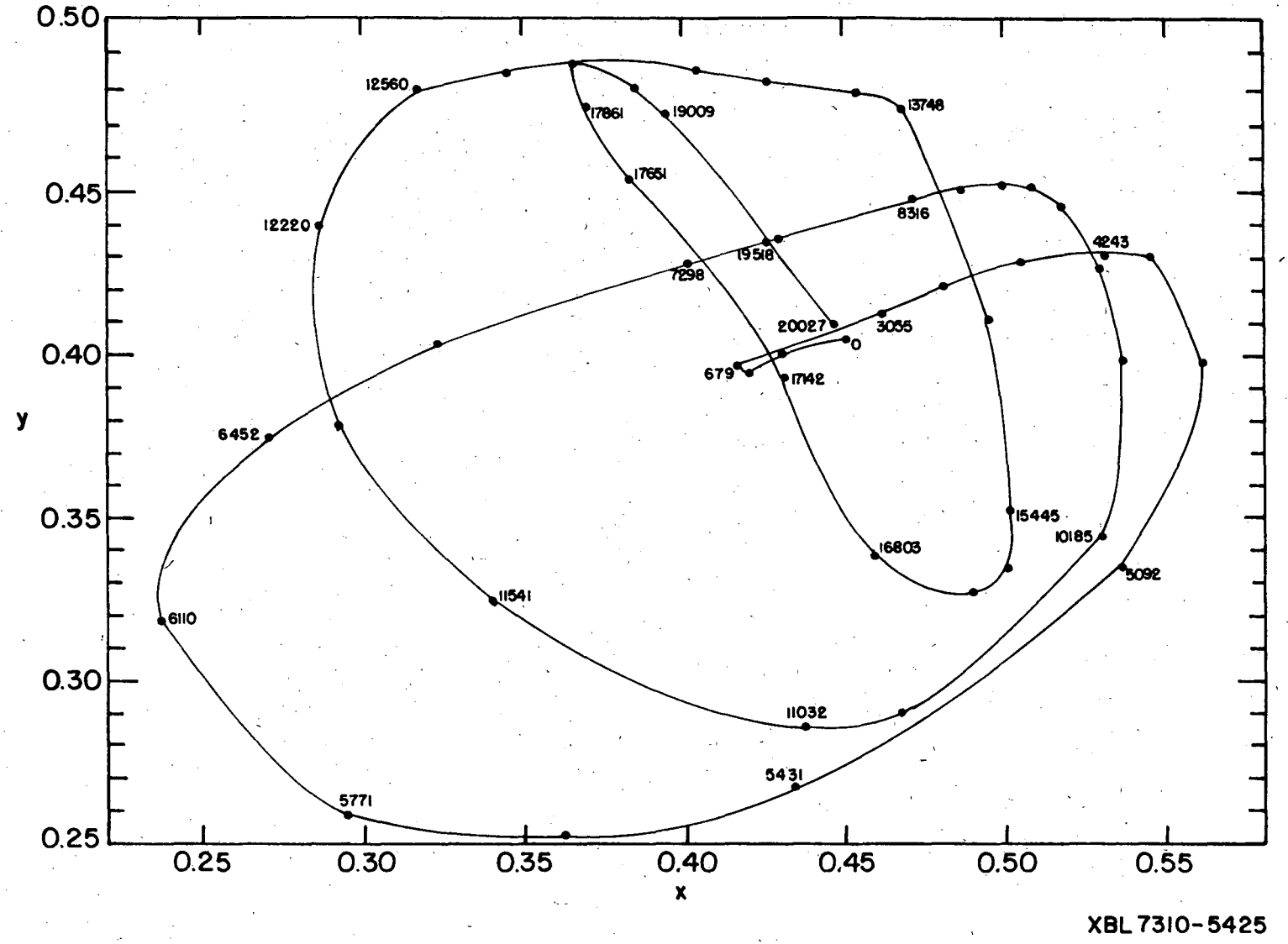

Fig. 46. Chromaticities of cryolite film on silicon substrate for p-component of light. $\phi=80°$, $\delta_{TOT}=180.00$, $r_{p1}=0.36$.

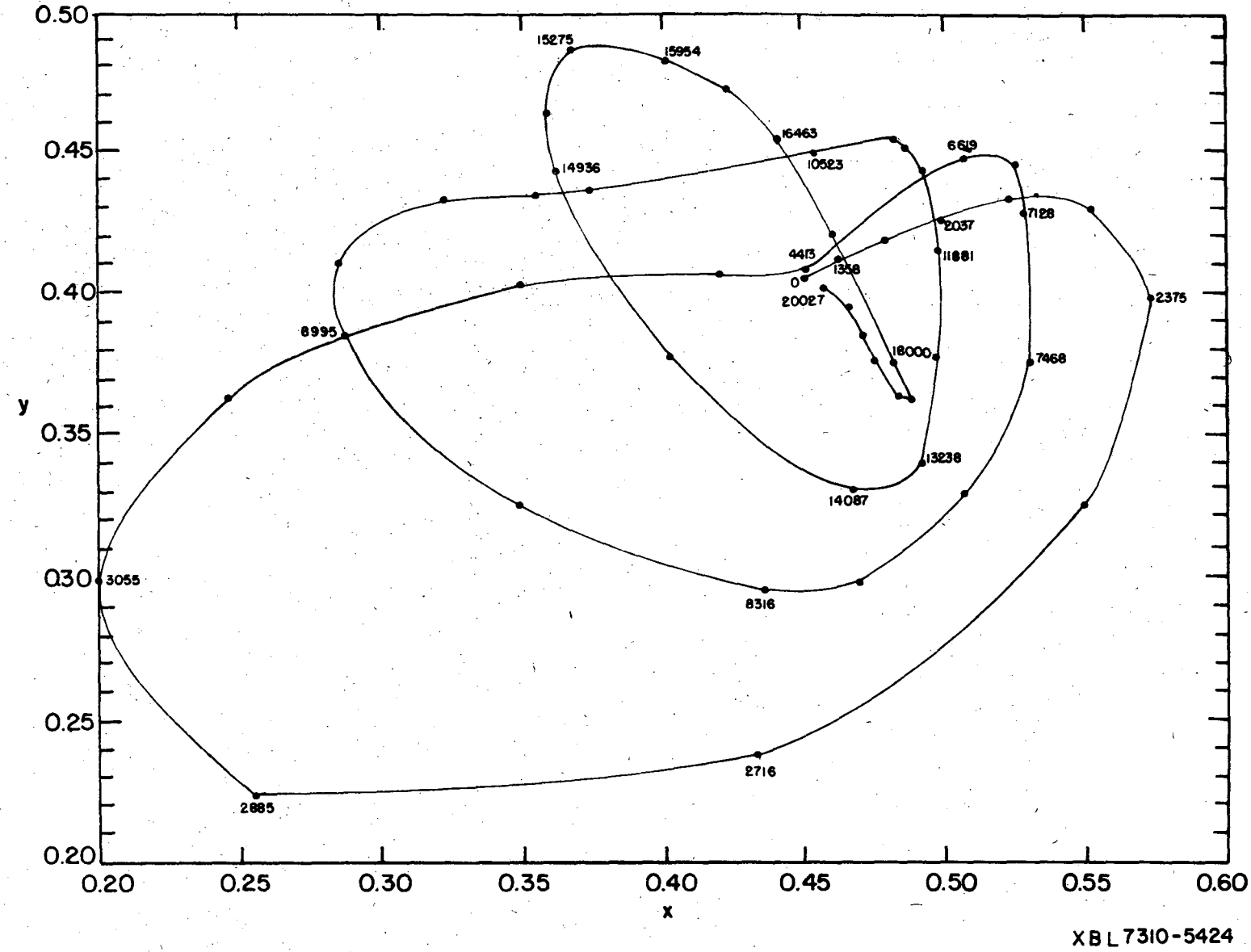

Fig. 47. Chromaticities of cryolite film on silicon substrate for s-component of light. $\phi=80°$, $\delta_{TOT}=0.00°$, $r_{s1}=0.65$.

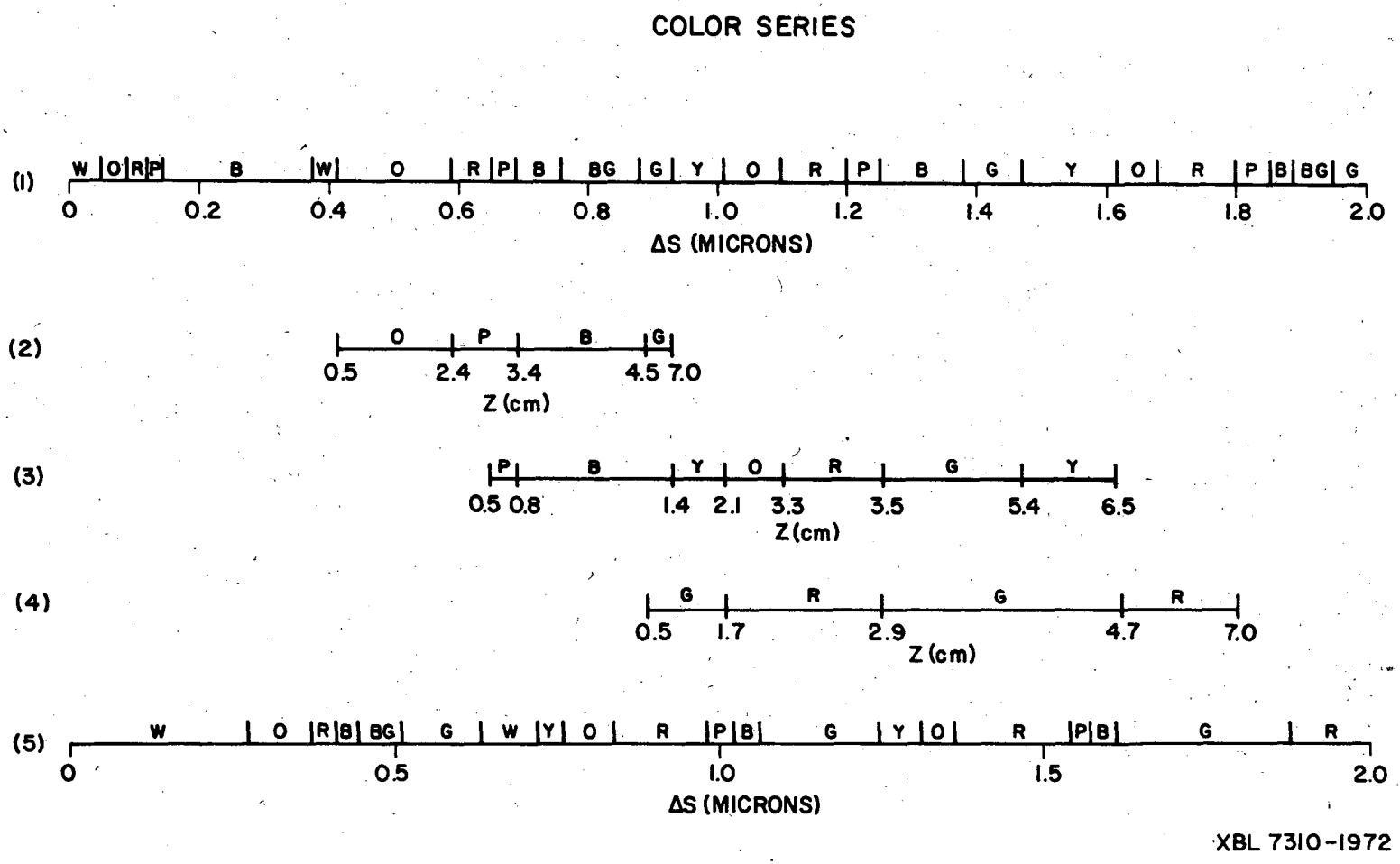

Fig. 48. Color series for ZnS films on chromium, p-polarization. (1) Present, calculated series: δ_{TOT}=270.00 (deg), r_{pl}=0.56, ϕ=80°. (2) Observed series, sample 1. (3) Observed series, sample 2. (4) Observed series, sample 3. (5) Previous series according to Turney: δ_{TOT}=270.00 (deg), r_{pl}=0.60. Film thickness, d = 0.241× ΔS.

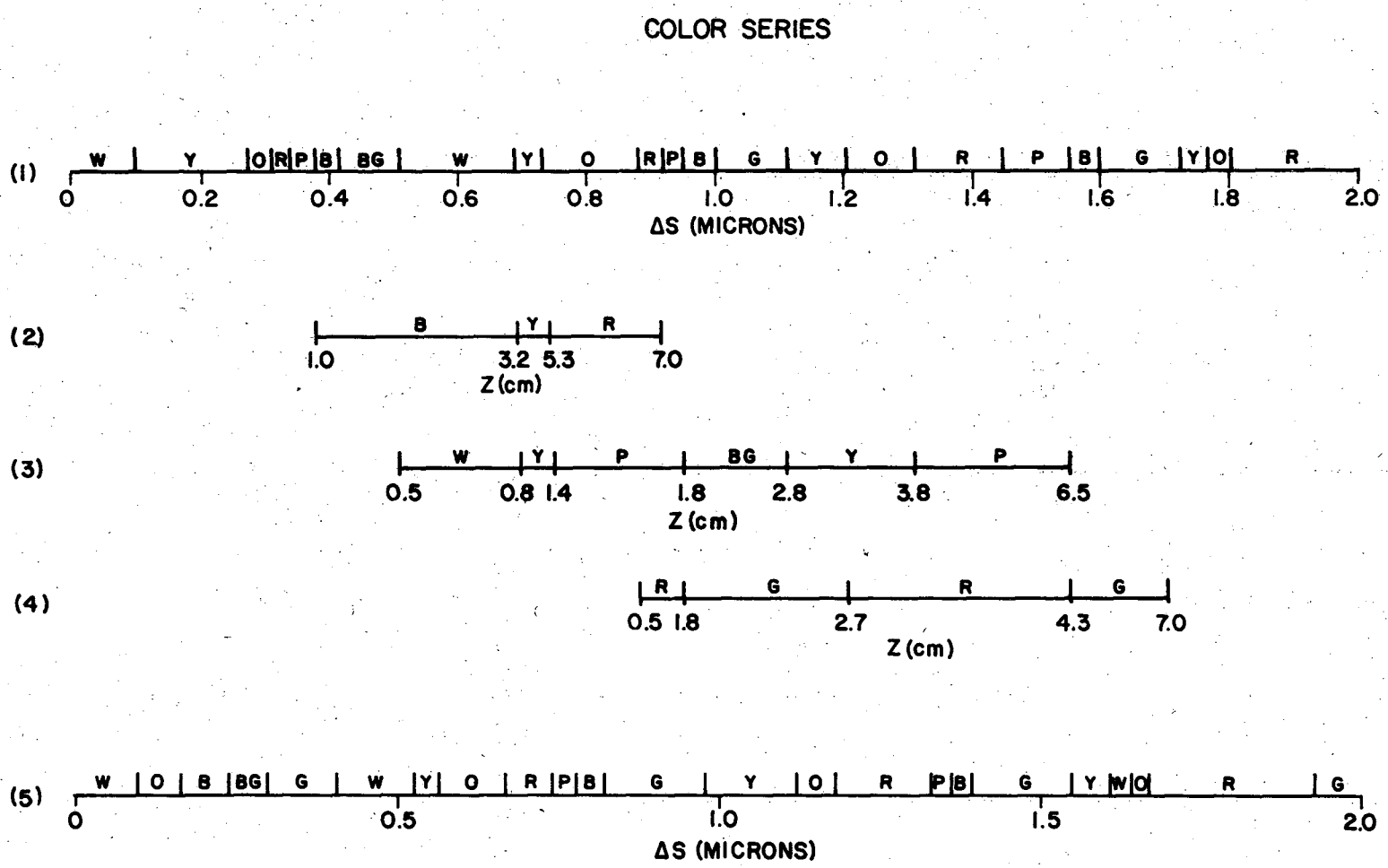

Fig. 49. Color series for ZnS films on chromium s-polarization. (1) Present, calculated series: δ_{TOT}=60.00 (deg), r_{s1}=0.63, ϕ=80 (deg). (2) Observed series, sample 1. (2) Observed series, sample 2. (4) Observed series, sample 3. (5) Previous series according to Turney: δ_{TOT}=60.00 (deg), r_{s1}=0.60. Film thickness, d = 0.241× ΔS

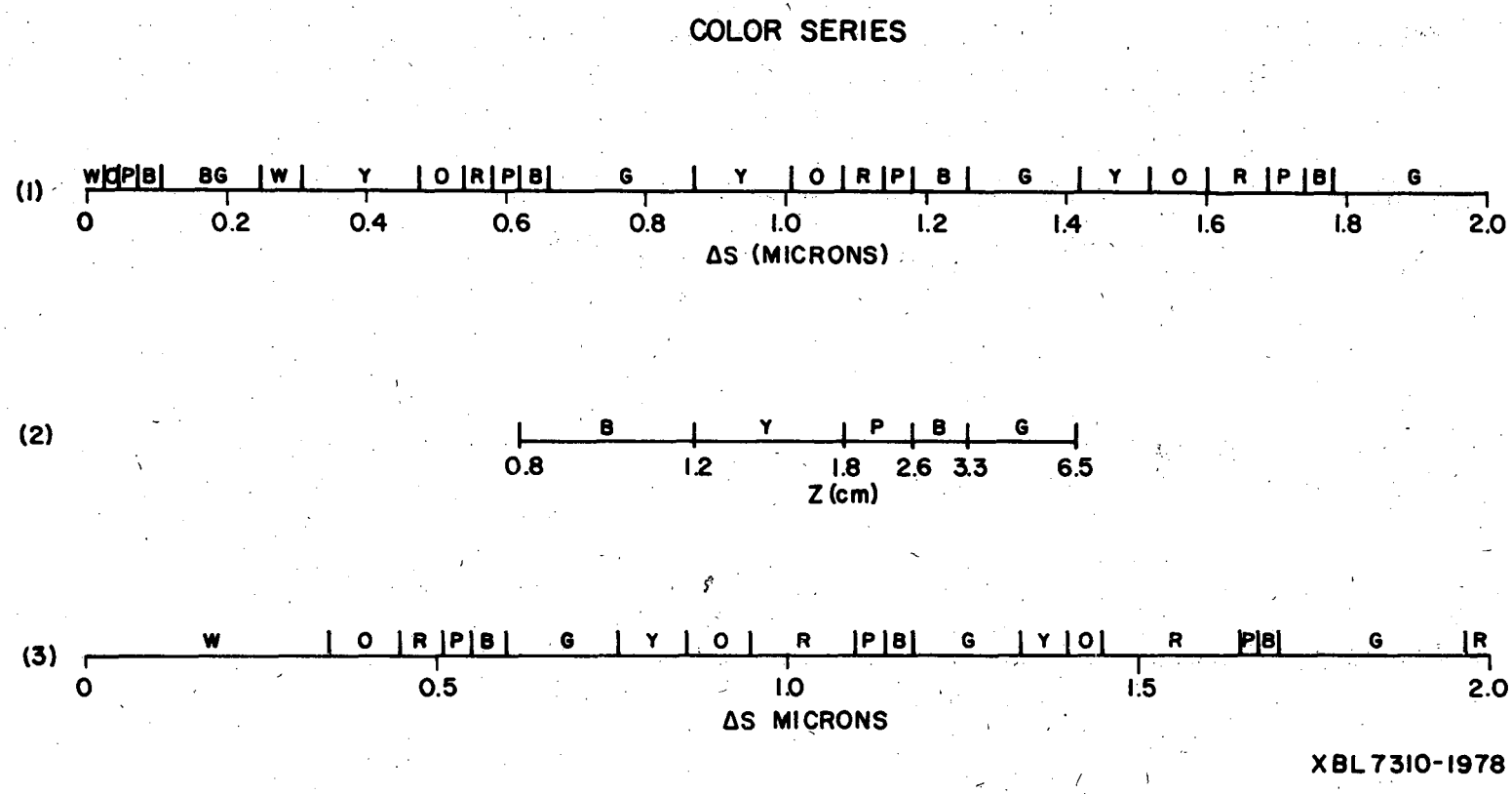

Fig. 50. Color series for cryolite films on chromium p-polarization. (1) Present, calculated series: δ_{TOT}=210.00 (deg), r_{pl}=0.61, ϕ=80 (deg). (2) Observed series. (3) Previous series according to Turney: δ^{pl}_{TOT}=210.00 (deg), r_{pl}=0.60. Film thickness, d = 0.588× ΔS.

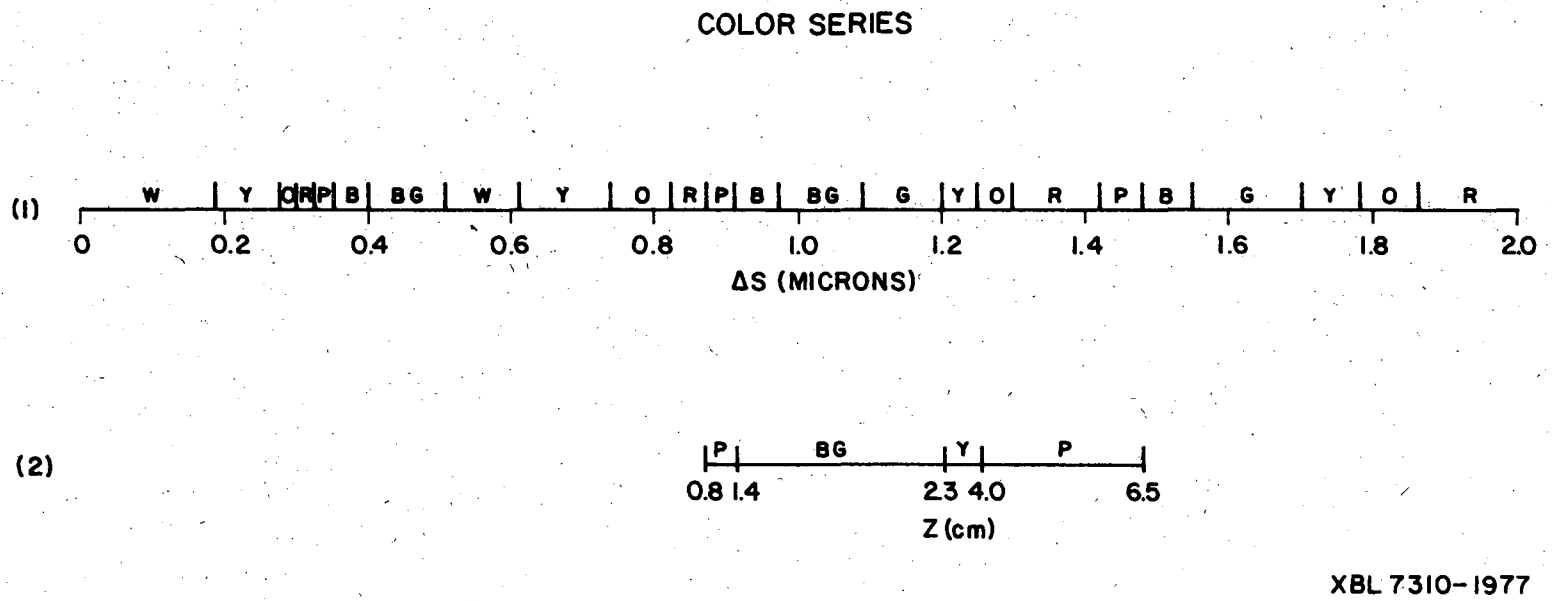

Fig. 51. Color series for cryolite films on chromium for s-polarization. (1) Present, calculated series: δ_{TOT}=30.00 (deg), r_{s1}=0.81, ϕ=80 (deg). (2) Observed series.

Turney charts do not cover high-reflectance. Film thickness, d = 0.588× ΔS.

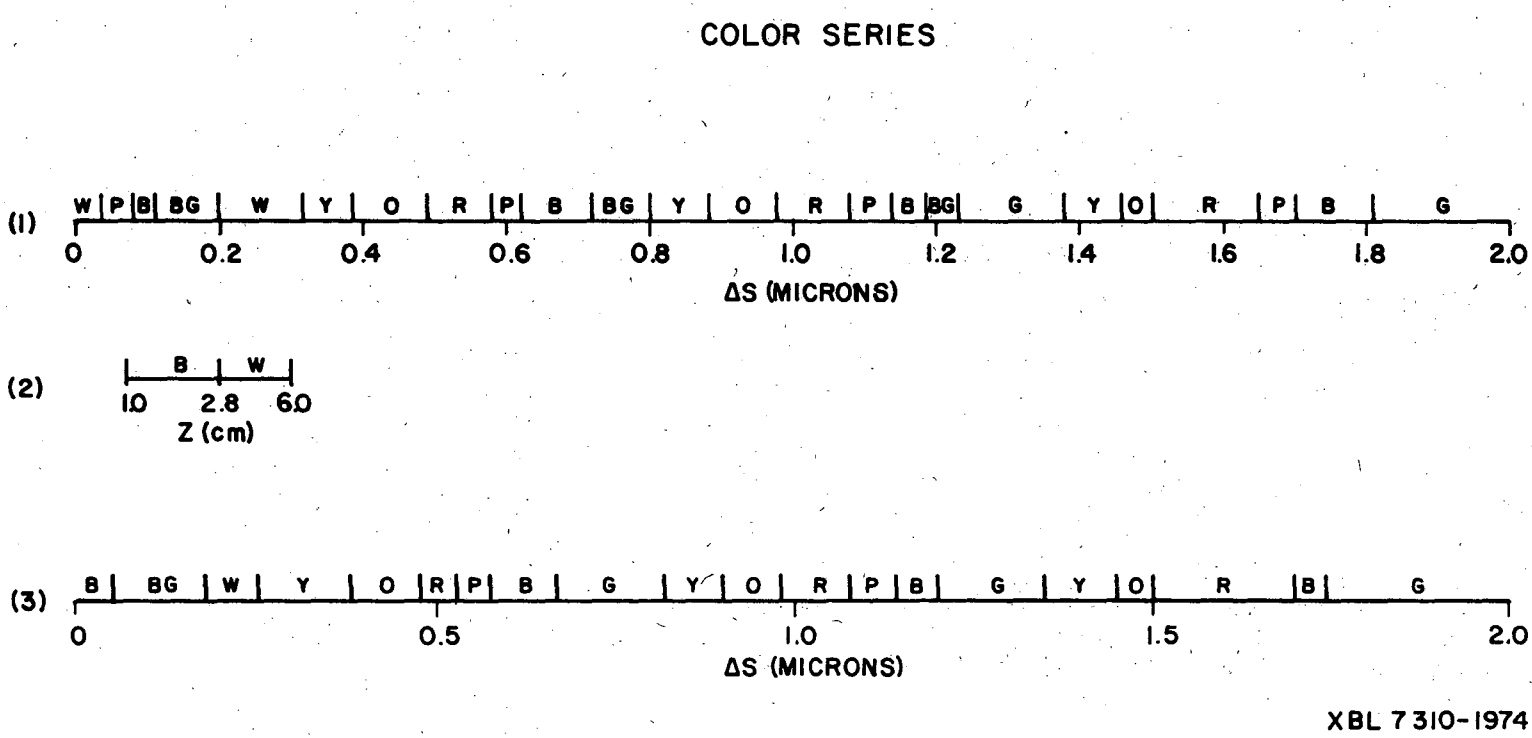

Fig. 52. Color series for ZnS films on silicon p-polarization.
(1) Present, calculated series: δ_{TOT}=180.00 (deg), r_{p1}=0.26, ϕ=80
(2) Observed series
(3) Previous series according to Turney: δ_{TOT}=180.00, r_{p1}=0.20
Film thickness, d = 0.241× ΔS.

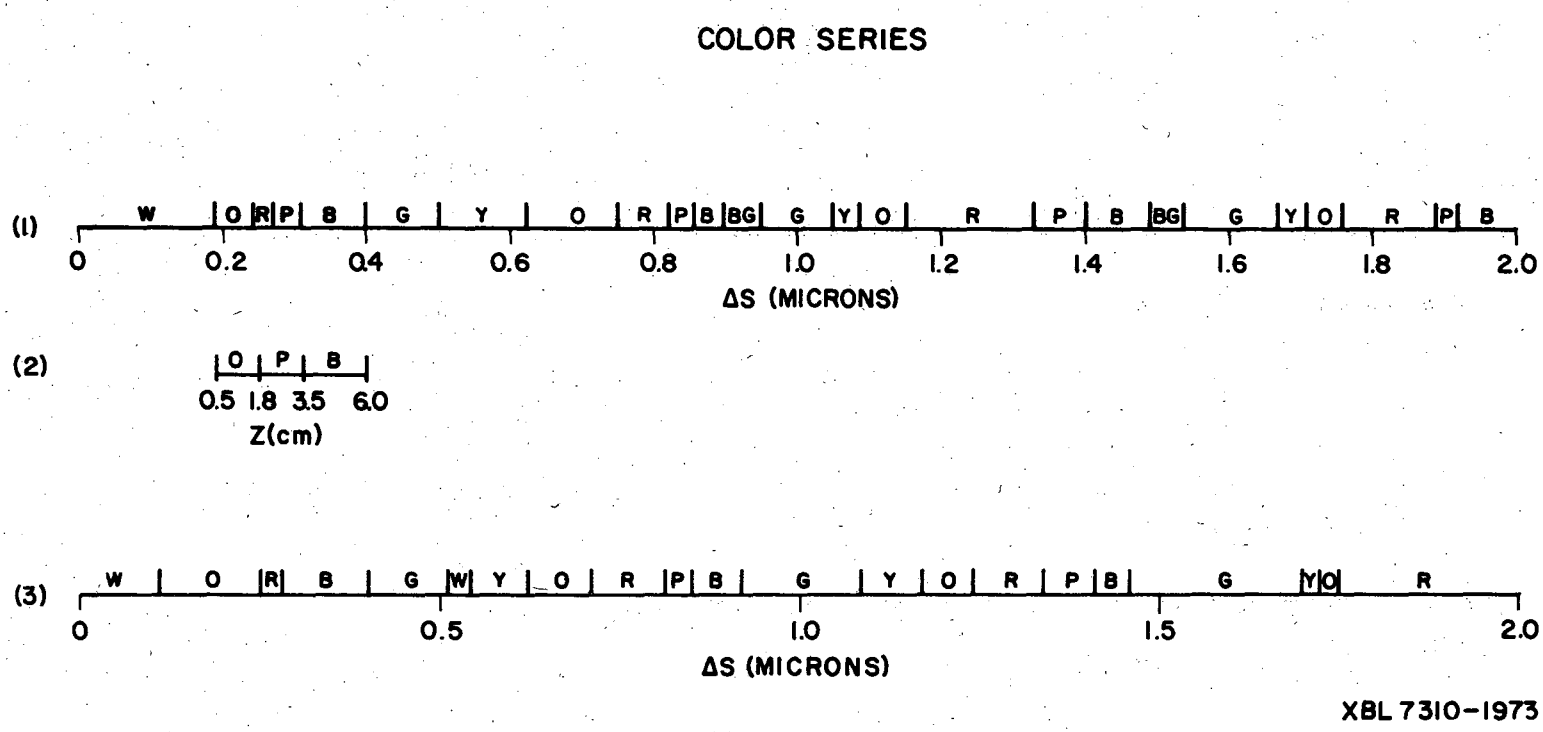

Fig. 53. Color series for ZnS film on silicon s-polarization. (1) Present, calculated series: δ_{TOT}=0.00 (deg), r_{s1}=0.32, ϕ=80 (deg). (2) Observed series. (3) Previous series according to Turney: δ_{TOT}=0.00 (deg), r_{s1}=0.20. Film thickness, d = 0.241× ΔS.

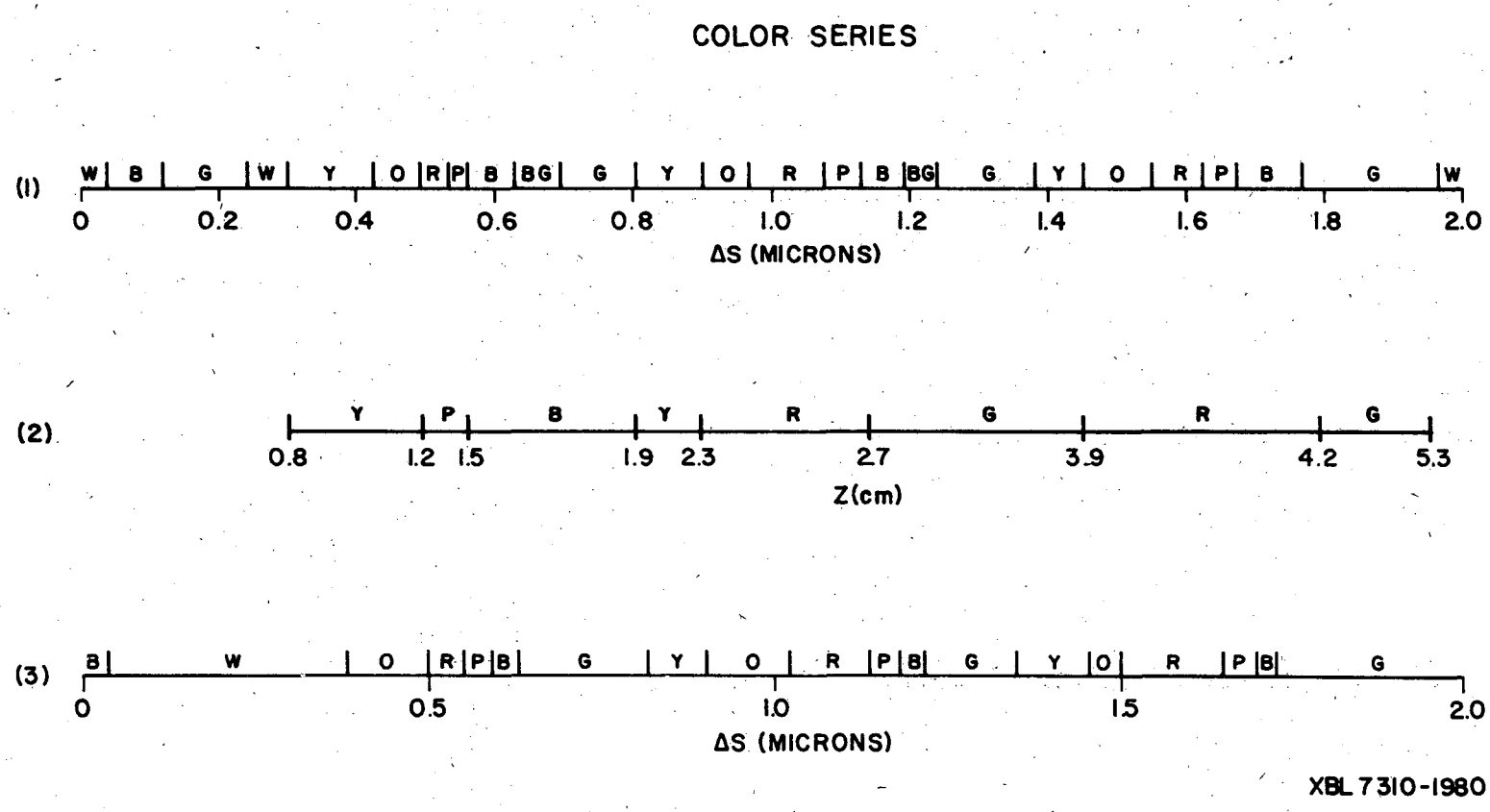

Fig. 54. Color series for cryolite films on silicon p-polarization. (1) Present, calculated series: ϕ_{TOT}=180.00 (deg), r_{p1}=0.49, ϕ=80 (deg). (2) Observed series. (3) Previous series according to Turney: δ_{TOT}=180.00 (deg), r_{p1}=0.60. Film thickness, d = 0.588× ΔS.

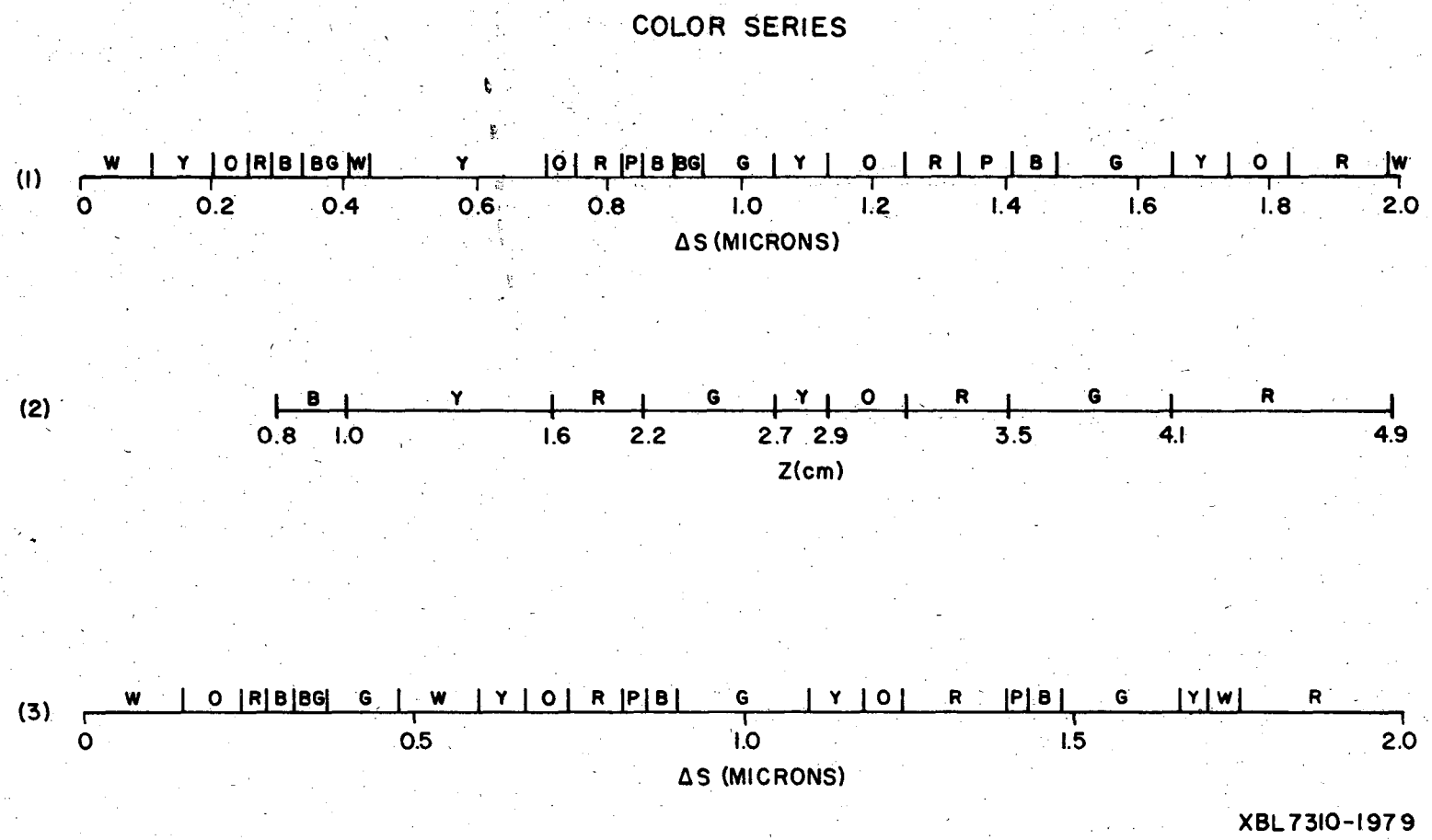

Fig. 55. Color series for cryolite films on silicon s-polarization. (1) Present, calculated series: δ_{TOT}=0.00 (deg), r_{s1}=0.65, ϕ=85 (deg). Film thickness, d = 0.588× ΔS.

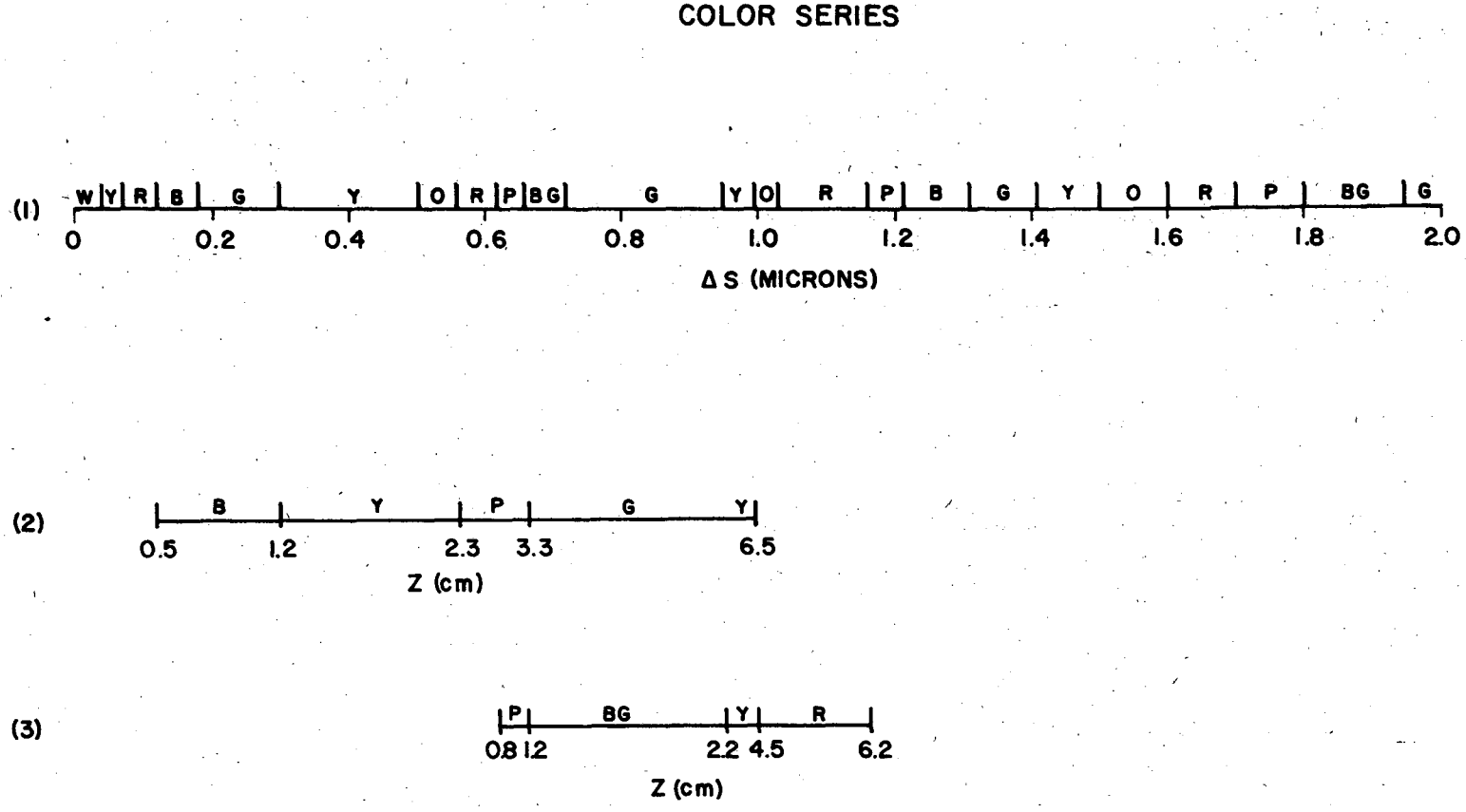

Fig. 56. Color series for ZnS films on aluminum p-polarization. (1) Present, calculated series: δ_{TOT}=240.00 (deg), r_{pl}=0.88, ϕ=80 (deg). (2) Observed series, sample 1. (3) Observed series, sample 2. Film thickness, d = 0.241× ΔS.

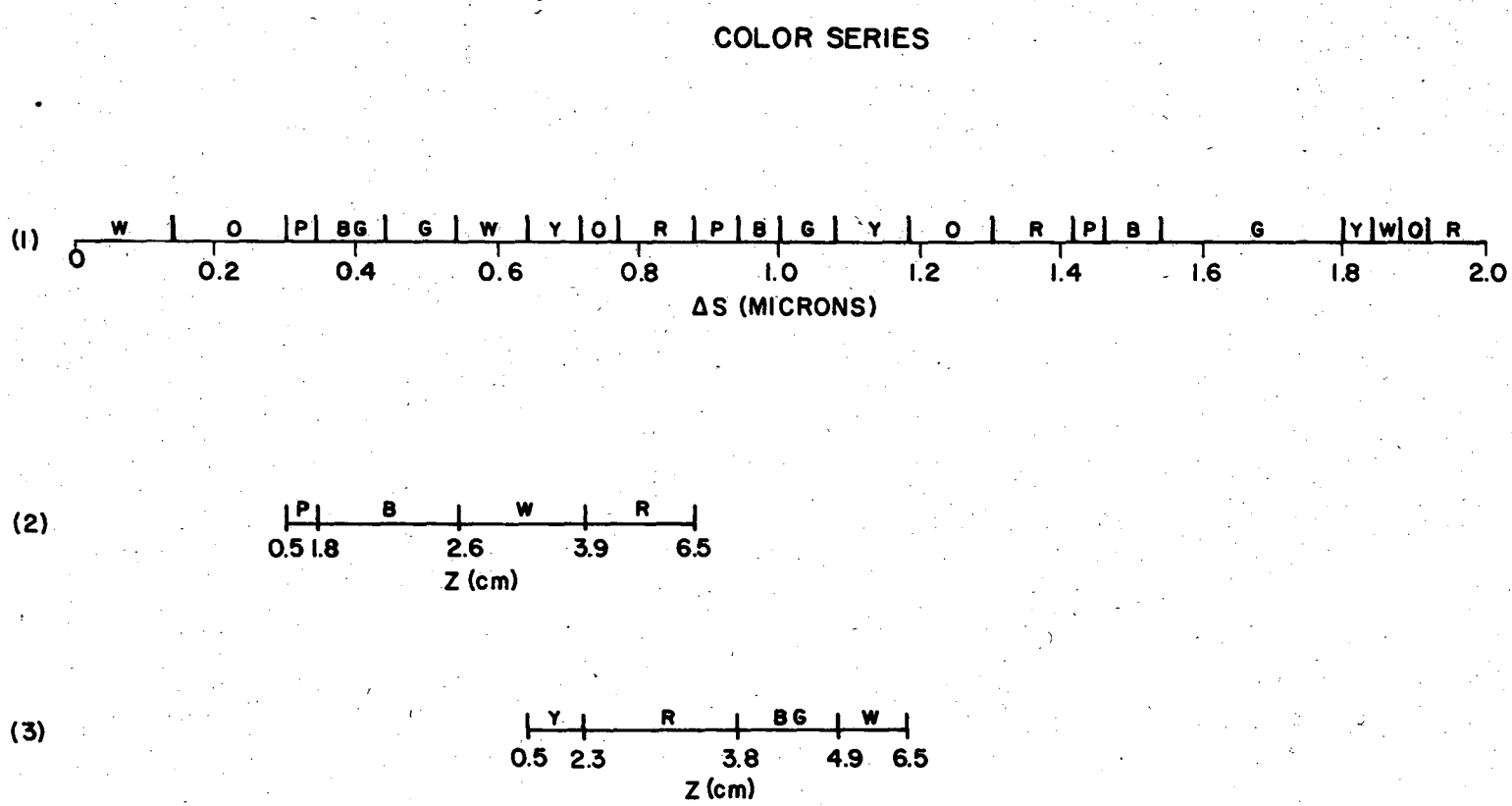

Fig. 57. Color series for ZnS films on aluminum s-polarization. (1) Present calculated series: δ_{TOT}=30.00 (deg), r_{sl}=0.90, ϕ=80.00 (deg). (2) Observed series, sample 1. (3) Observed series, sample 2. Film thickness, d = 0.241× ΔS.

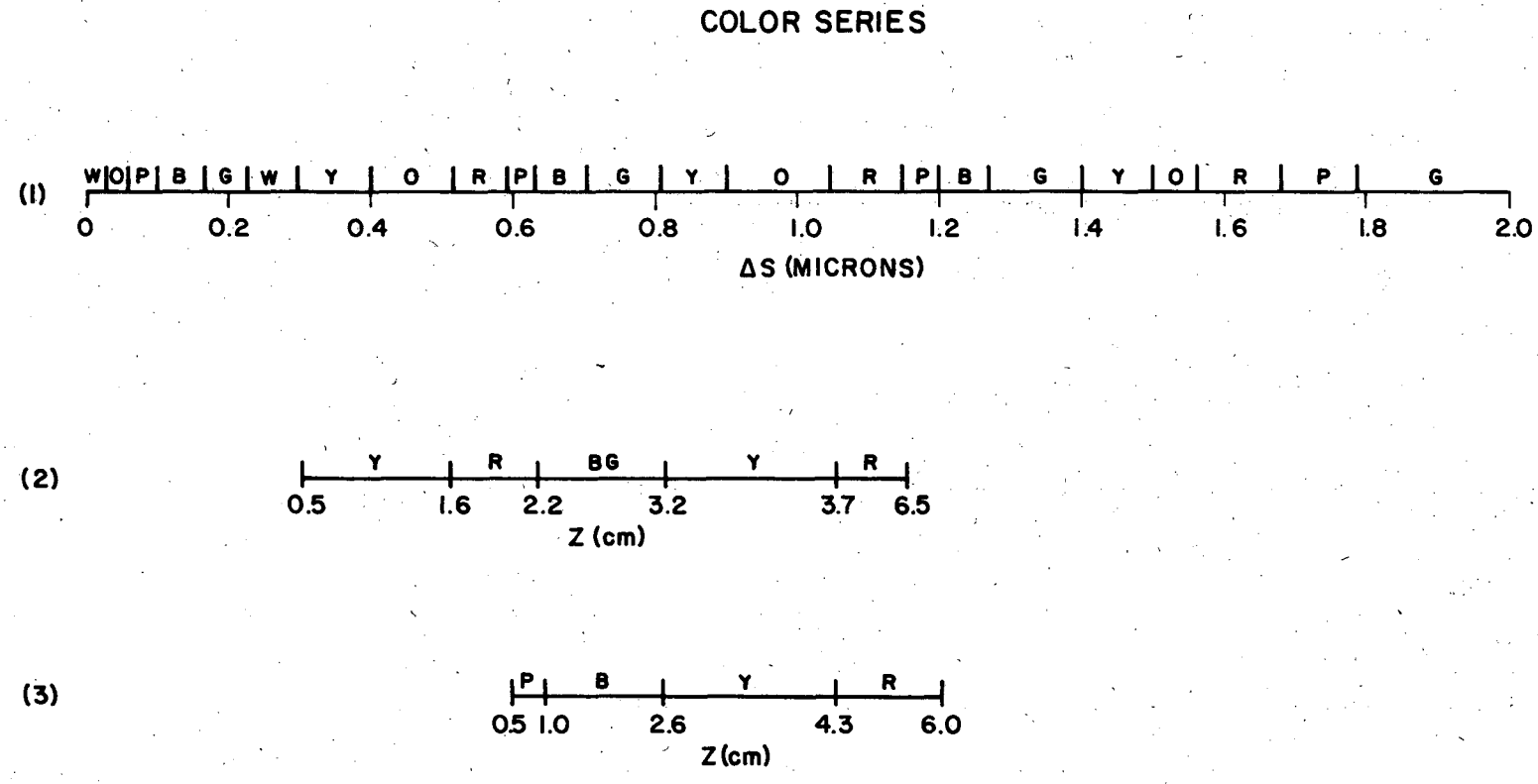

Fig. 58. Color series for cryolite films on aluminum p-polarization. (1) Present, calculated series: δ_{TOT}=210.00 (deg), r_{p1}=0.90, ϕ=80 (deg). (2) Observed series, sample 1. (3) Observed series, sample 2. Film thickness, d = 0.588× ΔS.

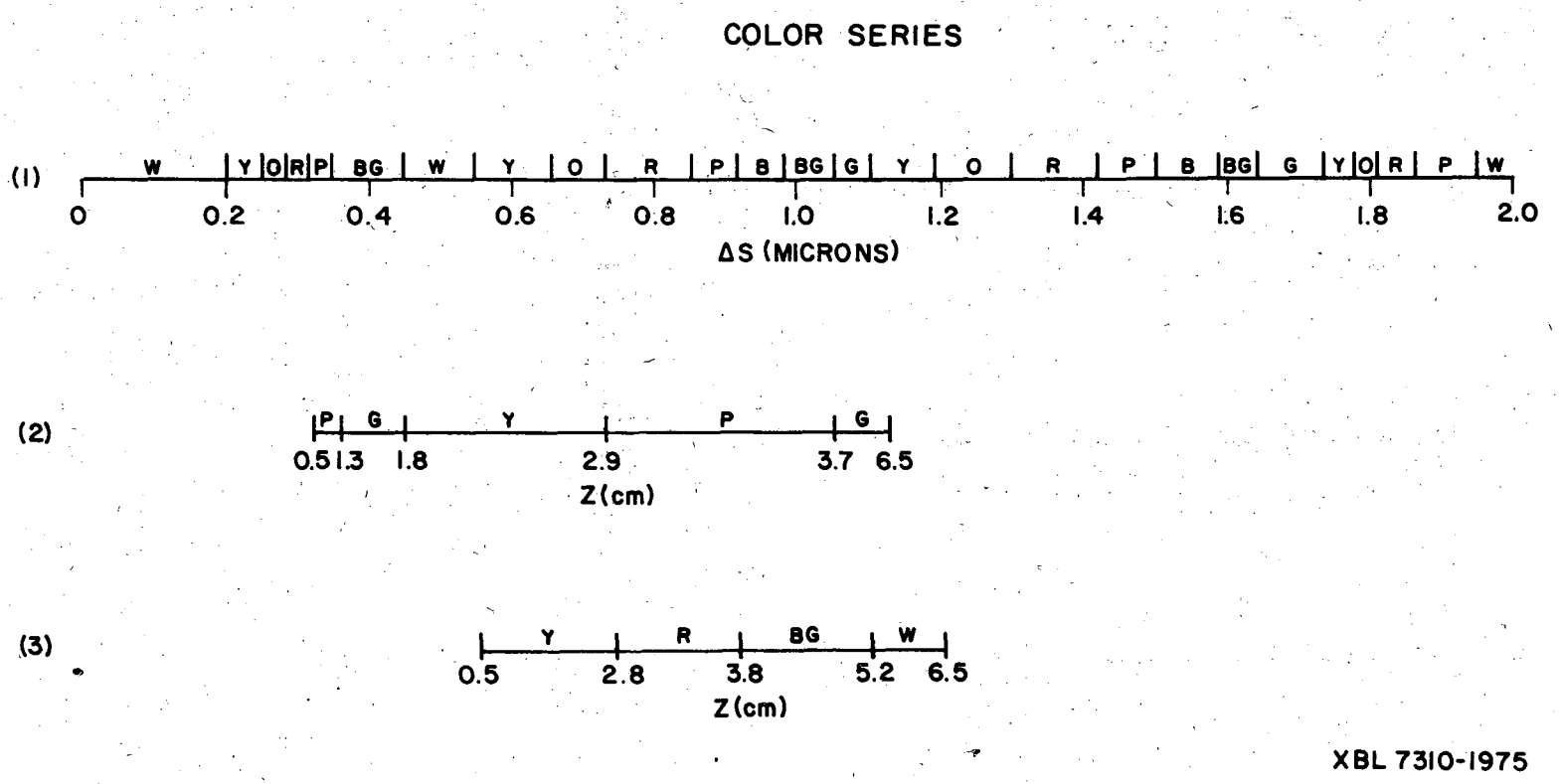

Fig. 59. Color series for cryolite films on aluminum s-polarization. (1) Present, calculated series: δ_{TOT}=30.00 (deg), r_{sl}=0.95, ϕ=80 (deg). (2) Observed series, sample 1. (3) Observed series, sample 2. Film thickness, d = 0.588× ΔS.

Figure 60

Examples of interference color series obtained with three different substrates. The nominal angle of incidence is 80°. Scribe markings are 0.5 cm apart. The narrow image is for p-polarization and the wide image is for s-polarization. The specimens are

left Cryolite film on aluminum substrate, sample 1.

center Cryolite film on silicon substrate.

right Zinc sulfide film on chromium substrate, sample 1.

The color series evaluated from the projection of the original slide are included in Figs. 59, 54 and 49. Colors on the photographic prints are less saturated than on the original color slides. In particular, distinction between yellow and orange is worse using the prints, made from the slides, than using the images of the slides.

(BBC 7310-6380)

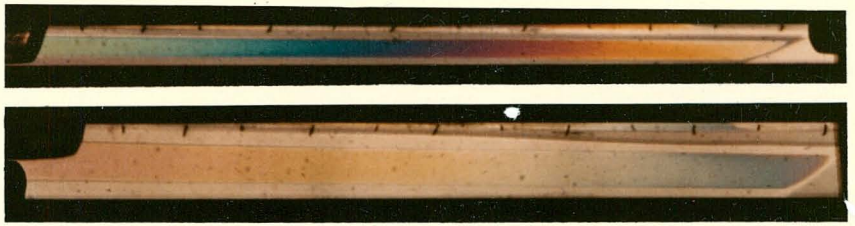

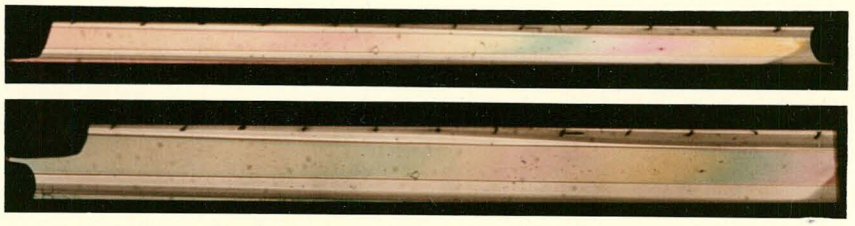

The probe in the reflected beam was placed in a rack and pinion mount in order to scan the film. The film was mounted on a machined surface and clamped securely. The lower edge of the taper was positioned at the lower edge of the camera field in order to provide a consistent reference for the probe. A variable resistor connected to the mount allowed potentiometric readout of the vertical motion of the probe. Horizontal motion of the probe was restricted by clamping. The acceptance diameter of the probes was 0.125 in. At an angle of incidence of 80°, the probe sampled an elliptical area of film surface 0.125 in. high and 0.375 in. wide. The probes (both Gamma Scientific Model 600-3C) were of equal 5-ft length to even out transmission losses.

Both probes were coupled with a matched pair of monochromators (Baush and Lomb Model 33-86-02) geared synchronously to give a uniform, reproducible sweep of the visible spectrum. Their wavelength bandwidths were 4 nm each. The useable range was limited on the blue by the output of the source and on the red by the response of two photomultiplier tubes connected to the monochromators. The photomultipliers were connected to the photometers.

For a spectral scan for maxima and minima at a discrete film position, the spectrophotometers were connected to a ratio-recording servo-recorder (a modified Heath Servo Recorder, Model EAW 20) as indicated in Fig. 62.

In order to scan the film for maxima and minima at discrete wavelengths, the photometers were connected to a ratiometer (Hewlett Packard Ratioing Voltmeter, Model A3200) as in Fig. 61. The output of the ratiometer, was connected to the vertical (Y) channel of an X-Y recorder. The horizontal (X) channel was connected with the output

Figures 61 and 62

Schematics of ratio recording spectrophotometer.

(1) Thin film covered surface

(2) Reference fiber optic probe

(3) Reflected beam fiber optic probe

(4) Matched, synchronous motor-driven monochromators

(5) Matched photomultiplier tubes

(6) Photomultiplier electronics

(7) Unity gain amplifier

(8) Ratio recorder

(9) Ratiometer

(10) X-Y recorder

(11) Rack and pinion potentiometer

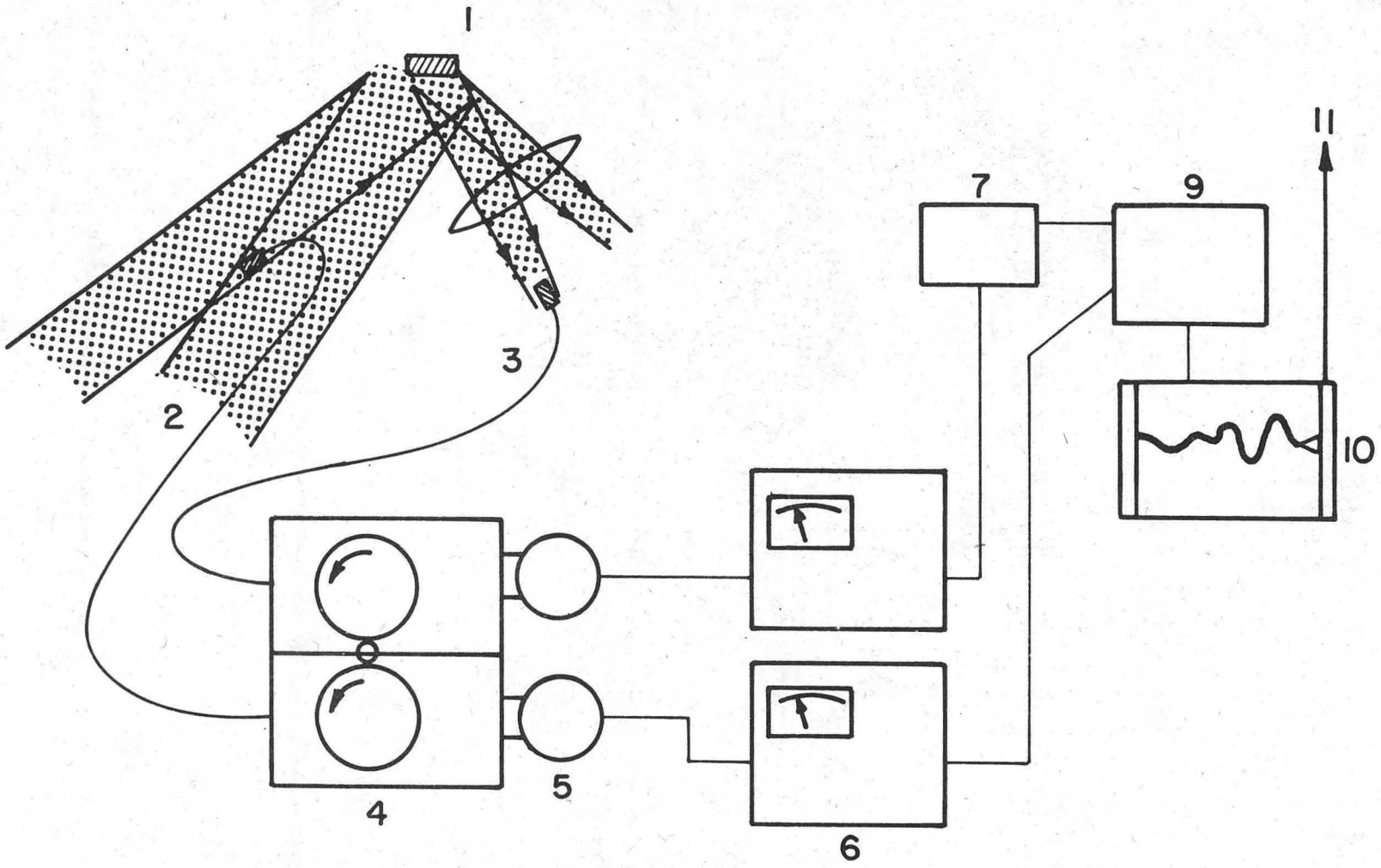

Fig. 61. Schematic of spectrophotometer system in Z-scanning mode

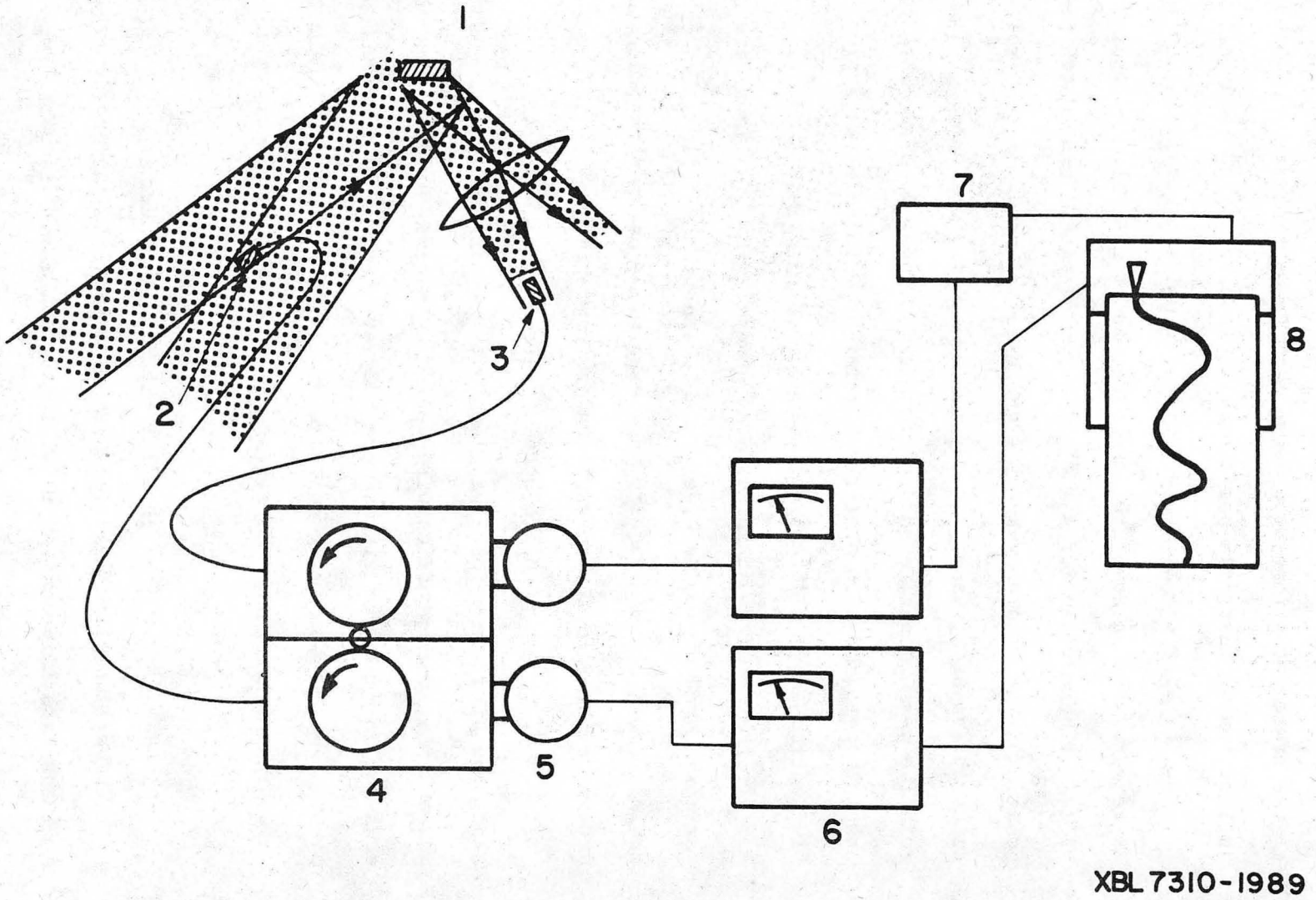

Fig. 62. Schematic of spectrophotometer system in λ-scanning mode.

of the probe potentiometer. Hence a trace of the ratios of beam intensities against film position was produced by the recorder.

Calibrating the instrument response using neutral density filters is required for an absolute determination of the ratio of incident to reflected beam intensities, I/I_o. Scanning either wavelength or position for maxima and minima eliminates the need for calibration since the value of the intensity ratio is not considered. Using a relative measurement, a ratio, in this instance, is preferable to absolute determination of intensity maxima or minima as source fluctuations do not affect the measurements.

In the spectral scanning mode, several film positions were scanned for maxima and minima in order to derive a film profile. Two or more maxima or minima were required for each film position in order to determine the film thickness using program MBINF.

The film-scan mode produced a trace of intensity ratio along the film for several wavelengths. By following the sequence of max and min, film profiles were derived. Several simultaneous or consecutive maxima or minima were adequate for a film thickness determination without assuming an order of the interference colors. Only in ambiguous instances where there were few maxima and minima was the order of interference assumed.

D. Ellipsometry of Thin Films

The ellipsometer used was a self-compensating automatic ellipsometer.[44] A mercury arc lamp source at 546.1 nm, with a bandwidth of 5 nm, was used. Samples of the dielectric-covered metal films were positioned in the beam by mounting the slides on a rack and pinion apparatus.

Vertical motion of the sample was then possible. The ellipsometric parameters were determined at discrete film positions by adjusting polarizers in the incident and reflected rays and reading azimuth angles. The film thickness obtained was an integrated average thickness over the lateral film dimension (+x). The data were analyzed using program FPLOT.[23] The film profiles were obtained by assuming a cycle of azimuth angle rotation based on independent film profile data.

E. Mechanical Step-Height Measurement

In order to measure step-height at the film-substrate boundary, a profilometer (Clevite Surfanalyzer, Model 150) was used. The instrument offered a maximum resolution, based on the absence of seismic vibrations and the negligibility of surface damage, of 25.4Å. Practical resolution using vibration damping and a lightweight (50 mg force) stylus was about 250Å.

A diamond-tipped, stylus of radius 2.54 microns was used. The profilometer operated in skidless mode to diminish datum distortions. The stylus traversed the specimen in the x direction such that the step between film and metal was in its path. A motor driven arm carried the stylus across the specimen at a rate of 0.1 in./sec to prevent skipping. The specimen was anchored to a polished flat glass slab using adhesive tape.

The lack of interference fringe bending across the film indicated that the step-height measurement was also the film thickness at the center of the film.

F. Optical Step-Height Measurement

Thin films of aluminum were deposited on top of the film and substrate in order to measure step height interferometrically. A Zeiss-Linnik double-beam interference microscope (Carl Zeiss, Model 2000) was used. A monochromatic, thallium light beam at 5400 Å was selected to produce fringes. Photographs of the fringes were made using PAN-X, black and white, 35 mm film and a Zeiss Ikon camera. The camera was released by cable tension to minimize disturbing the fringe pattern with vibration. No lenses were used with the camera. The pictures were taken of a circular area of surface along the boundary of the dielectric coated with aluminum at several film positions. Step-height was determined by measuring fringe displacement from projections of the photographic negatives. A typical photograph is shown in Fig. 63.

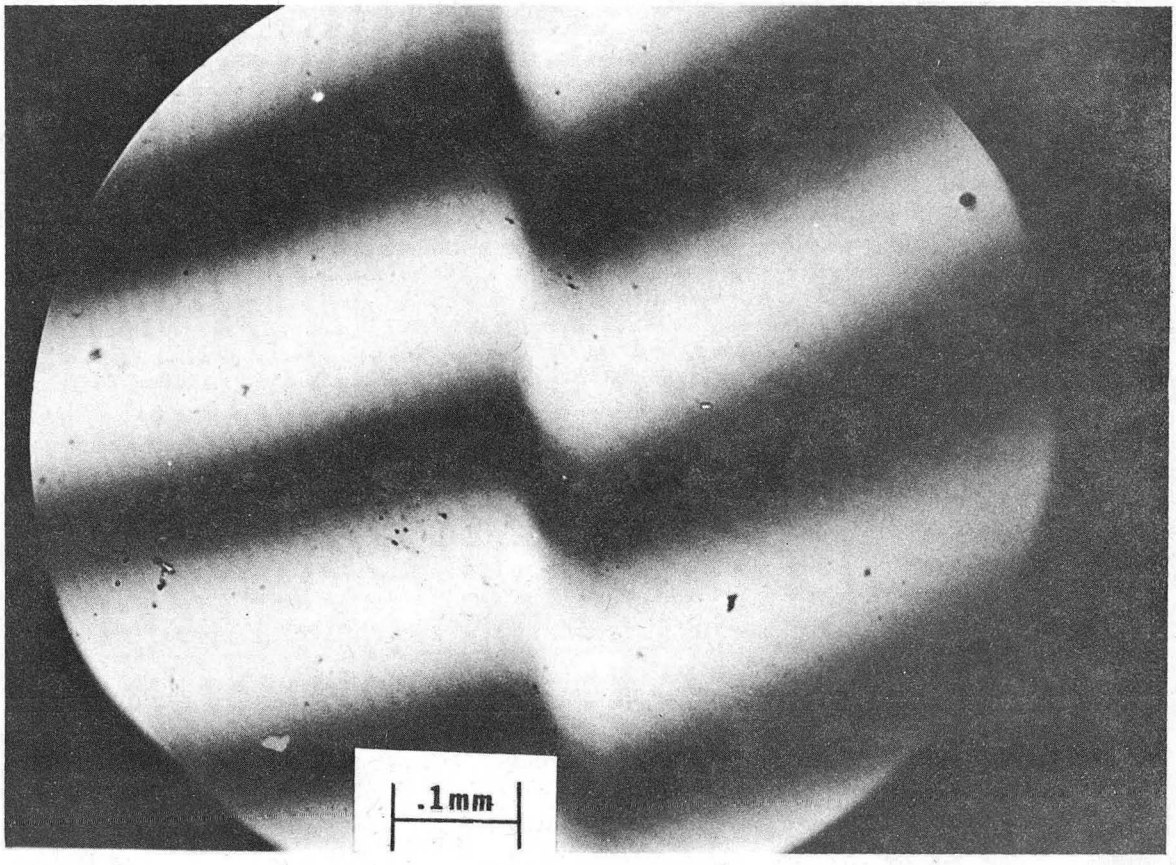

XBB 7310-6329

Fig. 63. Interference micrograph of the step between ZnS film (on the right) and chromium substrate (on the left).

IV. RESULTS

Film Profiles

Figures 64 through 69 show film profiles derived experimentally using methods described in Section III. A list of the symbols used is included. The mechanical and optical step-height measurements are the only profile measurements independent of the optical properties of the film and substrate.

In order to determine the interference order for colorimetric analysis and for the spectroscopic analysis of the interference colors, spectroscopically the film thicknesses derived by independent measurements were used to choose the order. The determination of film thickness using ellipsometer parameters, ψ and Δ, for a transparent film required a thickness reference obtained using methods independent of the optical properties of the film and substrate, also. The reason a reference was needed was that the curves generated in Figs. 23 through 34, which are ψ-Δ plots, are closed (closed curves are typical of non-absorbing films on absorbing substrates), resulting in cyclical variation of the ellipsometer parameters with increasing film thickness. Thus, a reference thickness was required to determine the cycle.

Eight different measurement techniques were used to determine each film profile. A possible ninth measurement, a spectroscopic measurement in the spectral scanning mode using p-polarized light, was not made.

The independently derived film profile data for dielectric films on aluminum substrates fell within a maximum scatter-band 450Å wide. The error in film thickness measurement was, then, ±225Å. Similarly,

CAPTIONS FOR FIGURES 64-69

Symbol	
○	Interference microscope step-height
●	Profilometer step-height
△	Spectrophotometer film thickness λ-scan, s-polarization
▲	Spectrophotometer film thickness z-scan, s-polarization
♦	Spectrophotometer film thickness z-scan, p-polarization
+	Ellipsometer film thickness
□	Colorimetric film thickness s-polarization, using present, calculated color series
■	Colorimetric film thickness p-polarization, using present, calculated color series

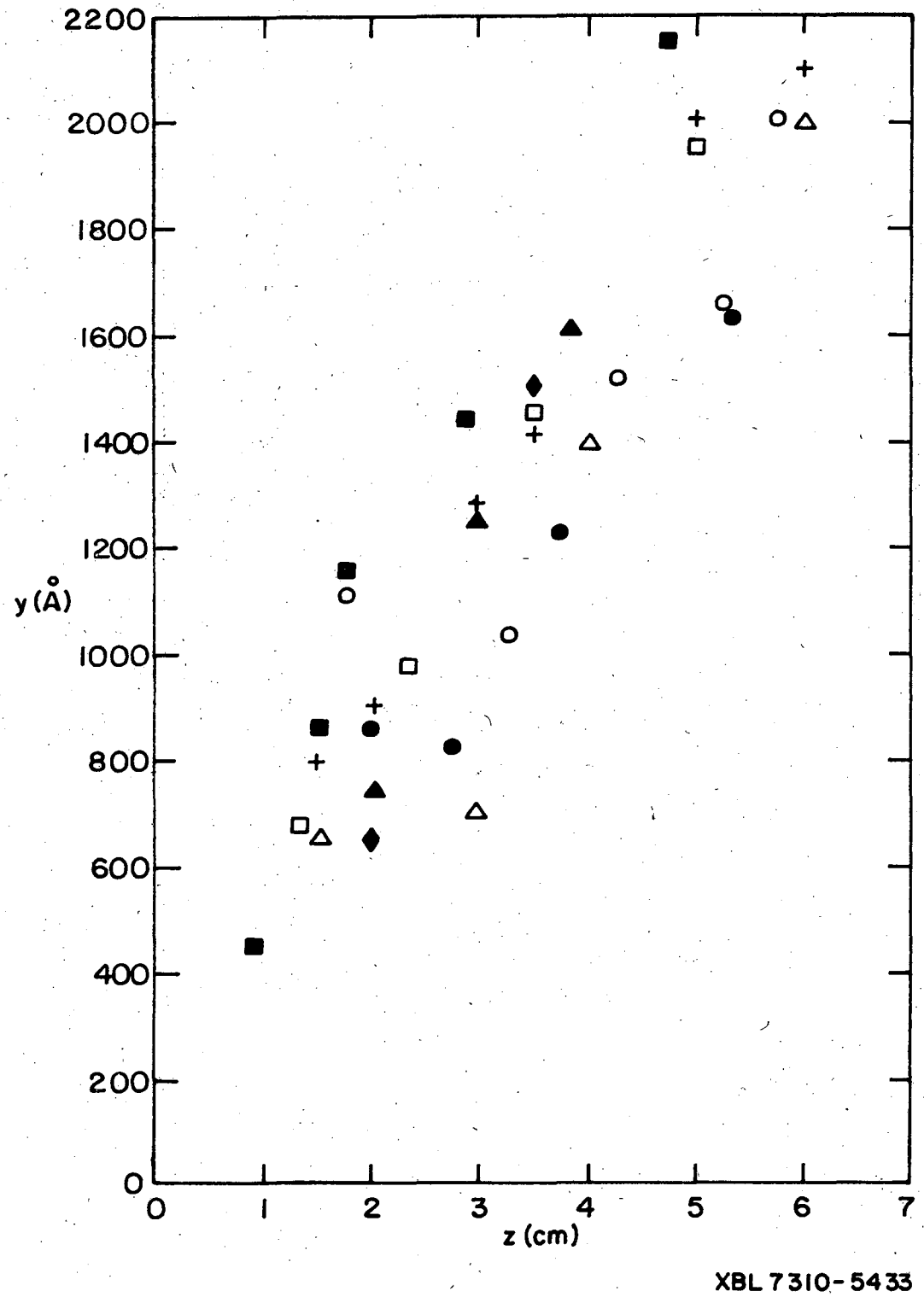

Fig. 64a. Profile of ZnS film on aluminum substrate, sample 1.

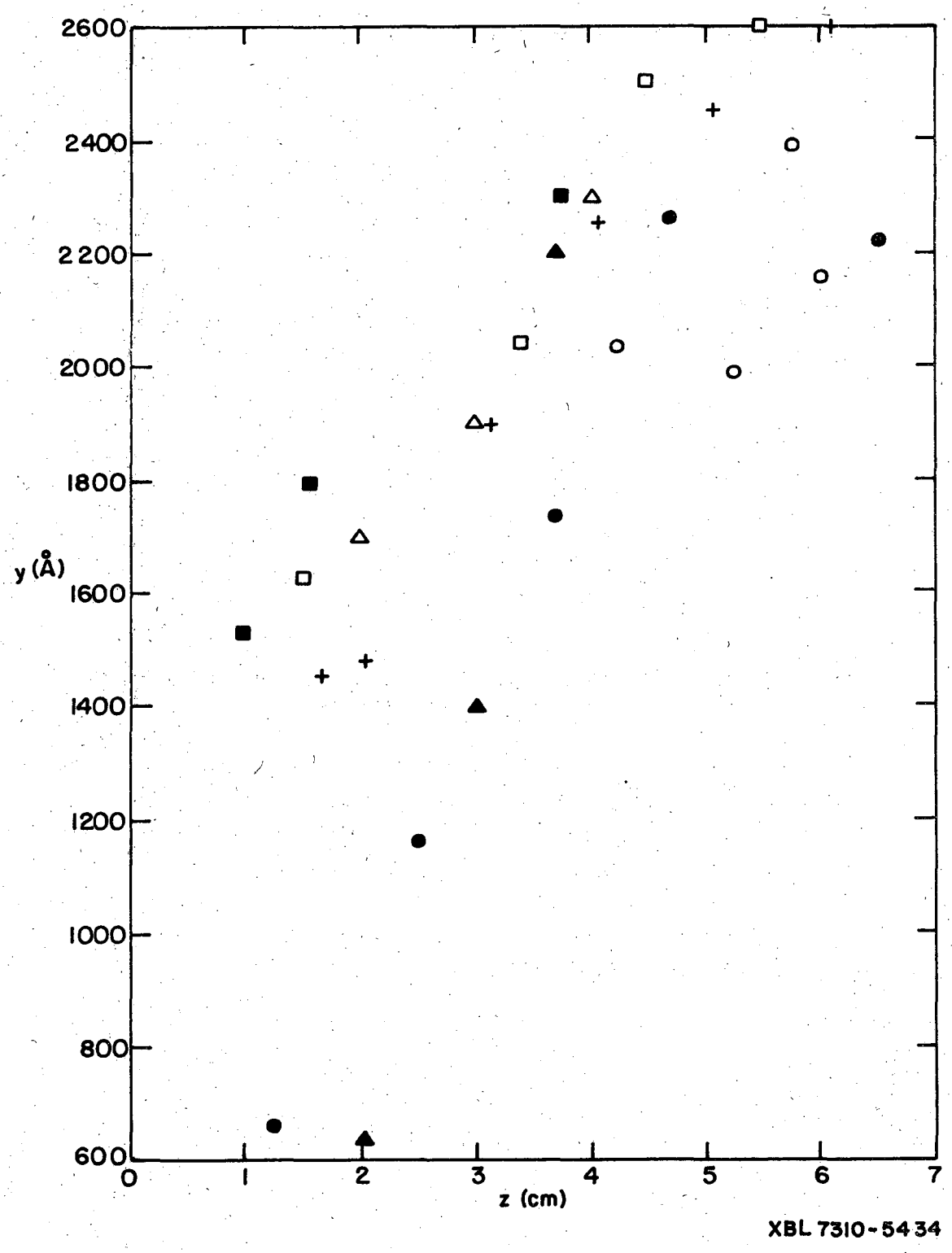

Fig. 64b. Film profile of ZnS film on aluminum substrate, sample 2.

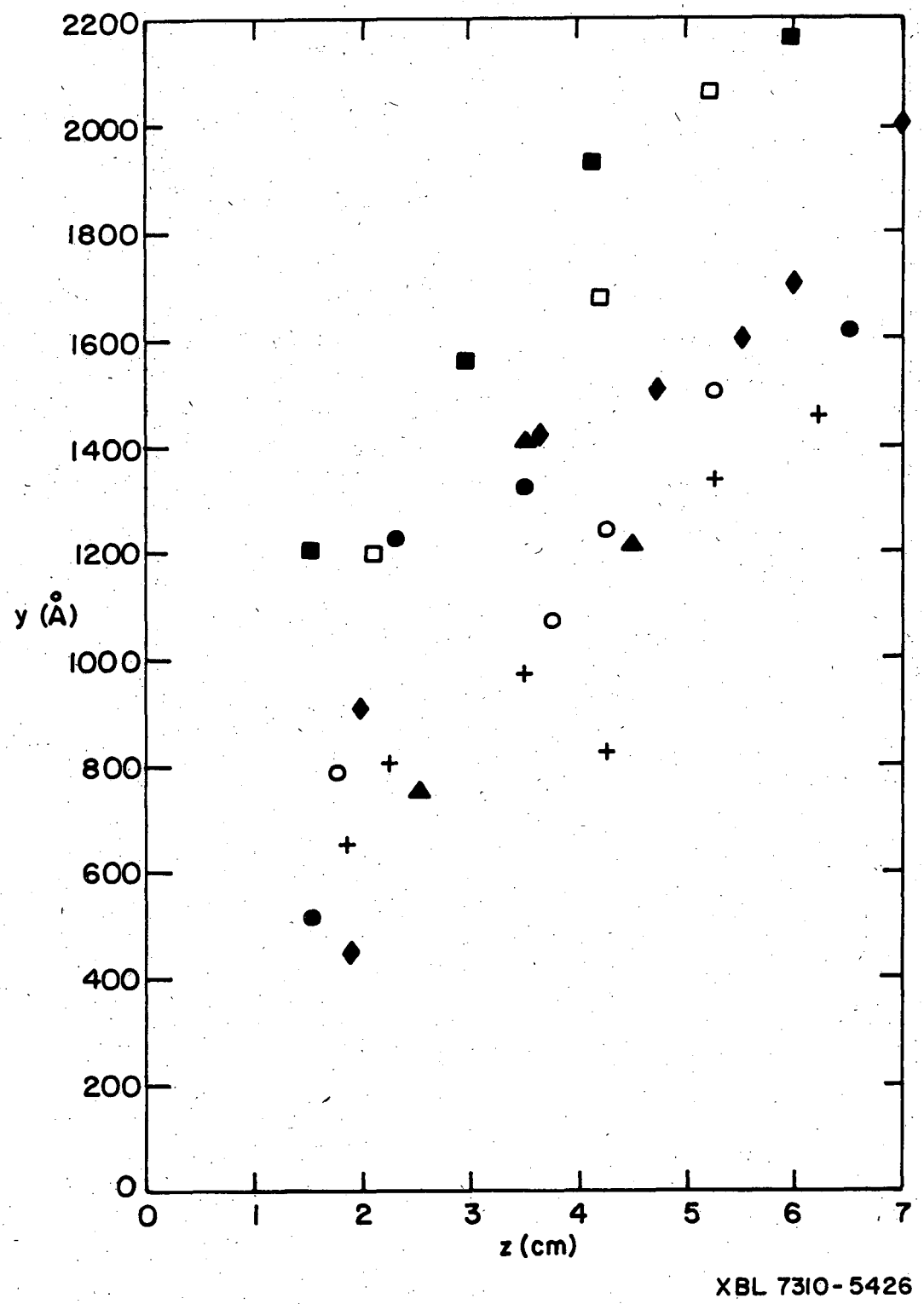

Fig. 65a. Film profile of ZnS film on chromium substrate, sample 1.

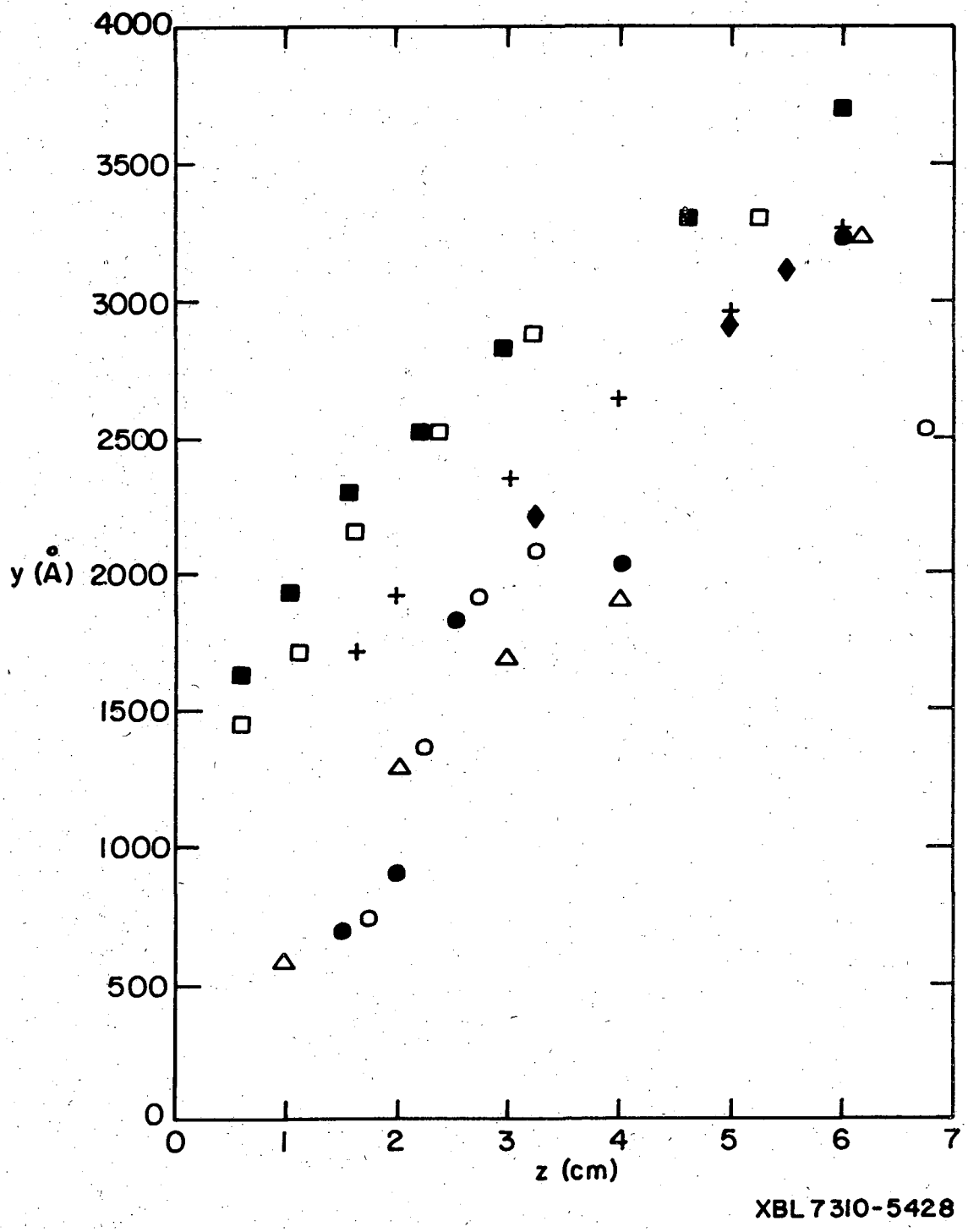

Fig. 65b. As in Fig. 65a, sample 2.

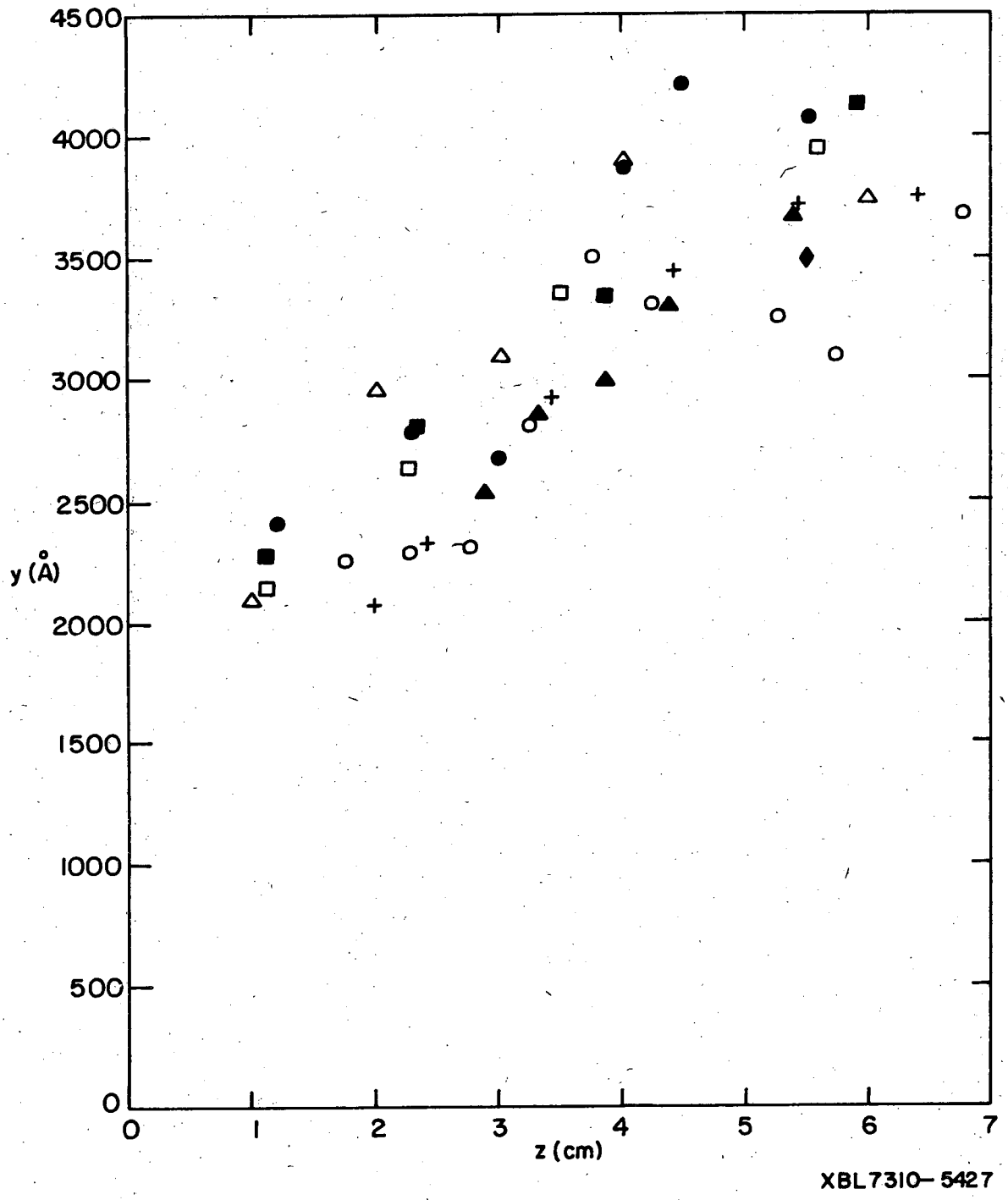

Fig. 65c. As in Fig. 65a, sample 3.

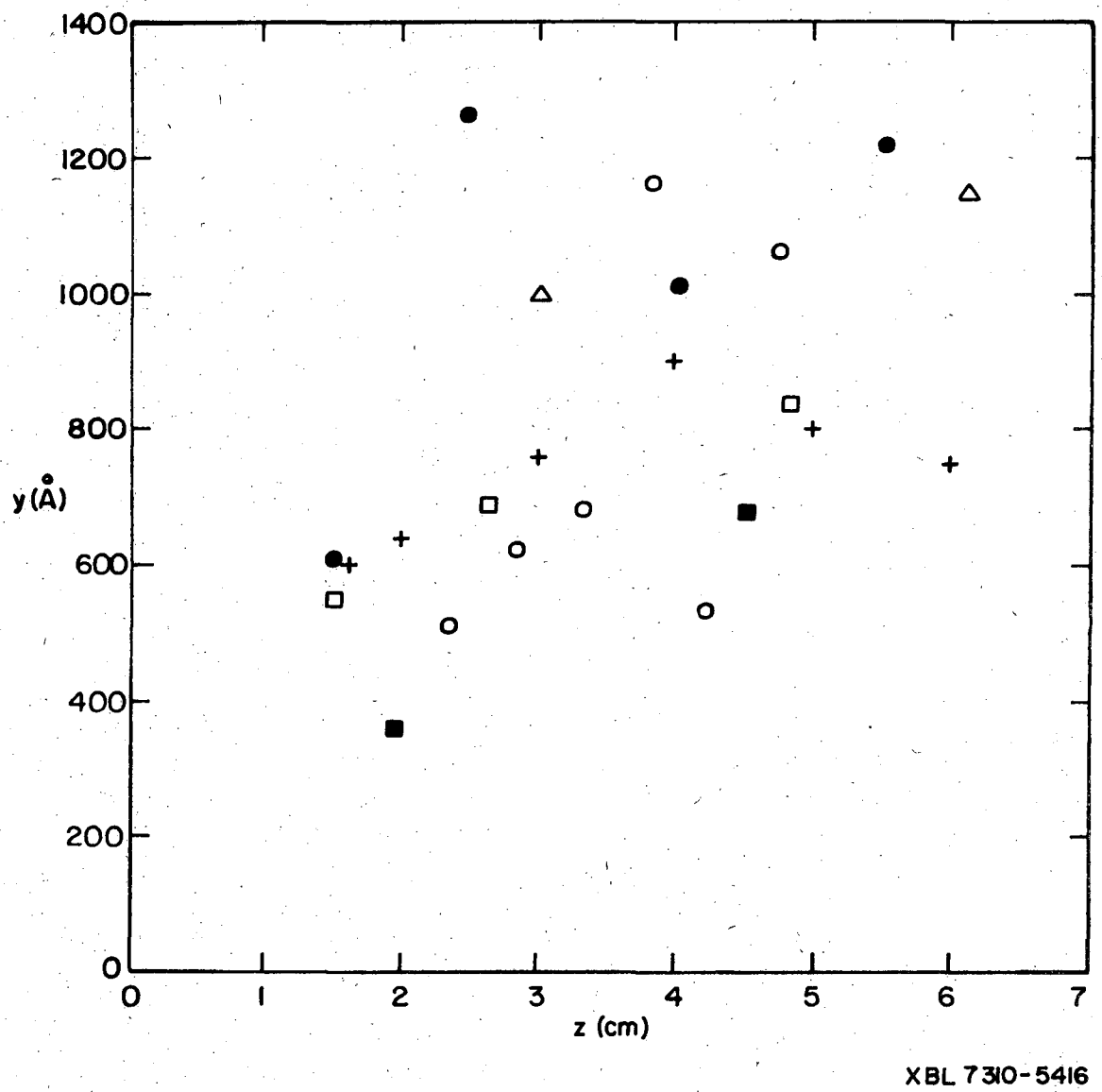

Fig. 66. Film profile of ZnS film on silicon substrate.

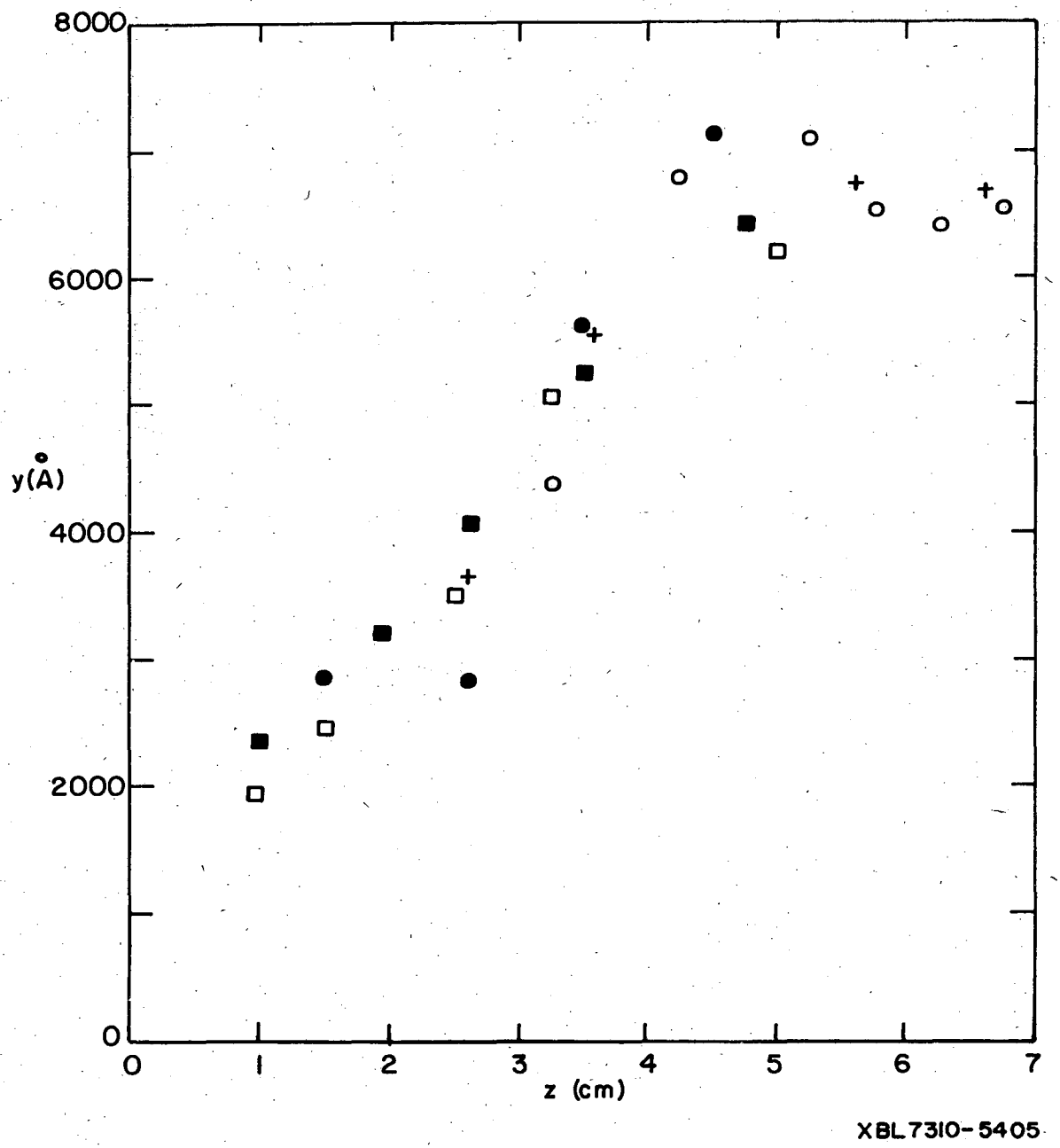

Fig. 67a. Film profile of cryolite film on aluminum substrate, sample 1.

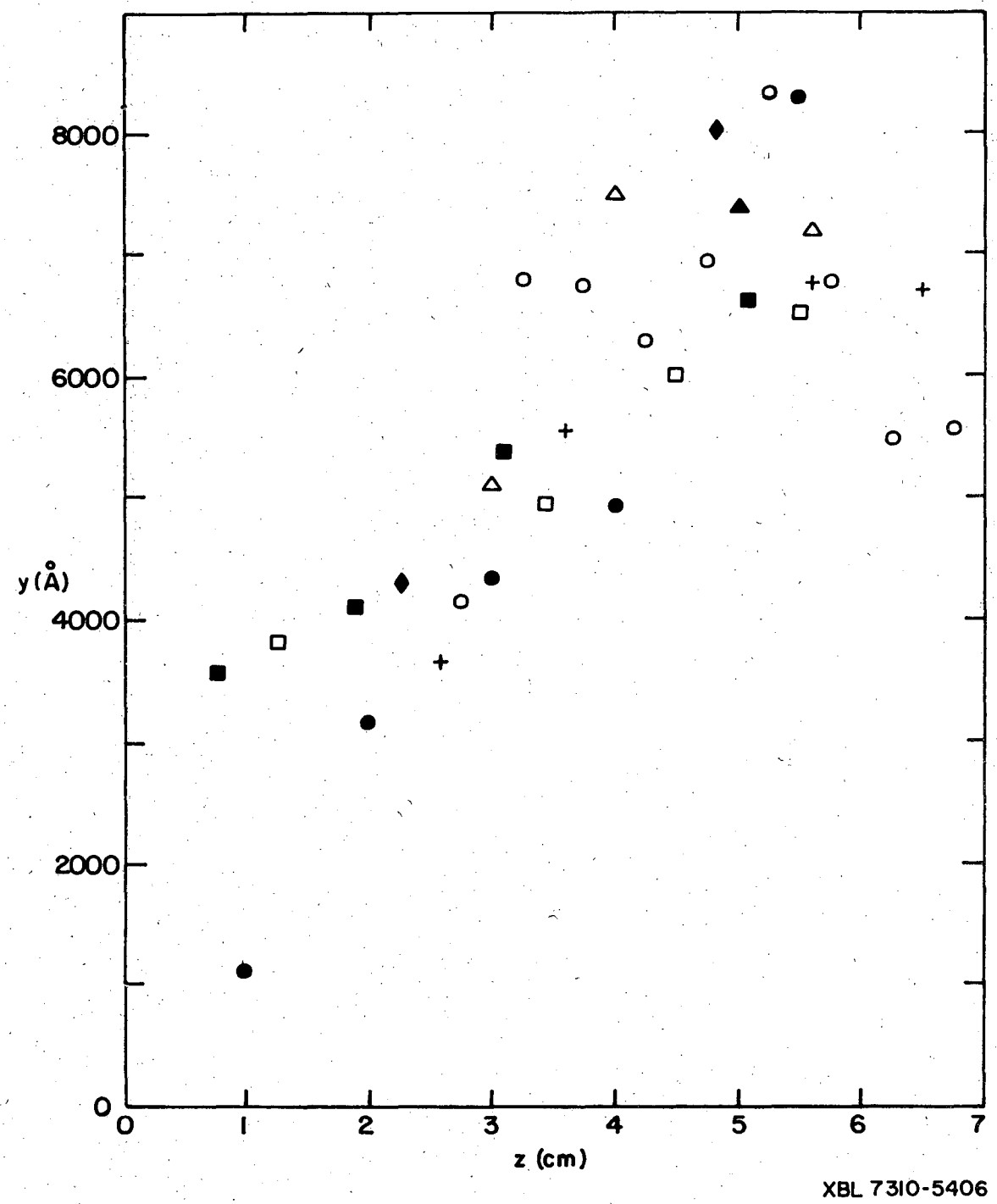

Fig. 67b. As in Fig. 67a, sample 2.

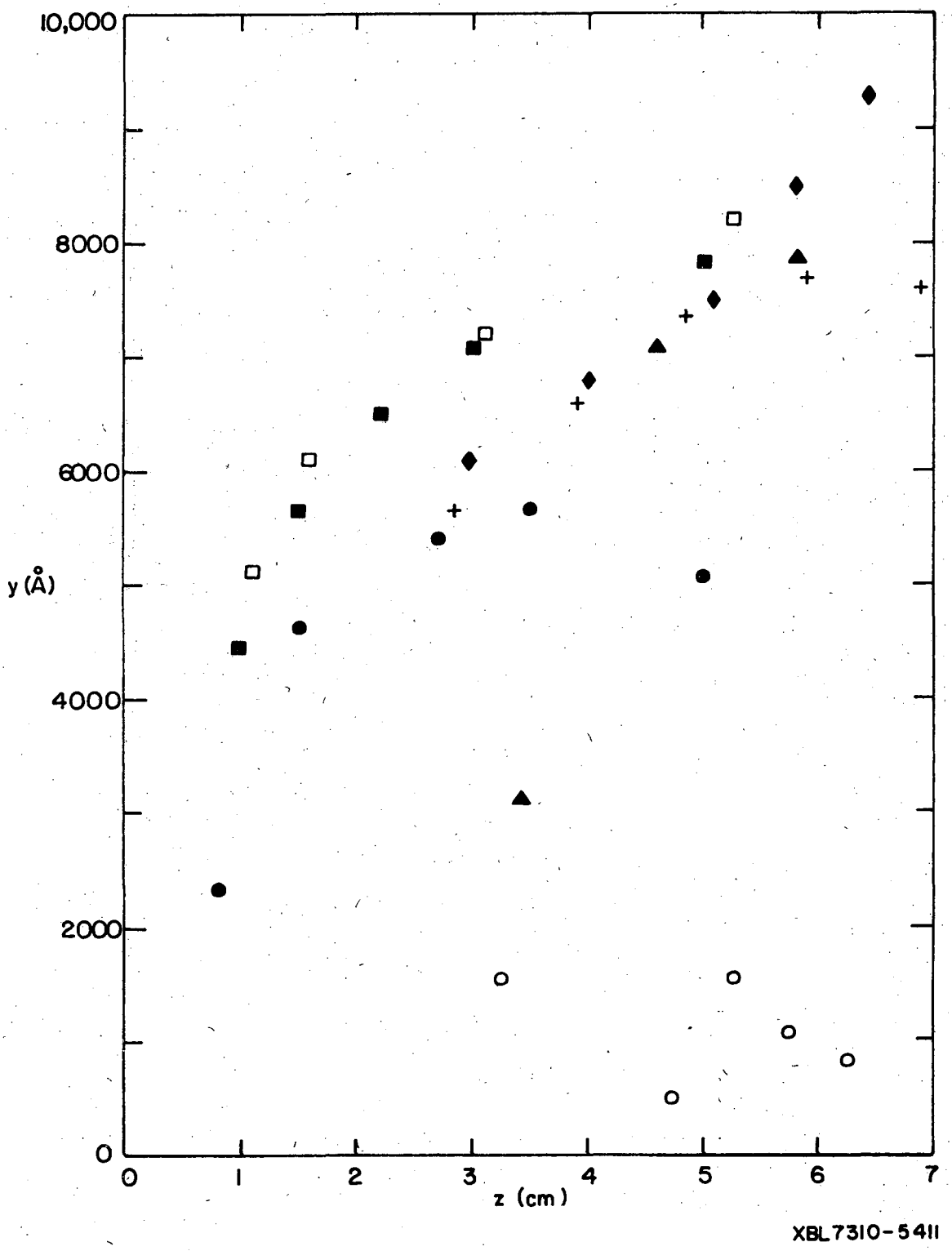

Fig. 68. Film profile of cryolite film on chromium substrate.

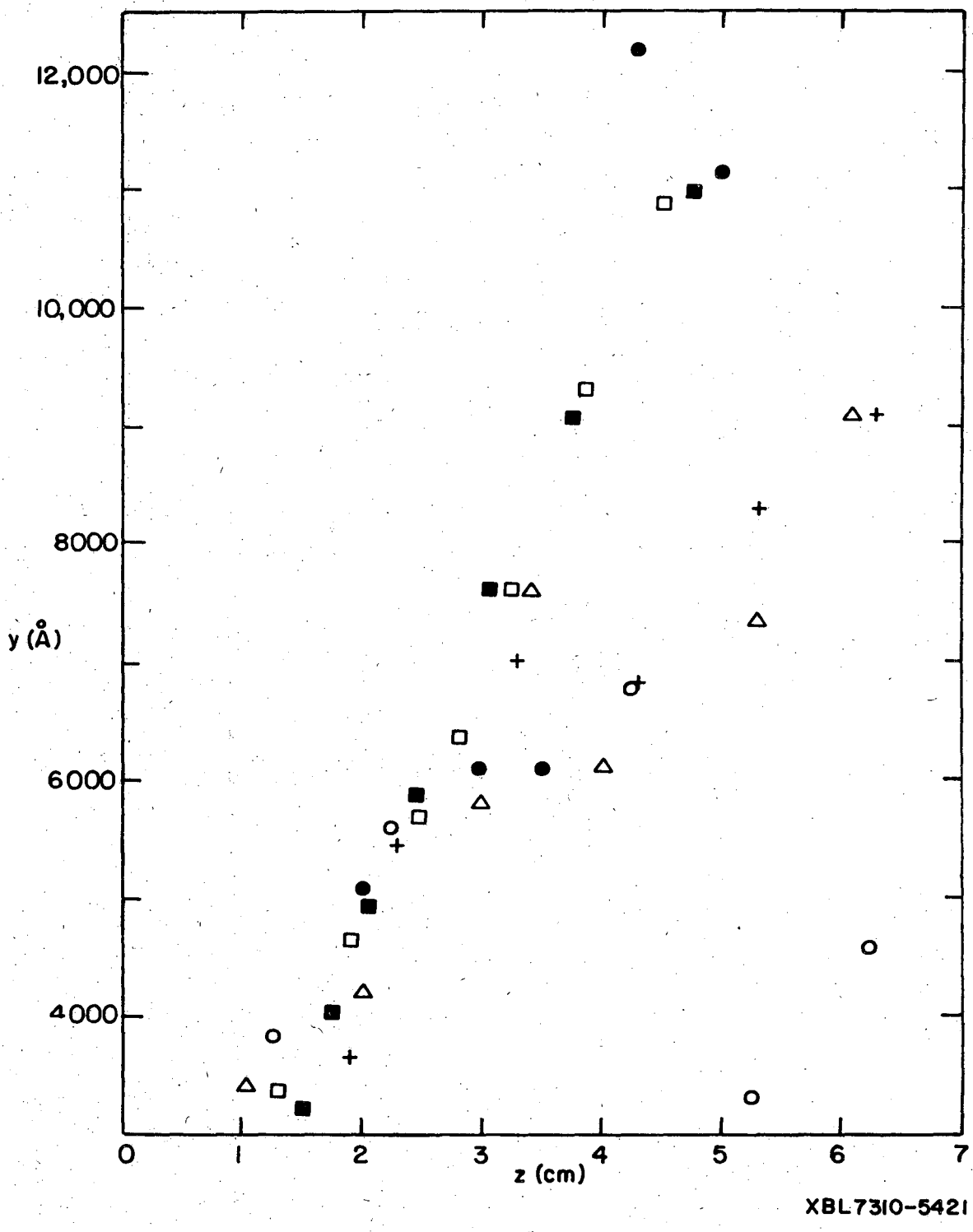

Fig. 69. Film profile of cryolite film on silicon substrate.

the error in film thickness measurement for dielectric films on chromium was ±190Å while for dielectric films on silicon the error was ±250Å

Agreement between colorimetrically derived film profiles and profiles derived otherwise was considered satisfactory if the colorimetry data fell within the scatter band of the other data. The agreement was found to be satisfactory for dielectric films on aluminum and silicon. The agreement for dielectric films on chromium was not satisfactory according to this criterion, but could, nevertheless, be considered satisfactory if the uncertainty of color interpretation was also taken into account.

Discussion of Color Series

Experimental color series were obtained photographically (Figs. 48 through 59). These series were analyzed using calculated color series of the present work based on the multiple beam interference model of Muller and Turney, using the optical properties of the film and substrate for the light range $380 \leqslant \lambda \leqslant 650$ nm. The range of film thickness for an observed color-fringe was derived from the corresponding range of optical path difference $\Delta\delta$, obtained from the analysis. The value of the film thickness at the center of the band was plotted against the film-location of the center of the color-fringe.

The present, calculated color series were, then, compared with previous color series obtained from the color charts of Turney shown in Figs. 5a and 5b. These color series are included on Figs. 50 through 62. The differences between the previous series and the present series were: (1) the size of the achromatic region was reduced by a factor of ten on the basis of observations of interference colors for high-reflectance substrates thus giving more colors, (2) the experimental angle was

used instead of the optimum angle of incidence, and (3) the reflectances of the metal-film interfaces of the experiments were not exactly those used by Turney.

Although the metal-film reflectance and δ_{TOT} do not change appreciably with respect to the angle of incidence on the dielectric surface, the color series generated using the experimental angle of incidence may differ from the color series using the optimum angle of incidence. Colors are most saturated at the optimum angle of incidence. Hence, the effect of varying the angle of incidence at constant reflectance and δ_{TOT} would be a change in the shape of the chromaticity diagrams. Whether or not this change in shape, corresponding to changes in the purity of colors, affects the color series for a particular metal-film pair is undetermined. Color series were, therefore, calculated for the experimental angle of incidence in order to determine any differences with the previous color series by Turney. Since films on chromium substrates were measured at an experimental angle of incidence slightly different from the optimum angle of incidence, discrepancies between the previous and present calculated color series were attributed to the difference in angles used and, to a lesser extent, the difference in reflectances of the color chart and the samples.

The sign convention adopted by the Nebraska conference[14] regarding the direction of the reflected p-electric field vector (see Fig. 1) does not affect the value of δ_{TOT} calculated by Turney for the color charts using the old convention (in which the direction of the p vector is reversed) because δ_{TOT} is the difference of absolute phase changes.

According to the analysis by Turney, colors with respect to films on highly reflecting substrates would be too impure (unsaturated) for visual resolution. However, the observation in this work that colors that result from dielectric films on aluminum can be resolved in regions quite near the achromatic center, considered white by Turney (see Figs. 45 through 49) indicates otherwise. Therefore, color charts can be constructed for high-reflectances at the film-substrate interface also.

Comparison of the present, calculated and previous color series by Turney (see Figs. 52, 53, 54 and 55) show good agreement for dielectric films on silicon.

Comparison of the present and previous color series for dielectric films on chromium shows a discrepancy of about 0.1 micron in optical path difference. The discrepancy, in terms of film thickness, is about 240 angstroms for zinc sulfide films and about 585 angstroms for cryolite films. The ability to discriminate colors visually is not as accurate as numerical capabilities of discrimination. Hence, the discrepancy between color series is negligible when considered experimentally.

Experimental film profiles derived from the present calculated color series for dielectric films on chromium show upward deviation from other measurements. Use of the Turney series alleviates the upward deviation somewhat.

Comparison of observed color series with the present calculated color series, based on chromaticities, indicated that the capability of visually resolving colors is considerably less than the capability of numerically resolving colors by calculation. There were fewer colors observed for a range of ΔS than are expected on the basis of the chromaticity values. The reason for the low resolution of visual observations may be that the eye does not distinguish colors nor gradations of color accurately.[19] There is, moreover, a loss in resolution using photography due to the insensitivity of photographic materials to small gradations of color.

The capability of visually resolving colors was determined by comparing the fringe width of a color, determined using chromaticities, with the fringewidth of the color determined by fitting a straight line through the film profile data from independent measurements for the region of the film bounded by the color fringe. Hence, fringe width of the narrowest band of yellow based on chromaticities for zinc sulfide films on chromium is 400Å in optical path difference, while the observed band of yellow is an average of 1450Å in optical path difference based on the independently measured film profiles. Assuming the minimum error in thickness measurement due to interpretation of the colors is equal to half the bandwidth of the narrowest fringe, the error using observed colors is ±725Å in optical path difference. This represents an error of ±173Å in film thickness of ZnS films due to color interpretation. The error for cryolite films on chromium was ±500Å using similar assumptions. This represents a considerable loss in resolution with respect to the error of ±147Å for resolution of the yellow color fringe based on chromaticities.

The ability of an observer to resolve colors affects the experimental determination of color series. This ability to resolve colors is dependent on: (1) the physiological response of the eye and the interpretation of color and (2) the influence of the color of the surface upon which the image of the interference colors was projected. Therefore, the resolution of colors will vary depending on the conditions of the observations.

ACKNOWLEDGEMENTS

I would like to express my thanks to Drs. R. H. Muller and H. J. Mathieu for their helpful conversation and aid in experimentation. This work was conducted under the auspices of the U. S. Atomic Energy Commission.

REFERENCES

1. R. H. Muller, J. Electrochem. Soc. 113, 943 (1966).
2. J. H. Turney, Profiles of Supermeniscus Electrolyte Films on Partially Submerged Gas Electrodes (M. S. Thesis), LBL-171, August 1971.
3. H. Gu, Ellipsometry of Surface Layers (M. S. Thesis), LBL-165 December 1971.
4. S. V. Chesnokov and Y. A. Chismadjev, Elektrochimia 5, 598 (1969).
5. R. H. Muller and J. R. Mowat, Reflection of Polarized Light from Absorbing Media, UCRL-11813, 1966.
6. K. Estermann, Z. Phys. Chem. 106, 403 (1923).
7. K. Estermann, Z. Fizichnii Phys. 33, 320 (1925).
8. R. W. Ditchburn, Proc. Roy. Soc. A141, 169 (1933).
9. A. Goswami and A. P. Goswami, Thin Solid Films 16, 175 (1973).
10. O. S. Heavers, Optical Properties of Thin Solid Films (Dover, New York, 1965), p. 6, 96.
11. Landolt-Bornstein Tables, Optische Constanten (Springer, Germany, 1962), Vol. II, part 8.
12. W. H. Steel, Interferometry (Cambridge University Press, 1967).
13. M. Francon, Optical Interferometry (Academic Press, 1966).
14. R. H. Muller, Surface Science 16, 14 (1969).
15. R. H. Muller and J. R. Mowat, Reflection of Polarized Light from Film Covered Surfaces, UCRL-17128, 1967.
16. C. E. Leberknight and B. Lustman, J. Opt. Soc. Am. 29, 59 (1939).
17. A. Vasicek, Optics of Thin Films (North Holland, 1960), p. 31

18. S. Tolansky, An Introduction to Interferometry (John Wiley and Sons, 1955).

19. Committee on Colorimetry Optical Society of America, The Science of America (Optical Society of America, Washington D. C., 1963), p. 259.

20. W. D. Wright, The Measurement of Color (Van Nostrand, 1969), p. 319.

21. W. D. Wright, J. Opt. Soc. of Amer. 33, 632 (1943).

22. R. H. Muller, Principles of Ellipsometry, LBL-187, 1966.

23. H. J. Mathieu, Computer Programs of Ellipsometry, LBL-1470, 1973.

24. E. Bickel, Some Fundamental Problems in the Measurement of Surface Roughness in International Research in Production Engineering, Production Engineers Research Conference ASME, Carnegie Inst. of Tech. 1963, p. 667.

25. R. E. Reason, ibid, p. 694.

26. H. Hasunuma, Japan Society of Percision Engineering 1(4), 205 (1966).

27. T. Nakamura, ibid, p. 240, 668.

28. J. L. Guerrero and J. T. Black, Trans. ASME 94(4), 1087 (1972).

29. R. R. Austin, R. Michaud, A. H. Guenther and J. Putman, Applied Optics 12(4), 665 (1973).

30. K. L. Chopra, Thin Film Phenomena (McGraw Hill, New York, 1969),

31. R. L. Meek, T. M. Buck and C. F. Gibbon, J. Electrochem. Soc. 120(9), 1241 (1973).

32. Sylvania Catalogue of Evaporation Sources, Sylvania, GTE TWX No. 510-297-4471.

33. R. E. Hohig and D. A. Kramer, RCA Review 30, 285 (1969).

34. R. W. Ditchburn, Light (Interscience, New York ,1964), Vol. II, p. 590.

35. J. V. Sanders in Chemisorption and Reactions on Metallic Films, J. R. Anderson, ed. (Academic Press, New York , 1971), Vol. I, p. 27.

36. W. E. J. Neal, R. W. Fane and N. W. Grimes, Philosophical Magazine 21(169) , 167 (1970).

37. W. Heitmann, Applied Optics 10(12), 2685 (1971).

38. K. R. Dixit in Thin Films in Optics, H. Anders, ed. (Focal Press, London, 1967), p. 21.

39. W. M. Feist, S. R. Steele and P. W. Readey in Physics of Thin Films, G. Hass and R. E. Thun, ed. (Academic Press, New York, 1969), Vol. 5.

40. S. C. Brown, Chemical Reactions in Electric Discharges (MIT Press, Cambridge , 1967).

41. N. Schwartz and R. W. Berry in Physics of Thin Films, G. Hass and R. E. Thun, eds. (Academic Press, N. Y. , 1969), Vol. II, p. 401.

42. G. R. Booker and B. A. Unvala, Philosophical Magazine 11(11), 11 (1964).

43. D. F. Klemperer in Chemisorption and Reactions on Metallic Thin Films, J. R. Anderson, ed. (Academic Press, New York, 1971), Vol. 1, p. 81.

44. H. J. Mathieu, D. E. McClure and R. H. Muller, Self-Compensating Automatic Ellipsometer, LBL-1478, 1973.

45. R. H. Muller, G. A. Somorjai, J. Morabito and K. Steiger, Surface Science 16, 234 (1969).

46. H. J. Mathieu, private communication.

47. K. Vedam, W. Krausemberger and F. Lukes, J. Opt. Soc. Amer. 59, 64 (1969).

48. J. O. M. Bockris, A. K. N. Reddy, B. Rao, J. Electrochem. Soc. 113(11), 1133 (1969).

49. Handbook of Chemistry and Physics, (Chemical Rubber Publ. Co., 1962), p. 3084.

50. G. Pfestorf, Ann. Phys. 81, 906 (1926).

51. H. O'Bryan, J. Opt. Soc. Amer. 26, 122 (1926).

52. R. Menard, J. Opt. Soc. Amer. 52, 427 (1962).

53. J. Carroll and A. Melmed, J. Opt. Soc. Amer. 61, 470 (1971).

54. C. J. Dell'Oca and L. Young, J. Electrochem. Soc. 117, 1545 (1970).

55. L. Young and F. Jobel, J. Electrochem. Soc. 113, 277 (1966).

56. A. Melmed, H. Layer and J. Kruger, Surface Science 9, 476 (1968).

57. H. Archer, Phys. Rev. 110, 354 (1958).

58. H. Phillip and H. Ehrenneich, Physical Review 129, 1550 (1963).

59. K. Volenik, Corrosion Science 9, 15 (1969).

60. C. J. Dell'Oca and L. Young, J. Electrochem. Soc. 118, 89 (1971).

61. H. Phillip and H. Ehrenreich, Phys. Rev. Lett. 8, 92 (1962).

62. M. Cardona, J. Appl. Phys. 36, 2181 (1965).

63. W. Spitzer and W. Kaiser, J. Phys. Chem. Solid 11, 339 (1959).

TECHNICAL INFORMATION DIVISION
LAWRENCE BERKELEY LABORATORY
UNIVERSITY OF CALIFORNIA
BERKELEY, CALIFORNIA 94720